

1976

A two-dimensional time-dependent numerical model investigation of the coastal sea circulation around the Chesapeake Bay entrance

Everett Michael Stanley

College of William and Mary - Virginia Institute of Marine Science

Follow this and additional works at: <https://scholarworks.wm.edu/etd>



Part of the [Oceanography Commons](#)

Recommended Citation

Stanley, Everett Michael, "A two-dimensional time-dependent numerical model investigation of the coastal sea circulation around the Chesapeake Bay entrance" (1976). *Dissertations, Theses, and Masters Projects*. Paper 1539616862.

<https://dx.doi.org/doi:10.25773/v5-0ncz-2780>

This Dissertation is brought to you for free and open access by the Theses, Dissertations, & Master Projects at W&M ScholarWorks. It has been accepted for inclusion in Dissertations, Theses, and Masters Projects by an authorized administrator of W&M ScholarWorks. For more information, please contact scholarworks@wm.edu.

INFORMATION TO USERS

This material was produced from a microfilm copy of the original document. While the most advanced technological means to photograph and reproduce this document have been used, the quality is heavily dependent upon the quality of the original submitted.

The following explanation of techniques is provided to help you understand markings or patterns which may appear on this reproduction.

1. The sign or "target" for pages apparently lacking from the document photographed is "Missing Page(s)". If it was possible to obtain the missing page(s) or section, they are spliced into the film along with adjacent pages. This may have necessitated cutting thru an image and duplicating adjacent pages to insure you complete continuity.
2. When an image on the film is obliterated with a large round black mark, it is an indication that the photographer suspected that the copy may have moved during exposure and thus cause a blurred image. You will find a good image of the page in the adjacent frame.
3. When a map, drawing or chart, etc., was part of the material being photographed the photographer followed a definite method in "sectioning" the material. It is customary to begin photoing at the upper left hand corner of a large sheet and to continue photoing from left to right in equal sections with a small overlap. If necessary, sectioning is continued again — beginning below the first row and continuing on until complete.
4. The majority of users indicate that the textual content is of greatest value, however, a somewhat higher quality reproduction could be made from "photographs" if essential to the understanding of the dissertation. Silver prints of "photographs" may be ordered at additional charge by writing the Order Department, giving the catalog number, title, author and specific pages you wish reproduced.
5. PLEASE NOTE: Some pages may have indistinct print. Filmed as received.

Xerox University Microfilms

300 North Zeeb Road
Ann Arbor, Michigan 48106

76-19,811

STANLEY, Everett Michael, 1938-
A TWO-DIMENSIONAL TIME-DEPENDENT
NUMERICAL MODEL INVESTIGATION OF THE
COASTAL SEA CIRCULATION AROUND THE
CHESAPEAKE BAY ENTRANCE.

The College of William and Mary in
Virginia, Ph.D., 1976
Physical Oceanography

Xerox University Microfilms, Ann Arbor, Michigan 48106

A TWO-DIMENSIONAL TIME-DEPENDENT
NUMERICAL MODEL INVESTIGATION OF THE
COASTAL SEA CIRCULATION AROUND THE
CHESAPEAKE BAY ENTRANCE

A Dissertation

Presented to

The Virginia Institute of Marine Science
The College of William and Mary in Virginia

In Partial Fulfillment

Of the Requirements for the Degree of

Doctor of Philosophy

by

Everett Michael Stanley

1976

APPROVAL SHEET

This dissertation is submitted in partial fulfillment of
the requirements for the degree of
Doctor of Philosophy

E. M. Stanley

E. M. Stanley

Approved, May 1976

Albert Y. Kuo

Dr. Albert Y. Kuo

Christopher S. Welch

Dr. Christopher S. Welch

Victor Goldsmith

Dr. Victor Goldsmith

W. G. MacIntyre

Dr. W. G. MacIntyre

Paul A. Haefner, Jr.

Dr. Paul A. Haefner, Jr.

Jerrold S. Rosenbaum

Dr. Jerrold S. Rosenbaum (Assistant
Professor of Mathematical Science,
Virginia Commonwealth University)

TABLE OF CONTENTS

	Page
ACKNOWLEDGMENTS	iv
LIST OF FIGURES	vi
DEFINITION OF SYMBOLS	x
ABSTRACT.	xiv
CHAPTER I INTRODUCTION AND BACKGROUND.	2
CHAPTER II DERIVATION OF TWO-DIMENSIONAL DIFFERENTIAL EQUATIONS.	10
CHAPTER III FORMULATION OF FINITE DIFFERENCE EQUATIONS.	25
CHAPTER IV METHOD OF SOLUTION FOR THE UNKNOWNNS OF U, V, δ , AND S	37
CHAPTER V COMPUTER PROGRAM	53
CHAPTER VI RESULTS AND DISCUSSION.	60
CHAPTER VII CONCLUSIONS AND RECOMMENDATIONS.	132
APPENDIX A	138
APPENDIX B	143
APPENDIX C	145
APPENDIX D	157
BIBLIOGRAPHY.	160

ACKNOWLEDGMENTS

I wish to thank the David W. Taylor Naval Ship Research and Development Center for making this work possible by providing the necessary funds and sabbatical leave.

I am grateful to Dr. A. Kuo, whose patience, guidance, and continuous support during this work will always be remembered, and to the members of the committee who read and commented on this work.

I am also indebted to the people at the computing centers of the Virginia Institute of Marine Science and the David W. Taylor Naval Ship Research and Development Center for their time and support in helping me to interface with the complex computing machinery necessary to do this work.

I wish to thank the Graphics Department of the Virginia Institute of Marine Science for furnishing Figure 1 of this report and Dr. W. Boicourt of Johns Hopkins University for furnishing Figure 42.

To Dr. E. C. Fischer, who not only backed my efforts in this work but also remained a friend and loyal supporter, I give my thanks.

Finally, to my wife and family, who gave up many days and weekends together and cheerfully supported this effort, I am forever grateful.

LIST OF FIGURES

Figure		Page
1.	Location of Chesapeake Bight	3
2.	Coördinate notation.	12
3.	Grid point arrangement	29
4.	Illustration of grid and boundary conditions .	39
5.	Computer flow diagram from program COASTAL MODEL	54
6.	Grid outline and bottom profiles	63
7	Tidal height as a function of time for grid point (m = 15, n = 25).	66
8	Maximum theoretical and computed velocity as a function of distance in x direction, wave reflection	67
9	Maximum theoretical and computed tidal height as a function of distance in x direction, wave reflection	68
10	Velocity vector plot, steady-state jet	72
11	Water level plot, steady-state jet, cm	73
12	Centerline velocity distribution resulting from different values of bottom friction, steady-state jet.	76
13	Decay time, steady-state jet	78
14	Velocity vector plot, steady-state jet with side friction	80

Figure		Page
15	$U_0/2$ as a function of x and y for side and bottom friction case, steady-state jet. .	81
16	Centerline velocity distribution for side and bottom friction case, steady-state jet	82
17	Cross-stream velocity distribution, steady-state jet	87
18	Velocity vector plot, steady-state jet with Coriolis force.	89
19	Water level plot, steady-state jet with Coriolis force, cm.	90
20	Velocity vector plot, steady-state jet with southerly ambient velocity.	93
21	Velocity and water level as a function of time at two grid points, oscillating jet. .	96
22	Water level plot, oscillating jet at slack before ebb, cm.	98
23	Velocity vector plot, oscillating jet at maximum ebb	99
24	Velocity vector plot, oscillating jet at a maximum centerline velocity of 12 cm sec^{-1}	100
25	Water level plot, oscillating jet at slack before flood, cm.	101
26	Velocity vector plot, oscillating jet at maximum flood	102
27	Tidal averaged flow, oscillating jet	104
28	Centerline velocity distribution for flat and sloping bottom, oscillating jet	105

Figure		Page
29	Velocity vector plot, oscillating jet at maximum ebb and with Coriolis force . .	108
30	Velocity vector plot, oscillating jet at maximum flood and with Coriolis force .	109
31	Tidal average flow, oscillating jet with Coriolis force.	110
32	Velocity vector plot, oscillating jet at maximum ebb and with sloping bottom . .	111
33	Velocity vector plot, oscillating jet at maximum flood and with sloping bottom .	112
34	Velocity vector plot, oscillating jet at maximum ebb and with onshore wind . . .	115
35	Velocity vector plot, oscillating jet at maximum flood and with onshore wind . .	116
36	Velocity vector plot, oscillating jet at maximum ebb and with northerly wind . .	117
37	Velocity vector plot, oscillating jet at maximum flood and with northerly wind .	118
38	Velocity vector plot, oscillating jet at maximum ebb and with a southerly ambient velocity of 5 cm sec ⁻¹	123
39	Velocity vector plot, oscillating jet at maximum flood and with a southerly ambient velocity of 5 cm sec ⁻¹	124
40	Velocity vector plot, oscillating jet at maximum ebb and with a southerly ambient velocity of 10 cm sec ⁻¹	125
41	Velocity vector plot, oscillating jet at maximum flood and with a southerly ambient velocity of 10 cm sec ⁻¹	126

Figure		Page
42	Chesapeake Bight surface salinity distribution, July-August 1972.	128
43	Velocity vector roses at two grid points . .	130

DEFINITION OF SYMBOLS

<u>Symbol</u>	<u>Definition</u>
<u>Lower Case</u>	
a_o	wave amplitude, cm
f	Coriolis parameter, $2\Omega\sin\theta$, sec^{-1}
g	gravitational constant, 980 cm sec^{-2}
h	water depth referenced to mean sea level, cm
\bar{h}	average water depth referenced to mean sea level, cm
k	wave number $(2\pi/L)$, cm^{-1}
m	subscripts in numerical notation indicating x direction
n	subscripts in numerical notation indicating y direction
n'	Manning coefficient
p	pressure, $\text{gm cm}^{-1} \text{ sec}^{-2}$
s	real time variation of salinity, $s = \rho\tilde{S}$, gm cm^{-3}
s'	salinity deviation from average, gm cm^{-3}
t	time, sec

<u>Symbol</u>	<u>Definition</u>
u	velocity in x direction, cm sec^{-1}
u'	velocity deviation from average, x direction, cm sec^{-1}
v	velocity in y direction, cm sec^{-1}
v'	velocity deviation from average, y direction, cm sec^{-1}
w	velocity in z direction, cm sec^{-1}
x	direction in right-hand coordinate system, positive to east
y	direction in right-hand coordinate system, positive to north
z	direction in right-hand coordinate system, positive up

Upper Case

A_i	turbulent eddy viscosity ($i = x, y, \text{ or } z$), $\text{cm}^2 \text{ sec}^{-1}$
C	Chezy coefficient, $\text{cm}^{1/2} \text{ sec}^{-1}$
D_i	dispersion ($i = x \text{ or } y$), $\text{cm}^2 \text{ sec}^{-1}$
E_i	turbulent eddy diffusion ($i = x, y, \text{ or } z$), $\text{cm}^2 \text{ sec}^{-1}$
H	total water depth $h + \delta$, cm

<u>Symbol</u>	<u>Definition</u>
H_{jB}^{it}, H_{jF}^{it}	shorthand notation for $h + \delta$ in finite difference notation, where $j = x$ or y and $it = t, 2t, \text{ etc.}$ (See Chapter IV.)
L	distance x or y direction, cm
S	salinity averaged with respect to depth, gm kg^{-1}
\bar{S}	real time variation of salinity, gm kg^{-1}
T	wave period, sec
U	velocity in x direction integrated with respect to depth, cm sec^{-1}
\bar{U}	average depth integrated velocity in x direction, cm sec^{-1}
V	velocity in y direction integrated with respect to depth, cm sec^{-1}
\bar{V}	average depth integrated velocity in y direction, cm sec^{-1}
W	wind speed, cm sec^{-1}
Y	jet or Bay mouth width, cm
A_j, A_j^i	constants in recursion equations, where $j = m$ or n . (These constants are defined in Chapter IV; computer notation is given in Appendix A.)
B_j, B_j^i	
C_j, C_j^i	
D_j, D_j^i	
E_j, E_j^i	
F_j, F_j^i	

<u>Symbol</u>	<u>Definition</u>
H_j	constants in recursion equations, where $j = m$
P_j Q_j	or n (cont)
R_j T_j	
<u>Greek</u>	
α	constant in mixing length theory, dimensionless
δ	tidal height, cm
θ	angle, degree of latitude
ρ	density, gm cm^{-3}
ρ'	density deviation from average, gm cm^{-3}
ρ_a'	density of air, gm cm^{-3}
$\bar{\rho}$	density, average, with respect to depth, gm cm^{-3}
σ	wave angular frequency ($2\pi/T$), cm sec^{-1}
τ_{ij}	general stress term, $\text{gm cm}^{-1} \text{sec}^{-2}$
τ_i^s τ_i^b	surface and bottom stress, $\text{gm cm}^{-1} \text{sec}^{-2}$
Ω	earth's angular velocity, $0.729211 \times 10^{-4} \text{sec}^{-1}$
ΔL	grid spacing, cm
ΔT	whole time step for numerical technique, sec
Δt	half time step for numerical technique ($\Delta T = 2\Delta t$), sec

A TWO-DIMENSIONAL TIME-DEPENDENT
NUMERICAL MODEL INVESTIGATION OF THE
COASTAL SEA CIRCULATION AROUND THE
CHESAPEAKE BAY ENTRANCE

ABSTRACT

A computer study was made of the resultant flow field arising from the discharge of a tidal estuary or river onto the continental shelf. The approach was to: (1) vertically integrate the continuity, momentum, and mass balance equations assuming incompressible flow and using the hydrostatic assumption and a Boussinesq approximation for density; (2) numerically model the vertically integrated equations; and (3) apply the equations to a simplified coastal geometry and determine the effects of different physical factors on the flow field. The numerical equations were written using a multi-operational computational technique which was found to be fast and stable. Velocity and/or tidal heights were found to be usable on open boundary conditions for the multi-operational computational scheme.

General conclusions from the study show that the outflow from an estuary can be divided into three types: dispersive, entraining, or a mixture of the two.

Specifically, results of the model study using a steady-state or oscillating jet to simulate the Chesapeake Bay time averaged (non-tidal) or tidal outflow show that for the cases studied: the longitudinal centerline velocity for both tidal and non-tidal flows decreases rapidly as a function of distance from the Bay mouth, the transverse U velocity profile for the non-tidal case (steady-state jet) is a hyperbolic secant squared function, the sea surface slope is important in modeling the flow and should be known to within 1-2 cm, the Coriolis force was not an important factor in the turning of the outflow due to the dominance of bottom friction, and the wind and ambient current were the most important factors in the turning of the outflow to the south. The model studies also showed the existence of a northern flow above the Bay entrance and a weak residual eddy motion above and below the Bay mouth for the tidal case.

EVERETT MICHAEL STANLEY

THE VIRGINIA INSTITUTE OF MARINE SCIENCE

THE COLLEGE OF WILLIAM AND MARY IN VIRGINIA

In chief, men marvel Nature renders not
Bigger and bigger the bulk of ocean, since
So vast the down-rush of the waters be,
And every river out of every realm
Cometh thereto; and add the random rains
And flying tempest, which spatter every sea
And every land bedew; add their own springs:
Yet all of these unto the ocean's sum
Shall be but as the increase of a drop.

Titus Lucretius Carus

A TWO-DIMENSIONAL TIME-DEPENDENT
NUMERICAL MODEL INVESTIGATION OF THE
COASTAL SEA CIRCULATION AROUND THE
CHESAPEAKE BAY ENTRANCE

CHAPTER I

INTRODUCTION AND BACKGROUND

The Middle Atlantic Bight extends from Cape Hatteras, North Carolina, to Cape Cod, Massachusetts. It can be broken into two main sections: the New York Bight, extending from the tip of Long Island, New York, to Cape May, New Jersey, and the Chesapeake Bight (Figure 1), which covers the area from Cape May, New Jersey, to Cape Hatteras, North Carolina. The region of the Chesapeake Bight was first explored and described by Captain John Smith who called it the Virginia Sea. One of the chief characteristics of the 314-km coastline of the Chesapeake Bight is the Chesapeake Bay entrance. The effluence from this Bay, its interaction with the surrounding shelf waters, and the resultant circulation constitute the primary physical problem investigated in this thesis.

The first general oceanographic descriptions of the Chesapeake Bight region were given by Parr (1933), Bigelow (1933), and Bigelow and Sears (1935). The surface flow is generally southerly (Miller (1952), Howe (1962), Bumpus and

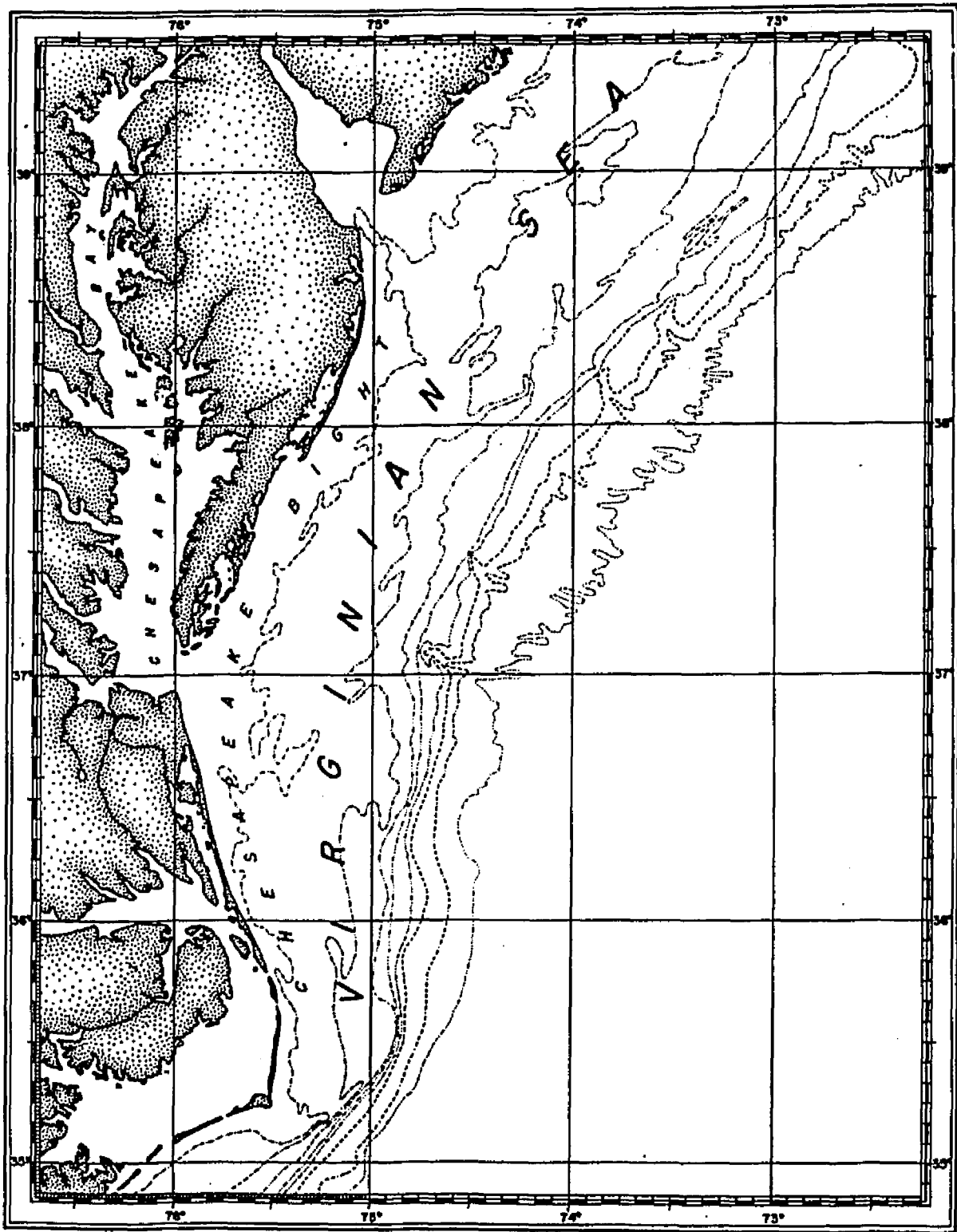


Figure 1
Location of Chesapeake Bight

Lauzier (1965), Harrison, Norcross, Pore, and Stanley (1967), Bumpus (1969)), but it is influenced by surface winds. The bottom drift is southerly in deep water and generally toward the Chesapeake Bay entrance in the shallow in-shore area (Bumpus (1965), Harrison et al (1967)), but it can vary with season, density stratification, and winds. The overall southerly surface flow is augmented by the discharge from the Chesapeake Bay and smaller coastal estuaries and lagoons, with the Chesapeake Bay being the largest contributor. This slow-moving southerly drift turns northward and is entrained in the Gulf Stream at Cape Hatteras (Ford and Miller (1952), Stommel (1965), Fisher (1972)). However, during periods of strong northerly winds, large segments of water from the Chesapeake Bight can be transported past Cape Hatteras into Raleigh Bay, and these have been documented by Harrison et al (1967), Bumpus and Pierce (1955), and Stefansson et al (1971).

Recently, work by Boicourt (1973) has shown that there may exist, during the summer, a return shoreward flow at mid-depths from the edge of the continental shelf. This return flow compensates for the off-shore drift of the Ekman layer caused by the predominately southerly winds at this time of year. Also, new current meter data (Boicourt (1973)) from the Bay mouth show great variability of the

efflux of the Bay waters onto the continental shelf and the possibility of this movement of water onto the shelf being controlled to some extent by the wind.

Thus, while a large amount of field data has been accumulated since Bigelow's pioneering work in 1933 and a basic understanding of the movement of the shelf waters has been outlined, there have been few attempts to understand the interrelationship between the outflow from the Chesapeake Bay and the circulation of the shelf waters. How this interrelationship changes and what factors are affecting it are difficult questions to answer.

A logical starting point to eradicate this deficiency would be to consider the application of the extensive work on plane submerged jets discharging into an infinite medium. Many papers and several books (Abramovich (1963), Birkhoff and Zarantonello (1957)) have been written on this subject. However, when the theory and experimental results of a plane jet are compared with what occurs when a large river or estuary empties into a coastal sea, little correlation can be found between the two. The major discrepancy occurs because the plane jet is an entraining one and its angle of spread is small. An estuary or river outflow is generally divergent and can be affected by tide, winds, stratification, ambient currents, and rotation of

the earth. This can be seen when comparing classical jet theory with the descriptive work of Stefansson and Richards (1963) and Park (1966) on the Columbia River, Ryther et al (1967) and Gibbs (1970) on the Amazon, Wright and Coleman (1971) on the south pass of the Mississippi, and Garvine (1974) on the Connecticut River. These investigations describe the circulation and distribution of salinity and nutrients which result from the discharge of the above rivers into the surrounding waters and discuss some of the physical factors affecting the circulation.

Recently, several investigators have tried to either apply the results of the theory of the classical jet (referenced above) to the natural environment or take a theoretical approach specifically formulated for the hydrodynamics of a river discharging into a larger body of water.

Bates (1953) suggested that the deceleration of river effluence discharging onto a continental shelf was in accordance with the theory of turbulent jet diffusion as described in Chapter VI. This reasoning was applied to the mouths of the Mississippi River to help understand the formation of deltas.

Iselin (1955) has given a physical description of factors which should affect the circulation in a coastal area and has outlined some rules which have been accepted

almost without question.

A more rigorous theoretical approach has been attempted by Takano (1954a, 1954b, 1955), Borichansky and Midhailov (1966), and Bondar (1970). They consider variables, such as bottom and side friction, geometry of the channel entrance, bottom slope, Coriolis force, and density differences, to describe the resultant flow patterns. Their results will also be discussed in Chapter VI.

Finally, Gadgil (1971) has determined the effect of a simple rotating and non-rotating system on the shape and velocity distribution of a steady jet. She has shown that, if a simple laboratory jet is rotated strongly, bottom friction dominates and the jet will be dispersive; while for a non-rotating jet, side friction will dominate and the jet will entrain the surrounding fluid.

The theoretical investigations described above are very useful in gaining an understanding of the physical factors affecting the flow field caused by a river or estuary discharging onto a continental shelf. These results, however, have been derived from the momentum equations where some terms have been left out or simplified to render an analytical solution possible. In like manner, the purely descriptive studies of jet and shelf circulations have given a view where individual factors affecting the flow

have been lumped together to give a mean, average, or seasonal pattern of flow, obliterating their individual contributions.

The intent of this investigation is to examine the characteristics of flow resulting from a tidal estuary (Chesapeake Bay) emptying onto a continental shelf using as many of the terms in the equations of motion and the mass balance equation as possible. No effort will be made to reproduce the physical geometry and dynamical situation of the shelf exactly because the extensive data needed for input into the model are not available. Instead the approach will be to vertically integrate the equations of continuity, momentum, and mass balance, assuming where applicable: (1) incompressible flow, (2) a Boussinesq-type approximation, (3) the hydrostatic assumption, and (4) that only the horizontal components of the rotational terms are important. The resultant equations will then be applied to a simplified geometry resembling that of the continental shelf and Chesapeake Bay entrance. Specifically, the effect of tidal flow, bottom and side frictions, force of Coriolis, bottom slope, wind, and ambient currents on the overall circulation patterns will be considered. Further, three circulation characteristics observed in field work of the area will be specifically looked for:

(1) deflection of the Bay effluent, (2) a northern flow above the Bay entrance, and (3) a clockwise eddy south of the Bay entrance.

CHAPTER II

DERIVATION OF TWO-DIMENSIONAL DIFFERENTIAL EQUATIONS

Basic Concepts

A right-hand coordinate system is assumed with x being positive to the right or east and z being positive upward. The velocity components are the usual u , v , and w for the x , y , and z directions, respectively. The basic equations describing the conservation of mass and momentum in a water body are:

continuity equation

$$\frac{\partial \rho}{\partial t} + \frac{\partial}{\partial x} (\rho u) + \frac{\partial}{\partial y} (\rho v) + \frac{\partial}{\partial z} (\rho w) = 0; \quad 2.1$$

momentum equation in the x direction

$$\begin{aligned} \frac{\partial}{\partial t} (\rho u) + \frac{\partial}{\partial x} (\rho u^2) + \frac{\partial}{\partial y} (\rho u v) + \frac{\partial}{\partial z} (\rho u w) = \\ - \frac{\partial P}{\partial x} + f \rho v + \frac{\partial}{\partial x} \tau_{xx} + \frac{\partial}{\partial y} \tau_{xy} + \frac{\partial}{\partial z} \tau_{xz}; \end{aligned} \quad 2.2$$

momentum equation in the y direction

$$\begin{aligned} \frac{\partial}{\partial t} (\rho v) + \frac{\partial}{\partial x} (\rho v u) + \frac{\partial}{\partial y} (\rho v^2) + \frac{\partial}{\partial z} (\rho v w) = \\ - \frac{\partial P}{\partial y} - f \rho u + \frac{\partial}{\partial x} \tau_{yx} + \frac{\partial}{\partial y} \tau_{yy} + \frac{\partial}{\partial z} \tau_{yz}; \end{aligned} \quad 2.3$$

momentum equation in the z direction

$$\frac{\partial}{\partial t}(\rho w) + \frac{\partial}{\partial x}(\rho w u) + \frac{\partial}{\partial y}(\rho w v) + \frac{\partial}{\partial z}(\rho w^2) =$$

$$-\frac{\partial p}{\partial z} - \rho g + \frac{\partial}{\partial x} \tau_{zx} + \frac{\partial}{\partial y} \tau_{zy} + \frac{\partial}{\partial z} \tau_{zz} ;$$

2.4

mass balance equation of salt

$$\frac{\partial A}{\partial t} + \frac{\partial}{\partial x}(uA) + \frac{\partial}{\partial y}(vA) + \frac{\partial}{\partial z}(wA) =$$

$$\frac{\partial}{\partial x} (E_x \frac{\partial A}{\partial x}) + \frac{\partial}{\partial y} (E_y \frac{\partial A}{\partial y}) + \frac{\partial}{\partial z} (E_z \frac{\partial A}{\partial z}) ;$$

2.5

where t , ρ , p , f , g , s , and E_i represent time, density, pressure, Coriolis parameter, gravitational acceleration, real time variation of salinity, and turbulent diffusion coefficient in the i direction. τ_{ij} represents the shear stress, where the subscript i is the direction of the stress and the plane in which the stress acts is given by the normal to the plane j .

Integration of Equation of Continuity

As shown in Figure 2, let the depth of water be h (referenced to mean sea level), δ the tidal height, and H the total water depth ($H = h + \delta$).

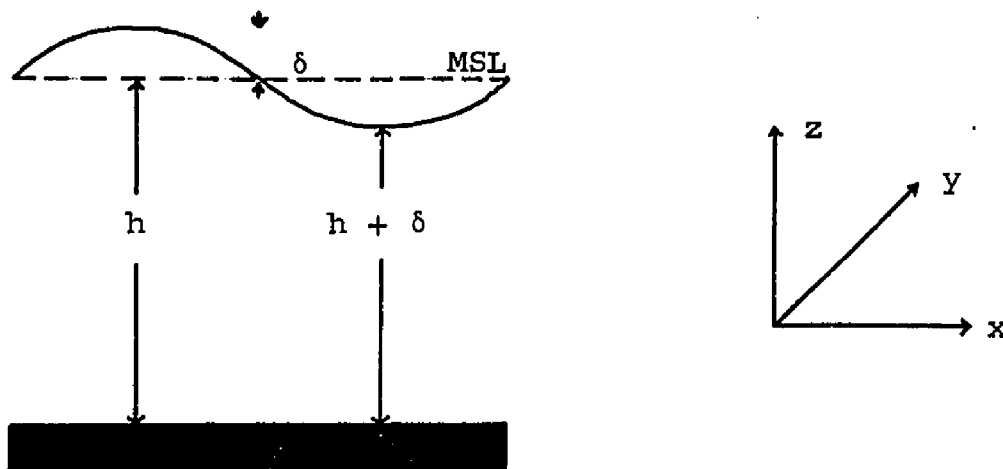


Figure 2

Coordinate notation

In an incompressible flow field, equation 2.1 may be simplified to give

$$\frac{\partial U}{\partial x} + \frac{\partial V}{\partial y} + \frac{\partial W}{\partial z} = 0. \quad 2.6$$

Integrating with respect to z from $-h$ to δ gives

$$\int_{-h}^{\delta} \frac{\partial U}{\partial x} dz + \int_{-h}^{\delta} \frac{\partial V}{\partial y} dz + \int_{-h}^{\delta} \frac{\partial W}{\partial z} dz = 0. \quad 2.7$$

Applying Leibnitz's rule, the boundary conditions $w = \frac{\partial \delta}{\partial t} + u \frac{\partial \delta}{\partial x} + v \frac{\partial \delta}{\partial y}$ at the free surface and $u = v = w = 0$ at the bottom give for 2.7

$$\frac{\partial}{\partial t} (\delta) + \frac{\partial}{\partial x} \int_{-h}^{\delta} U dz + \frac{\partial}{\partial y} \int_{-h}^{\delta} V dz = 0. \quad 2.8$$

Since the velocity in a natural environment is seldom constant with respect to depth, we set

$$u = u(z) = \bar{U} + u'(z) \quad 2.9$$

where \bar{U} is the velocity averaged with respect to depth, and $u'(z)$ is the variation of the velocity u from the average \bar{U} .

By definition,

$$\int_{-h}^{\delta} u'(z) dz = 0 \quad 2.10$$

and

$$\frac{1}{H} \int_{-h}^{\delta} u dz = \bar{U}; \quad 2.11$$

or, rearranging,

$$\bar{U}H = \int_{-h}^{\delta} u dz.$$

Doing the same for the velocity v gives

$$v = v(z) = \bar{V} + v'(z) \quad 2.12$$

and

$$\bar{V}H = \int_{-h}^{\delta} v dz. \quad 2.13$$

Now, substitution of 2.11 and 2.13 into 2.8 gives

$$\frac{\partial \delta}{\partial t} + \frac{\partial}{\partial x} (UH) + \frac{\partial}{\partial y} (VH) = 0. \quad 2.14$$

Integration of Momentum Equations

Now, applying equations 2.1 and 2.6 to 2.2 and 2.3 and integrating with respect to depth between the limits of $-h$ and δ give for the equation in the x direction

$$\int_{-h}^{\delta} \frac{\partial}{\partial t} u dz + \int_{-h}^{\delta} \frac{\partial}{\partial x} (u^2) dz + \int_{-h}^{\delta} \frac{\partial}{\partial y} (uv) dz + \int_{-h}^{\delta} \frac{\partial}{\partial z} (uw) dz = - \int_{-h}^{\delta} \frac{1}{\rho} \frac{\partial p}{\partial x} dz +$$

$$\int_{-h}^{\delta} f v dz + \int_{-h}^{\delta} \frac{1}{\rho} \frac{\partial}{\partial x} \tau_{yx} dz + \int_{-h}^{\delta} \frac{1}{\rho} \frac{\partial}{\partial y} \tau_{xy} dz + \int_{-h}^{\delta} \frac{1}{\rho} \frac{\partial}{\partial z} \tau_{xz} dz ; \quad 2.15$$

and for the equation in the y direction

$$\int_{-h}^{\delta} \frac{\partial}{\partial t} v dz + \int_{-h}^{\delta} \frac{\partial}{\partial x} (uv) dz + \int_{-h}^{\delta} \frac{\partial}{\partial y} (v^2) dz + \int_{-h}^{\delta} \frac{\partial}{\partial z} (vw) dz = - \int_{-h}^{\delta} \frac{1}{\rho} \frac{\partial p}{\partial y} dz -$$

$$\int_{-h}^{\delta} f u dz + \int_{-h}^{\delta} \frac{1}{\rho} \frac{\partial}{\partial x} \tau_{yx} dz + \int_{-h}^{\delta} \frac{1}{\rho} \frac{\partial}{\partial y} \tau_{yy} dz + \int_{-h}^{\delta} \frac{1}{\rho} \frac{\partial}{\partial z} \tau_{yz} dz. \quad 2.16$$

Using Leibnitz's rule, the boundary conditions for the surface and bottom (as in the equation of continuity) and equations 2.11 and 2.13 on 2.15 and 2.16 give for the equation in the x direction

$$\begin{aligned}
& \frac{\partial}{\partial t} (UH) + \frac{\partial}{\partial x} (U^2H) + \frac{\partial}{\partial y} (UVH) + \frac{\partial}{\partial x} \int_{-h}^{\delta} (u')^2 dz + \frac{\partial}{\partial y} \int_{-h}^{\delta} (u'v') dz = \\
& - \int_{-h}^{\delta} \frac{1}{\rho} \frac{\partial p}{\partial x} dz + fVH + \int_{-h}^{\delta} \frac{1}{\rho} \frac{\partial}{\partial x} \tau_{xx} dz + \int_{-h}^{\delta} \frac{1}{\rho} \frac{\partial}{\partial y} \tau_{yx} dz + \int_{-h}^{\delta} \frac{1}{\rho} \frac{\partial}{\partial z} \tau_{xz} dz
\end{aligned} \tag{2.17}$$

and the equation in the y direction

$$\begin{aligned}
& \frac{\partial}{\partial t} (VH) + \frac{\partial}{\partial x} (UVH) + \frac{\partial}{\partial y} (V^2H) + \frac{\partial}{\partial x} \int_{-h}^{\delta} (u'v') dz + \frac{\partial}{\partial y} \int_{-h}^{\delta} (v')^2 dz = \\
& - \int_{-h}^{\delta} \frac{1}{\rho} \frac{\partial p}{\partial y} dz - fUH + \int_{-h}^{\delta} \frac{1}{\rho} \frac{\partial}{\partial x} \tau_{yx} dz + \int_{-h}^{\delta} \frac{1}{\rho} \frac{\partial}{\partial y} \tau_{yy} dz + \int_{-h}^{\delta} \frac{1}{\rho} \frac{\partial}{\partial z} \tau_{yz} dz.
\end{aligned} \tag{2.18}$$

To further simplify the above two equations, several assumptions must be made. First is the hydrostatic assumption and the resultant equation

$$\frac{\partial p}{\partial z} = -\rho g \tag{2.19}$$

Second, a Boussinesq-type approximation is assumed in which the vertical variation of density ρ is ignored except in the gravitational term. Now, considering only the pressure gradient term in 2.17 for the time being, applying the above assumptions and Leibnitz's rule gives

$$- \int_{-h}^{\delta} \frac{1}{\rho} \frac{\partial p}{\partial x} dz = - \frac{1}{\rho} \int_{-h}^{\delta} \frac{\partial p}{\partial x} dz = - \frac{1}{\rho} \left[\int_{-h}^{\delta} \rho dz + \rho|_{-h} \frac{\partial(-h)}{\partial x} - \rho|_{\delta} \frac{\partial \delta}{\partial x} \right], \tag{2.20}$$

where $p|_{\delta} = 0$ is the pressure at the free surface or sea-air interface. If the same type of convention for the density variation as a function of depth is used as was for the velocity, i.e., the density consists of a depth averaged part plus a variation from this average,

$$\rho = \bar{\rho} + \rho' \quad 2.21$$

To expand 2.20 to a form which can be used, 2.21 is substituted into equation 2.19 and integrated from the surface $z = \delta$ to any depth z

$$p = \int_{\delta}^z -g(\bar{\rho} + \rho') dz$$

or

$$p = \bar{\rho}g(\delta - z) + g \int_z^{\delta} \rho' dz. \quad 2.22$$

Integrating 2.22 over depth gives

$$\begin{aligned} \int_{-h}^{\delta} p dz &= \bar{\rho}g \int_{-h}^{\delta} (\delta - z) dz + g \int_{-h}^{\delta} \left(\int_z^{\delta} \rho' dz \right) dz \\ &= \bar{\rho}g \frac{(\delta + h)^2}{2} + g \int_{-h}^{\delta} \left(\int_z^{\delta} \rho' dz \right) dz. \end{aligned}$$

2.23

Differentiating the above with respect to x yields

$$\frac{\partial}{\partial x} \int_{-h}^{\delta} p dz = \bar{p} g (\delta+h) \left(\frac{\partial \delta}{\partial x} + \frac{\partial h}{\partial x} \right) + g \frac{(\delta+h)^2}{2} \frac{\partial \bar{p}}{\partial x} +$$

$$g \frac{\partial}{\partial x} \int_{-h}^{\delta} \left(\int_3^{\delta} \rho' dz \right) dz.$$

2.24

The term $p|_{-h}$ can be evaluated from 2.22, giving

$$p|_{-h} = \bar{p} g H, \quad 2.25$$

since

$$\int_{-h}^{\delta} \rho' dz = 0.$$

Substituting equations 2.24 and 2.25 into 2.20 and simplifying yields

$$-\int_{-h}^{\delta} \frac{1}{\rho} \frac{\partial p}{\partial x} dz = -g H \frac{\partial \delta}{\partial x} - \frac{g H^2}{2 \bar{\rho}} \frac{\partial \bar{p}}{\partial x} - \frac{g}{\bar{\rho}} \frac{\partial}{\partial x} \int_{-h}^{\delta} \left(\int_3^{\delta} \rho' dz \right) dz. \quad 2.26$$

Likewise, for the y direction without repeating the derivation, the results using the same approach will be

$$-\int_{-h}^{\delta} \frac{1}{\rho} \frac{\partial p}{\partial y} dz = -g H \frac{\partial \delta}{\partial y} - \frac{g H^2}{2 \bar{\rho}} \frac{\partial \bar{p}}{\partial y} - \frac{g}{\bar{\rho}} \frac{\partial}{\partial y} \int_{-h}^{\delta} \left(\int_3^{\delta} \rho' dz \right) dz. \quad 2.27$$

For homogeneous or weakly stratified water columns, as considered here, the last term in 2.26 and 2.27 can be dropped

due to its small value (Appendix A).

The shear stress terms of 2.17 and 2.18 can also be simplified using the Boussinesq approximation to give

$$\int_{-h}^{\delta} \frac{1}{\rho} \frac{\partial}{\partial x} \tau_{xz} dz + \int_{-h}^{\delta} \frac{1}{\rho} \frac{\partial}{\partial y} \tau_{yz} dz + \int_{-h}^{\delta} \frac{1}{\rho} \frac{\partial}{\partial z} \tau_{z3} dz =$$

$$\frac{1}{\rho} \left[\frac{\partial}{\partial x} \int_{-h}^{\delta} \tau_{xz} dz + \frac{\partial}{\partial y} \int_{-h}^{\delta} \tau_{yz} dz + \tau_x^s - \tau_x^b \right]$$

2.28

and

$$\int_{-h}^{\delta} \frac{1}{\rho} \frac{\partial}{\partial x} \tau_{yx} dz + \int_{-h}^{\delta} \frac{1}{\rho} \frac{\partial}{\partial y} \tau_{yy} dz + \int_{-h}^{\delta} \frac{1}{\rho} \frac{\partial}{\partial z} \tau_{y3} dz =$$

$$\frac{1}{\rho} \left[\frac{\partial}{\partial x} \int_{-h}^{\delta} \tau_{yx} dz + \frac{\partial}{\partial y} \int_{-h}^{\delta} \tau_{yy} dz + \tau_y^s - \tau_y^b \right],$$

2.29

where τ_x^s , τ_x^b , τ_y^s , τ_y^b are the surface and bottom stresses in planes of the local surface and bottom in the x and y directions, respectively. Substituting 2.26 through 2.29 into the proper places in 2.17 and 2.18 results in

$$\begin{aligned}
& \frac{\partial}{\partial t} (UH) + \frac{\partial}{\partial x} (U^2H) + \frac{\partial}{\partial y} (UVH) + \frac{\partial}{\partial x} \int_{-h}^{\delta} (u')^2 dz + \frac{\partial}{\partial y} \int_{-h}^{\delta} (u'n') dz = \\
& -gH \frac{\partial \delta}{\partial x} - \frac{gH^2}{2\rho} \frac{\partial \bar{p}}{\partial x} + fUH + \frac{1}{\rho} \frac{\partial}{\partial x} \int_{-h}^{\delta} \tau_{xz} dz + \frac{1}{\rho} \frac{\partial}{\partial y} \int_{-h}^{\delta} \tau_{xy} dz + \\
& \frac{1}{\rho} (\tau_x^s - \tau_x^b)
\end{aligned}$$

2.30

and

$$\begin{aligned}
& \frac{\partial}{\partial t} (VH) + \frac{\partial}{\partial x} (VUH) + \frac{\partial}{\partial y} (V^2H) + \frac{\partial}{\partial x} \int_{-h}^{\delta} (u'n') dz + \frac{\partial}{\partial y} \int_{-h}^{\delta} (v'n')^2 dz = \\
& -gH \frac{\partial \delta}{\partial x} - \frac{gH^2}{2\rho} \frac{\partial \bar{p}}{\partial x} + fUH + \frac{1}{\rho} \frac{\partial}{\partial x} \int_{-h}^{\delta} \tau_{yx} dz + \frac{1}{\rho} \frac{\partial}{\partial y} \int_{-h}^{\delta} \tau_{yy} dz + \\
& \frac{1}{\rho} (\tau_y^s - \tau_y^b).
\end{aligned}$$

2.31

Further, the turbulent velocity fluctuation and the shear stress terms in 2.30 can be combined and approximated (Leendertse et al (1973)) by

$$\frac{\partial}{\partial x} \int_{-h}^{\delta} \left(\frac{\tau_{xx}}{\rho} - u'v' \right) dz = \frac{\partial}{\partial x} A_x H \frac{\partial U}{\partial x} = \frac{\partial}{\partial x} \alpha H^2 U \frac{\partial U}{\partial x}$$

$$\frac{\partial}{\partial y} \int_{-h}^{\delta} \left(\frac{\tau_{xy}}{\rho} - u'v' \right) dz = \frac{\partial}{\partial y} A_y H \frac{\partial U}{\partial y} = \frac{\partial}{\partial y} \alpha H^2 V \frac{\partial U}{\partial y}$$

side
friction 2.32
terms

Following the lead of Dronkers (1964), the bottom stress term can also be approximated by

$$-\frac{\tau_x^b}{\rho} = -\frac{gU[U^2+V^2]^{1/2}}{C^2}$$

bottom
friction 2.33
term

For the y direction the approximations for equation 2.31 give

$$\frac{\partial}{\partial x} \int_{-h}^{\delta} \left(\frac{\tau_{yx}}{\rho} - u'v' \right) dz = \frac{\partial}{\partial x} A_x H \frac{\partial V}{\partial x} = \frac{\partial}{\partial x} \alpha H^2 U \frac{\partial V}{\partial x}$$

$$\frac{\partial}{\partial y} \int_{-h}^{\delta} \left(\frac{\tau_{yy}}{\rho} - v'v' \right) dz = \frac{\partial}{\partial y} A_y H \frac{\partial V}{\partial y} = \frac{\partial}{\partial y} \alpha H^2 V \frac{\partial V}{\partial y}$$

side
friction 2.34
terms

and

$$-\frac{\tau_y^b}{\rho} = -\frac{gV[U^2+V^2]^{1/2}}{C^2}$$

bottom
friction 2.35
term

In equations 2.32 through 2.35, C is the Chézy coefficient and A the turbulent eddy viscosity. The Chézy coefficient can be related (Henderson (1966)) to depth by the equation

$$C = \frac{h^{1/6}}{n'} \quad 2.36$$

where h is the depth in meters and n' is the Manning coefficient. The turbulent eddy viscosities were simplified by relating them to the mixing length theory, giving

$$A_x = \alpha H U \quad 2.37$$

$$A_y = \alpha H V \quad 2.38$$

where α is a constant. Substituting the terms in 2.32 through 2.35 into 2.30 and 2.31 and applying equation 2.13 gives the final momentum equations of

$$\begin{aligned} \frac{\partial U}{\partial t} + U \frac{\partial U}{\partial x} + V \frac{\partial U}{\partial y} = fV - g \frac{\partial \delta}{\partial x} - \frac{gH}{2\bar{P}} \frac{\partial \bar{P}}{\partial x} - \frac{gU[U^2 + V^2]^{1/2}}{HC^2} + \\ \frac{\tau_x^s}{\bar{P}H} + \frac{1}{H} \left[\frac{\partial}{\partial x} \alpha H^2 U \frac{\partial U}{\partial x} \right] + \frac{1}{H} \left[\frac{\partial}{\partial y} \alpha H^2 V \frac{\partial U}{\partial y} \right] \end{aligned} \quad 2.39$$

and

$$\begin{aligned} \frac{\partial V}{\partial t} + U \frac{\partial V}{\partial x} + V \frac{\partial V}{\partial y} = -fU - g \frac{\partial \delta}{\partial y} - \frac{gH}{2\bar{P}} \frac{\partial \bar{P}}{\partial y} - \frac{gV[U^2 + V^2]^{1/2}}{HC^2} \\ \frac{\tau_y^s}{\bar{P}H} + \frac{1}{H} \left[\frac{\partial}{\partial x} \alpha H^2 U \frac{\partial V}{\partial x} \right] + \frac{1}{H} \left[\frac{\partial}{\partial y} \alpha H^2 V \frac{\partial V}{\partial y} \right]. \end{aligned} \quad 2.40$$

Integration of Mass Balance Equation

Lastly, the two-dimensional mass balance equation is derived by starting with 2.5, integrating with respect to z between the limits of δ and $-h$, and applying Leibnitz's rule, giving

$$\begin{aligned} & \frac{\partial}{\partial t} \int_{-h}^{\delta} \rho dz + \frac{\partial}{\partial x} \int_{-h}^{\delta} (\rho u) dz + \frac{\partial}{\partial y} \int_{-h}^{\delta} (\rho v) dz - \left[\rho \left(\frac{\partial \delta}{\partial t} + u \frac{\partial \delta}{\partial x} + v \frac{\partial \delta}{\partial y} - w \right) \right]_{\delta} \\ & \left[\rho \left(-\frac{\partial h}{\partial t} - u \frac{\partial h}{\partial x} - v \frac{\partial h}{\partial y} - w \right) \right]_{-h} - \frac{\partial}{\partial x} \int_{-h}^{\delta} E_x \frac{\partial \rho}{\partial x} dz - \frac{\partial}{\partial y} \int_{-h}^{\delta} E_y \frac{\partial \rho}{\partial y} dz + \\ & \left[\left(E_x \frac{\partial \rho}{\partial x} \right) \frac{\partial \delta}{\partial x} + \left(E_y \frac{\partial \rho}{\partial y} \right) \frac{\partial \delta}{\partial y} - E_z \frac{\partial \rho}{\partial z} \right]_{\delta} + \left[\left(E_x \frac{\partial \rho}{\partial x} \right) \frac{\partial h}{\partial x} + \left(E_y \frac{\partial \rho}{\partial y} \right) \frac{\partial h}{\partial y} + \right. \\ & \left. E_z \frac{\partial \rho}{\partial z} \right]_{-h} = 0, \end{aligned} \tag{2.41}$$

where $[]_{\delta}$ and $[]_{-h}$ designate the quantities in the brackets being evaluated at $z = \delta$ and $z = -h$, respectively.

Again, using the same technique for representing the variation of s as a function of depth as was done previously for the velocity and density, i.e.,

$$s = \bar{s} + s'(z) \tag{2.42}$$

and

$$\frac{1}{H} \int_{-h}^{\delta} s' dz = 0, \tag{2.43}$$

gives upon integration of 2.42 with respect to depth

$$\int_{-h}^{\delta} a \, dz = H \delta'. \quad 2.44$$

Substitution of 2.44 into 2.41, setting the boundary conditions that the salt flux through the surface and bottom is 0, and using the results of 2.11 and 2.12 give

$$\begin{aligned} \frac{\partial}{\partial t} (H \delta') + \frac{\partial}{\partial x} (H U \delta') + \frac{\partial}{\partial y} (H V \delta') = - \frac{\partial}{\partial x} \int_{-h}^{\delta} (u' a') \, dz - \frac{\partial}{\partial y} \int_{-h}^{\delta} (v' a') \, dz + \\ \frac{\partial}{\partial x} \int_{-h}^{\delta} E_x \frac{\partial \delta'}{\partial x} \, dz + \frac{\partial}{\partial y} \int_{-h}^{\delta} E_y \frac{\partial \delta'}{\partial y} \, dz. \end{aligned} \quad 2.45$$

Finally, letting the turbulent diffusion terms be replaced by a dispersion term D_i such that

$$D_x H \frac{\partial \delta'}{\partial x} = \int_{-h}^{\delta} (E_x \frac{\partial \delta'}{\partial x} - u' a') \, dz \quad 2.46$$

and

$$D_y H \frac{\partial \delta'}{\partial y} = \int_{-h}^{\delta} (E_y \frac{\partial \delta'}{\partial y} - v' a') \, dz \quad 2.47$$

gives

$$\frac{\partial}{\partial t} (H \delta') + \frac{\partial}{\partial x} (H U \delta') + \frac{\partial}{\partial y} (H V \delta') = \frac{\partial}{\partial x} \left[D_x H \frac{\partial \delta'}{\partial x} \right] + \frac{\partial}{\partial y} \left[D_y H \frac{\partial \delta'}{\partial y} \right]. \quad 2.48$$

Expanding the left-hand side and applying the equation of continuity (2.14) gives

$$\frac{\partial S'}{\partial t} + \frac{\partial (Us')}{\partial x} + \frac{\partial (Vs')}{\partial y} = \frac{1}{H} \left[\frac{\partial}{\partial x} D_x H \frac{\partial S}{\partial x} \right] + \frac{1}{H} \left[\frac{\partial}{\partial y} D_y H \frac{\partial S'}{\partial y} \right]. \quad 2.49$$

CHAPTER III

FORMULATION OF FINITE DIFFERENCE EQUATIONS

Basic Concepts

The final equations in the previous chapter (2.14, 2.39, 2.40, and 2.49) form a set of partial differential equations which together and without further assumptions have no known analytical solution. For these equations to be applied, as outlined in the Introduction, it will be necessary to use numerical techniques to approximate their exact solution.

The approach in forming a numerical approximation was: first, choosing a finite difference technique and computational scheme for the equations; second, formulating a computational grid for the equations; third, writing the analytical equations in finite difference form with the computational scheme and grid governing the formulation of the equations; fourth, solving the numerical equations for the unknown parameters; and fifth, programming the finite difference solution derived from step four for machine computation of the unknown parameters.

Finite Difference Equations and Computational Scheme -

For the final equations of Chapter II, several computational

schemes were possible. As an example, Gordon and Spaulding (1974) recently referenced over 160 different numerical models for tidal rivers, estuaries, and coastal rivers. Because of the need to include non-linear terms and the desire to have a fast stable finite difference scheme, the formulations of Leendertse (1970) were chosen for the hyperbolic equations of flow and the ADI (Alternating Direction Implicit) technique of Peaceman and Rachford (1955) and Douglas and Gunn (1964) was chosen for the parabolic equations of transport.

The computational scheme requires a set of finite difference equations (consisting of one each of the continuity, momentum, and mass balance equations) for both the x and y directions. The first set of equations are written implicitly for the unknowns of δ , U, and S in the x direction for the first half of the forward time step (details of the time step will be explained shortly), while δ , V, and S (known from a previous time step) are written explicitly for the y direction in the same equations. For the second half of the forward time step, δ , V, and S for the y direction are written implicitly and δ , U, and S for the x direction are written explicitly. This results in a solution scheme which has better stability than a purely explicit set of equations and requires fewer simultaneous equations to solve

than a straight implicit formulation. This is important since the computational effort increases as the cube of the number of simultaneous equations.

A detailed description of how to solve the finite difference equations for U , V , δ , and S will be given in Chapter IV. However, some idea of the approach to be used in solving these equations after they are written in finite difference form will be necessary in order to write them in their proper format.

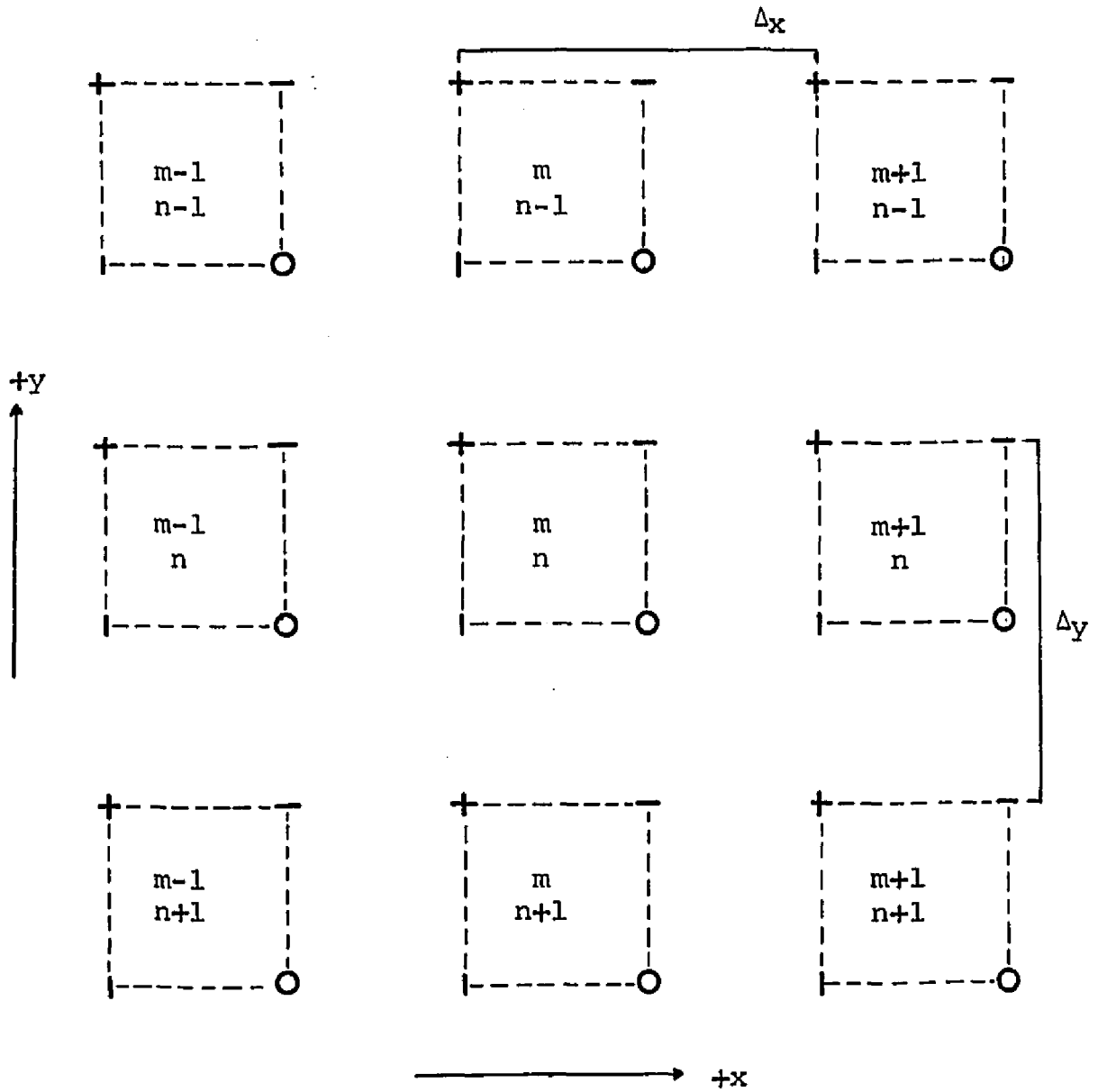
In brief, the solution technique will consist of first solving simultaneously for the unknowns of tidal height δ and velocity U for the x direction at the first half of the forward time step. This technique requires the simultaneous solution of the continuity and momentum equations whose value of δ and U when determined are then used to solve for S in the mass balance equations for the same time step. Next, δ and V are determined simultaneously in the y direction for the last half of the forward time step, and their values are used to calculate S for this half time step. This procedure eliminates the need of the solution of four simultaneous equations (for U , V , δ , and S) and makes computation easier.

Grid - The grid of points to be used in writing the equations is similar to that used by Leendertse (1967, 1970)

and is illustrated in Figure 3. Grid points for tidal height δ , density ρ , and salinity S are located at the $+$ points; while values for mean water depth h , velocity U and V are located at the points 0 , $-$, and $|$, respectively. All like points are separated by a distance Δx or Δy . The grid points are grouped into squares as shown in Figure 3, with a $+$, 0 , $-$, and $|$ forming the corner of each square.

The squares are numbered with integer values of m and n for the x and y directions. The values of m for the x direction increase from right to left, and the values of n increase from top to bottom. The grid is set up so that the predominantly southern flow of water in the area enters the grid at the top (i.e., northern edge) and leaves at the bottom and in the negative y direction. Formulation of the finite difference equations should present no difficulty because of this notation and can be handled by a sign reversal for the first order derivative terms of the y direction.

Stability - The stability of explicit numerical equations is a function of the grid size and time step, and expressions, such as the Courant-Friedrichs-Lewy criterion, are available to predict the maximum allowable time step for a specific grid size. For a multi-operational method as described above, no such formula exists. Leendertse (1970)



Legend

- $-$ grid points for velocity U in x direction
- $|$ grid points for velocity V in y direction
- O grid points for water depth, $-h$
- $+$ grid points for salinity S , density ρ , tidal height δ

Figure 3
Grid point arrangement

has taken a simplified approach in evaluating the stability and some of the factors affecting a multi-operational scheme. He used a linear analysis on a one-dimensional transport equation to study the effects of grid size and time step. He found that, for a time centered multi-operational method, the dispersion of the solution will be independent of the grid size if a sufficient representation of the concentration field is present.

In the discussion to come, the Courant-Friedrichs-Lewy criterion will be quoted to give an indication of how the time step chosen for the multi-operational technique compares with that of a pure explicit scheme.

Convention - For the equations to follow, the time step ΔT consists of two halves, one each for the x and y directions such that $\Delta T = 2\Delta t$. The time notations below will be used to conserve space in writing the numerical equations.

Time x direction, calculation of δ , U, and S

$$(2k-1)\Delta t = t = \text{past time}$$

$$2k\Delta t = 2t = \text{present time}$$

$$(2k+1)\Delta t = 3t = \text{future time}$$

Time y direction, calculation of δ , V, and S

$$2k\Delta t = 2t = \text{past time}$$

$$(2k+1)\Delta t = 3t = \text{present time}$$

$$(2k+2)\Delta t = 4t = \text{future time,}$$

where $k = 1, 2, \dots, k_{\max}$. The above notation t , $2t$, $3t$, and $4t$ will appear as a superscript of the variables.

The location of the variable in the grid will be given by subscripts m and n . Wind stress was assumed to be constant over the grid, although it could be made to vary, and no subscripts were used. Depth below mean sea level h was not allowed to vary with time; therefore, no time superscript will be used.

The finite difference equations are to be written so that they are centered in both space (centered differences tend to be more stable) and time. The centering in space (on the grid) is around the local derivative (time derivative) variable, i.e., either δ , U, V, or S of the equation being written.

Equation of Continuity

The finite difference form of the equation of continuity, upon applying the previously described operations and conditions for time $(2k+1)\Delta t$ (stepping in time from the present time $2k\Delta t$ to $(2k+1)\Delta t$), is

$$\begin{aligned}
& (\delta_{m,n}^{3t} - \delta_{m,n}^{2t}) \frac{1}{\Delta t} + [(h_{m,n} + h_{m,n-1} + \delta_{m+1,m}^{2t} + \delta_{m,n}^{2t}) U_{m,n}^{3t} - \\
& (h_{m-1,m} + h_{m-1,m-1} + \delta_{m-1,m}^{2t} + \delta_{m,n}^{2t}) U_{m-1,m}^{3t}] \frac{1}{2\Delta x} + \\
& [(h_{m,m-1} + h_{m-1,m-1} + \delta_{m,n}^{2t} + \delta_{m,m-1}^{2t}) V_{m,m-1}^{2t} - \\
& (h_{m,n} + h_{m-1,m} + \delta_{m,m+1}^{2t} + \delta_{m,n}^{2t}) V_{m,n}^{2t}] \frac{1}{2\Delta y} = 0.
\end{aligned}$$

3.1

Likewise, for time $(2k+2)\Delta t$, stepping from $(2k+1)\Delta t$ above to $(2k+2)\Delta t$, the equation of continuity is

$$\begin{aligned}
& (\delta_{m,n}^{4t} - \delta_{m,n}^{3t}) \frac{1}{\Delta t} + [(h_{m,n} + h_{m,n-1} + \delta_{m+1,m}^{3t} + \delta_{m,n}^{3t}) U_{m,n}^{3t} - \\
& (h_{m-1,m} + h_{m-1,m-1} + \delta_{m-1,m}^{3t} + \delta_{m,n}^{3t}) U_{m-1,m}^{3t}] \frac{1}{2\Delta x} + \\
& [(h_{m,m-1} + h_{m-1,m-1} + \delta_{m,n}^{3t} + \delta_{m,m-1}^{3t}) V_{m,m-1}^{4t} - \\
& (h_{m,n} + h_{m-1,m} + \delta_{m,m+1}^{3t} + \delta_{m,n}^{3t}) V_{m,n}^{4t}] \frac{1}{2\Delta y} = 0.
\end{aligned}$$

3.2

Momentum Equations

Using the same techniques for the momentum equation in the x direction yields

$$\begin{aligned}
& (U_{m,m}^{3t} - U_{m,m}^t) \frac{1}{2\Delta t} + (U_{m+1,n}^t - U_{m-1,n}^t) (U_{m,m}^{3t}) \left(\frac{1}{2\Delta x} \right) + \\
& (U_{m,m-1}^t - U_{m,m+1}^t) (V_{m+1,n}^{2t} + V_{m+1,n-1}^{2t} + V_{m,m-1}^{2t} + V_{m,m}^{2t}) \left(\frac{1}{8\Delta y} \right) + \\
& (\delta_{m+1,m}^{3t} - \delta_{m,m}^{3t} + \delta_{m+1,n}^t + \delta_{m,m}^t) \left(\frac{g}{2\Delta x} \right) + (\bar{P}_{m+1,n}^{2t} - \bar{P}_{m,n}^{2t}) (h_{m,m} + \\
& h_{m,m-1} + \delta_{m+1,n}^{2t} + \delta_{m,m}^{2t}) \left(\frac{g}{2\Delta x} \right) \left(1 / (\bar{P}_{m+1,n}^{2t} + \bar{P}_{m,n}^{2t}) \right) - \\
& (f/4) (V_{m+1,n}^{2t} + V_{m+1,n-1}^{2t} + V_{m,m-1}^{2t} + V_{m,m}^{2t}) + \\
& \frac{(g) (U_{m,m}^{3t} + U_{m,m}^t) \left[(U_{m,m}^t)^2 + (1/16) (V_{m+1,n}^{2t} + V_{m+1,n-1}^{2t} + V_{m,m-1}^{2t} + V_{m,m}^{2t})^2 \right]^{1/2}}{(h_{m,m} + h_{m,m-1} + \delta_{m+1,n}^{2t} + \delta_{m,m}^{2t}) \left[(C_{m+1,n}^{2t} + C_{m,n}^{2t}) / 2 \right]^2} - \\
& (4\gamma^5 / (\bar{P}_{m+1,n}^{2t} + \bar{P}_{m,n}^{2t}) (h_{m,m} + h_{m,m-1} + \delta_{m+1,n}^{2t} + \delta_{m,m}^{2t})) - \\
& (2 / (h_{m,m} + h_{m,m-1} + \delta_{m,m}^{2t} + \delta_{m+1,n}^{2t})) \left[\left((h_{m+1,n} + h_{m,m-1} + h_{m,m} + h_{m+1,n}) / 4 \right) + \right. \\
& \left. \delta_{m+1,n}^{2t} \right]^2 \alpha (U_{m,m}^t + U_{m+1,n}^t) (U_{m+1,n}^t - U_{m,m}^t) - \left((h_{m,m} + h_{m,m-1} + h_{m-1,m-1} + \right. \\
& \left. h_{m-1,n}) / 4 \right) + \delta_{m,m}^{2t} \left. \alpha (U_{m,m}^t + U_{m-1,n}^t) (U_{m,m}^t - U_{m-1,n}^t) \right] \frac{1}{2(\Delta x)^2} - \\
& (2 / (h_{m,m} + h_{m,m-1} + \delta_{m,m}^{2t} + \delta_{m+1,n-1}^{2t})) \left[\left((\delta_{m,m-1}^{2t} + \delta_{m+1,n}^{2t} + \delta_{m,m}^{2t} + \delta_{m+1,n-1}^{2t}) / 4 \right) + \right. \\
& \left. h_{m,m-1} \right]^2 \alpha (V_{m,m-1}^{2t} + V_{m+1,n-1}^{2t}) (U_{m,m-1}^t - U_{m,m}^t) - \left((\delta_{m,m}^{2t} + \delta_{m+1,n}^{2t} + \delta_{m,m+1}^{2t} + \right. \\
& \left. \delta_{m+1,n+1}^{2t}) / 4 \right) + h_{m,m} \left. \alpha (V_{m,m}^{2t} + V_{m+1,n}^{2t}) (U_{m,m}^t - U_{m,m+1}^t) \right] \frac{1}{2(\Delta y)^2} = 0.
\end{aligned}$$

The resultant equation in the y direction is

$$\begin{aligned}
 & (V_{m,n}^{4t} - V_{m,n}^{2t}) \frac{1}{2\Delta t} + (U_{m,n}^{3t} + U_{m-1,n+1}^{3t} + U_{m,n+1}^{3t} + U_{m-1,n}^{3t}) (V_{m+1,n}^{2t} - \\
 & V_{m-1,n}^{2t}) \left(\frac{1}{8\Delta x} \right) + (V_{m,n}^{4t}) (V_{m,m-1}^{2t} - V_{m,n+1}^{2t}) \left(\frac{1}{2\Delta y} \right) + \\
 & (\delta_{m,n}^{4t} - \delta_{m,n+1}^{4t} + \delta_{m,n}^{2t} - \delta_{m,n+1}^{2t}) \left(\frac{g}{2\Delta y} \right) + (\bar{P}_{m,n}^{3t} - \bar{P}_{m,n+1}^{3t}) (h_{m,n} + \\
 & h_{m-1,n} + \delta_{m,n+1}^{3t} + \delta_{m,n}^{3t}) \left(\frac{g}{2\Delta y} \right) \left(1 / (\bar{P}_{m,n+1}^{3t} + \bar{P}_{m,n}^{3t}) \right) + \\
 & (f/4) (U_{m,n+1}^{3t} + U_{m,n}^{3t} + U_{m-1,n+1}^{3t} + U_{m-1,n}^{3t}) + \\
 & \frac{(g)(V_{m,n}^{4t} + V_{m,n}^{2t}) \left[(V_{m,n}^{2t})^2 + (1/16) (U_{m,n+1}^{3t} + U_{m,n}^{3t} + U_{m-1,n+1}^{3t} + U_{m-1,n}^{3t})^2 \right]^{1/2}}{(h_{m,n} + h_{m-1,n} + \delta_{m,n+1}^{3t} + \delta_{m,n}^{3t}) \left[(C_{m,n+1}^{3t} + C_{m,n}^{3t}) / 2 \right]^2} - \\
 & (4\gamma_s / (\bar{P}_{m,n+1}^{3t} + \bar{P}_{m,n}^{3t})) (h_{m,n} + h_{m-1,n} + \delta_{m,n+1}^{3t} + \delta_{m,n}^{3t}) - \\
 & (2 / (h_{m,n} + h_{m-1,n} + \delta_{m,n}^{3t} + \delta_{m,n+1}^{3t})) \left[(((\delta_{m,n}^{3t} + \delta_{m+1,n}^{3t} + \delta_{m,n+1}^{3t} + \delta_{m+1,n+1}^{3t}) / 4) + \right. \\
 & h_{m,n})^2 \alpha (U_{m,n}^{3t} + U_{m,n+1}^{3t}) (V_{m+1,n}^{2t} - V_{m,n}^{2t}) - (((\delta_{m,n}^{3t} + \delta_{m,n+1}^{3t} + \delta_{m-1,n+1}^{3t} + \\
 & \delta_{m-1,n}^{3t}) / 4) + h_{m-1,n})^2 \alpha (U_{m-1,n}^{3t} + U_{m-1,n+1}^{3t}) (V_{m,n}^{2t} - V_{m-1,n}^{2t}) \left. \right] \frac{1}{2(\Delta x)^2} - \\
 & (2 / (h_{m,n} + h_{m-1,n} + \delta_{m,n}^{3t} + \delta_{m,n+1}^{3t})) \left[(((h_{m,n} + h_{m-1,n} + h_{m-1,n-1} + h_{m,n-1}) / 4) + \right. \\
 & \delta_{m,n}^{3t})^2 \alpha (V_{m,n-1}^{2t} + V_{m,n}^{2t}) (V_{m,n-1}^{2t} - V_{m,n}^{2t}) - (((h_{m-1,n} + h_{m,n} + h_{m-1,n+1} + \\
 & h_{m,n+1}) / 4) + \delta_{m,n+1}^{3t})^2 \alpha (V_{m,n}^{2t} + V_{m,n+1}^{2t}) (V_{m,n}^{2t} - V_{m,n+1}^{2t}) \left. \right] \frac{1}{2(\Delta y)^2} = 0.
 \end{aligned}$$

Mass Balance Equation

Remembering that U and δ for the x direction at time $(2k+1)\Delta t$ are known before S is calculated, the following results for the mass balance equation in the x direction

are derived

$$\begin{aligned}
 & \left[\delta_{m,n}^{3t} \left((h_{m,n} + h_{m,n-1} + h_{m-1,n-1} + h_{m-1,n}) / 4 \right) + \delta_{m,n}^{3t} \right] - \\
 & \left[\delta_{m,n}^{2t} \left((h_{m,n} + h_{m,n-1} + h_{m-1,n-1} + h_{m-1,n}) / 4 \right) + \delta_{m,n}^{2t} \right] \frac{1}{\Delta t} + \\
 & \left[(h_{m,n} + h_{m,n-1} + \delta_{m+1,n}^{2t} + \delta_{m,n}^{2t}) U_{m,n}^{3t} (\delta_{m+1,n}^{3t} + \delta_{m,n}^{3t}) - \right. \\
 & \left. (h_{m-1,n} + h_{m-1,n-1} + \delta_{m-1,n}^{2t} + \delta_{m,n}^{2t}) U_{m-1,n}^{3t} (\delta_{m,n}^{3t} + \delta_{m-1,n}^{3t}) \right] \frac{1}{4\Delta x} + \\
 & \left[(h_{m,n-1} + h_{m-1,n-1} + \delta_{m,n}^{2t} + \delta_{m,n-1}^{2t}) V_{m,n-1}^{2t} (\delta_{m,n}^{2t} + \delta_{m,n-1}^{2t}) - \right. \\
 & \left. (h_{m,n} + h_{m-1,n} + \delta_{m,n}^{2t} + \delta_{m,n+1}^{2t}) V_{m,n}^{2t} (\delta_{m,n+1}^{2t} + \delta_{m,n}^{2t}) \right] \frac{1}{4\Delta y} - \\
 & \left[(h_{m,n} + h_{m,n-1} + \delta_{m+1,n}^{3t} + \delta_{m,n}^{3t}) D_{x,m,n}^{3t} (\delta_{m+1,n}^{3t} - \delta_{m,n}^{3t}) - \right. \\
 & \left. (h_{m-1,n} + h_{m-1,n-1} + \delta_{m-1,n}^{3t} + \delta_{m,n}^{3t}) D_{x,m-1,n}^{3t} (\delta_{m,n}^{3t} - \delta_{m-1,n}^{3t}) \right] \frac{1}{2(\Delta x)^2} - \\
 & \left[(h_{m-1,n-1} + h_{m,n-1} + \delta_{m,n}^{2t} + \delta_{m,n-1}^{2t}) D_{y,m,n-1}^{2t} (\delta_{m,n-1}^{2t} - \delta_{m,n}^{2t}) - \right. \\
 & \left. (h_{m,n} + h_{m-1,n} + \delta_{m,n+1}^{2t} + \delta_{m,n}^{2t}) D_{y,m,n}^{2t} (\delta_{m,n}^{2t} - \delta_{m,n+1}^{2t}) \right] \frac{1}{2(\Delta y)^2} = 0.
 \end{aligned}$$

3.5

Likewise, the mass balance equation in the y direction

becomes

$$\begin{aligned}
& \left[\delta_{m,n}^{4t} \left((h_{m,m} + h_{m,m-1} + h_{m-1,m-1} + h_{m-1,m}) / 4 \right) + \delta_{m,m}^{4t} \right] - \\
& \left[\delta_{m,n}^{3t} \left((h_{m,m} + h_{m,m-1} + h_{m-1,m-1} + h_{m-1,m}) / 4 \right) + \delta_{m,m}^{3t} \right] \frac{1}{\Delta t} + \\
& \left[(h_{m,m} + h_{m,m-1} + \delta_{m+1,m}^{3t} + \delta_{m,m}^{3t}) U_{m,m}^{3t} (\delta_{m+1,m}^{3t} + \delta_{m,m}^{3t}) - \right. \\
& \left. (h_{m-1,m} + h_{m-1,m-1} + \delta_{m-1,m}^{3t} + \delta_{m,m}^{3t}) U_{m-1,m}^{3t} (\delta_{m,m}^{3t} + \delta_{m-1,m}^{3t}) \right] \frac{1}{4\Delta x} + \\
& \left[(h_{m,m-1} + h_{m-1,m-1} + \delta_{m,m}^{3t} + \delta_{m,m-1}^{3t}) V_{m,m-1}^{4t} (\delta_{m,m}^{4t} + \delta_{m,m-1}^{4t}) - \right. \\
& \left. (h_{m,m} + h_{m-1,m} + \delta_{m,m}^{3t} + \delta_{m,m+1}^{3t}) V_{m,m}^{4t} (\delta_{m,m+1}^{4t} + \delta_{m,m}^{4t}) \right] \frac{1}{4\Delta y} - \\
& \left[(h_{m,m} + h_{m,m-1} + \delta_{m+1,m}^{3t} + \delta_{m,m}^{3t}) D_{x,m,n}^{3t} (\delta_{m+1,m}^{3t} - \delta_{m,m}^{3t}) - \right. \\
& \left. (h_{m-1,m} + h_{m-1,m-1} + \delta_{m,m}^{3t} + \delta_{m-1,m}^{3t}) D_{x,m-1,n}^{3t} (\delta_{m,m}^{3t} - \delta_{m-1,m}^{3t}) \right] \frac{1}{2(\Delta x)^2} - \\
& \left[(h_{m,m-1} + h_{m-1,m-1} + \delta_{m,m}^{4t} + \delta_{m,m-1}^{4t}) D_{y,m,n-1}^{4t} (\delta_{m,m-1}^{4t} - \delta_{m,m}^{4t}) - \right. \\
& \left. (h_{m,m} + h_{m-1,m} + \delta_{m,m+1}^{4t} + \delta_{m,m}^{4t}) D_{y,m,n}^{4t} (\delta_{m,m}^{4t} - \delta_{m,m+1}^{4t}) \right] \frac{1}{2(\Delta y)^2} = 0. \quad 3.6
\end{aligned}$$

CHAPTER IV

METHOD OF SOLUTION FOR THE UNKNOWNNS OF U, V, δ , AND S

Basic Concepts

Starting Values - Values of velocity, tidal height, and salinity must be specified at all computational points on the grid at time $t = 0$ (initial conditions). Thereafter, at the advanced time step the values of U, V, δ , and S need only be specified on the boundaries of the grid when needed to predict their values in the interior at the same time step. These boundary values can be specified on either an open or closed boundary and can be grouped as described below.

Boundaries - Closed boundaries are the easiest to work with from a computational standpoint because here velocities and mass fluxes become zero, requiring no field data, and the only dynamic variable, tidal height, can be easily measured with tide gauges or calculated from tables. Open boundaries present more serious difficulties in the sense that more detailed data, particularly if time-dependent models are used, are needed, requiring more complex numerical and computational techniques. Thus, it is desirable to

have all closed boundaries; but, for a coastal situation, this is impossible, and the physical layout sometimes requires as many as three open boundaries.

To show how boundaries are used in this thesis, Figure 4 was drawn to illustrate a simple coastal situation of an estuary or river emptying onto a continental shelf. The closed boundaries are drawn through points that include the depth data points (0) and always one of the velocity data points (1 or -).

The open boundary can be drawn through points representing either tidal height (+) or velocity (1 or -) so that one of these variables must be defined on the boundary in order to calculate tidal heights and velocities in the interior of the grid (boundary value problem). If salinity is being calculated, it must be defined on all four boundaries (+) in order to calculate values in the interior of the grid at the advanced time step. If two open boundaries in the same direction exist, then a combination of boundary conditions can be used, i.e., tidal height or velocity on both boundaries or a combination of each. For the situation in this thesis, two of the above combinations were tried: tidal height at both boundaries and tidal height and velocity, one on each boundary.

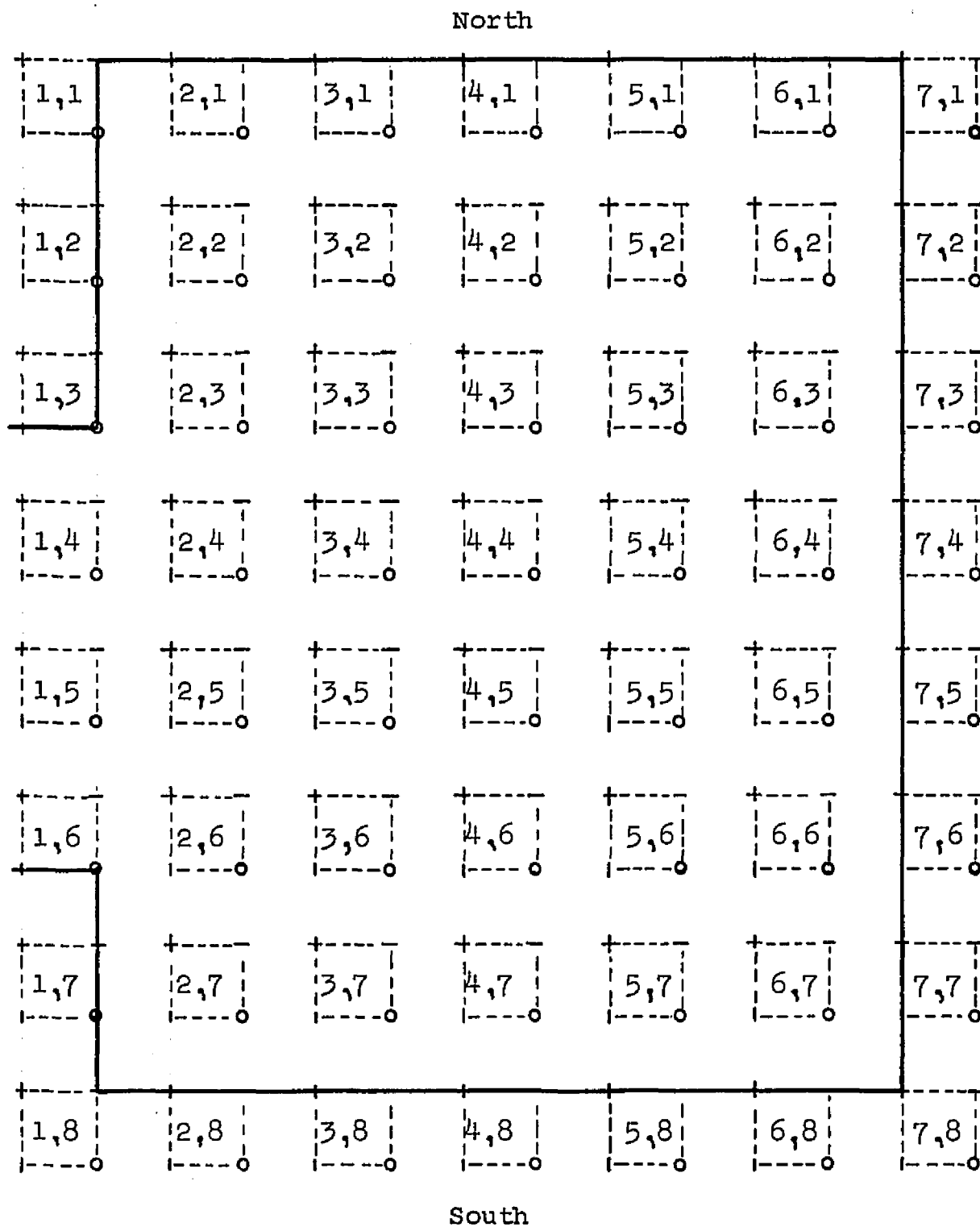


Figure 4

Illustration of
grid and boundary conditions

The reason for this choice was dictated by the availability of historical data for use with the model at a future date. The boundary condition chosen on the western side of the computational area was velocity since data were available from continuous current meter records at the Bay entrance and the realization that the investigation was to study the effect of fresh water runoff from the Bay. The boundary on the eastern side was chosen to be tidal height, since it was felt that this could be calculated accurately (Redfield (1958)). The northern boundary condition was chosen as either velocity, because of the availability of data and the weak southern flow, or tidal height. It was felt in the beginning that, if either of these boundaries were placed well above the Bay entrance, any error caused by the data would not affect the overall results and, more importantly, the boundary conditions would not be affected by the flux from the Bay mouth (this point will be discussed in the results). The southern boundary was chosen as tidal height because of the lack of good velocity data across the shelf in this region and the ease of estimating tidal height.

Upon the choice of the boundary conditions as stated above, the final finite difference equations must be solved so that the input of the boundary conditions will result

in their solution giving values of U, V, δ , and S.

Recursion Equations

Grouping of Terms - The first step in solving for the unknown values of U, V, δ , and S in equations 3.1 through 3.6 is to group the resultant equation around the unknown values of δ , U, V, and S. In order to simplify the results of this step, the following shorthand notations common to all equations will be used:

$$\bar{h} = (h_{m,m} + h_{m,m-1} + h_{m-1,m-1} + h_{m-1,m})/4$$

$$H_{XF}^{it} = h_{m,m} + h_{m,m-1} + \delta_{m+1,m}^{it} + \delta_{m,m}^{it}$$

$$H_{XB}^{it} = h_{m-1,m} + h_{m-1,m-1} + \delta_{m-1,m}^{it} + \delta_{m,m}^{it}$$

$$H_{YF}^{it} = h_{m,m-1} + h_{m-1,m-1} + \delta_{m,m}^{it} + \delta_{m,m-1}^{it}$$

$$H_{YB}^{it} = h_{m,m} + h_{m-1,m} + \delta_{m,m}^{it} + \delta_{m,m+1}^{it}$$

$$\bar{U}^{it} = (U_{m,m+1}^{it} + U_{m,m}^{it} + U_{m-1,m+1}^{it} + U_{m-1,m}^{it})/4$$

$$\bar{V}^{it} = (V_{m+1,m} + V_{m+1,m-1} + V_{m,m-1} + V_{m,m})/4,$$

where it is the general notation for the time t, 2t, 3t, or 4t.

Using the notation in the continuity equation for the x direction (equation 3.1) yields the simplified form

$$A_m \delta_{m,n}^{3t} + B_m U_{m,n}^{3t} + C_m U_{m-1,n}^{3t} = D_m. \quad 4.1$$

Since all unknowns are at the same time $3t$ and on the same row n , these notations can be dropped, giving

$$A_m \delta_m + B_m U_m + C_m U_{m-1} = D_m, \quad 4.2$$

where

$$A_m = 1/\Delta t$$

$$B_m = (1/2\Delta L) H_{XF}^{2t}$$

$$C_m = -(1/2\Delta L) H_{XB}^{2t}$$

and

$$D_m = -\left[(-\delta_{m,n}^{2t})\frac{1}{\Delta t} + \frac{1}{2\Delta L} (H_{YF}^{2t} V_{m,m-1}^{2t} - H_{YB}^{2t} V_{m,m}^{2t})\right]$$

are constants which can be calculated from known information. ΔL is a general notation denoting grid spacing Δx and Δy (for this study $\Delta x = \Delta y$).

Using the same procedure for the momentum equation 3.3 yields

$$E_m U_{m,n}^{3t} + F_m \delta_{m+1,n}^{3t} - F_m \delta_{m,n}^{3t} = H_m. \quad 4.3$$

Dropping the time and row notation as before, 4.3 becomes

$$E_m U_m + F_m \delta_{m+1} - F_m \delta_m = H_m \quad 4.4$$

where

$$E_m = \frac{1}{2\Delta t} + (U_{m+1,n}^{2t} - U_{m-1,n}^{2t})\frac{1}{2\Delta L} + \frac{g[(U_{m,n}^{2t})^2 + (\bar{V}^{2t})^2]^{1/2}}{H_{YF}^{2t} [(C_{m+1,n}^{2t} + C_{m,n}^{2t})/2]^2}$$

$$F_m = (g/2\Delta L)$$

and

$$\begin{aligned}
 H_m = & - \left\{ (-1/2\Delta t) U_{m,n}^t + (U_{m,n-1}^t - U_{m,n+1}^t) \bar{V}^{2t} (1/2\Delta L) + \right. \\
 & (\delta_{m+1,n}^t - \delta_{m,n}^t) (g/2\Delta L) + (\bar{P}_{m+1,n}^{2t} - \bar{P}_{m,n}^{2t}) \left(1/(\bar{P}_{m+1,n}^{2t} + \bar{P}_{m,n}^{2t}) \right) H_{XF}^{2t} (g/2\Delta L) - \\
 & f \bar{V}^{2t} + \frac{g U_{m,n}^t [(U_{m,n}^t)^2 + (\bar{V}^{2t})^2]^{1/2}}{H_{XF}^{2t} [(C_{m+1,n}^{2t} + C_{m,n}^{2t})/2]^2} - (4 \tau_y^s / (\bar{P}_{m+1,n}^{2t} + \bar{P}_{m,n}^{2t})) H_{XF}^{2t} - \\
 & (2/H_{XF}^{2t}) \left[\left((h_{m,n-1} + h_{m+1,n-1} + h_{m,n} + h_{m+1,n})/4 \right) + \delta_{m+1,n}^{2t} \right]^2 \\
 & \alpha (U_{m,n}^t + U_{m+1,n}^t) (U_{m+1,n}^t - U_{m,n}^t) - (\bar{h} + \delta_{m,n}^{2t})^2 \alpha (U_{m,n}^t + \\
 & U_{m-1,n}^t) (U_{m,n}^t - U_{m-1,n}^t) \left(1/2(\Delta L)^2 \right) - (2/H_{XF}^{2t}) \left[\left((\delta_{m,n-1}^{2t} + \delta_{m+1,n}^{2t} + \right. \right. \\
 & \left. \left. \delta_{m,n}^{2t} + \delta_{m+1,n-1}^{2t})/4 \right) + h_{m,n-1} \right]^2 \alpha (V_{m,n-1}^{2t} + V_{m+1,n-1}^{2t}) (U_{m,n-1}^t - \\
 & U_{m,n}^t) - \left((\delta_{m,n}^{2t} + \delta_{m+1,n}^{2t} + \delta_{m,n+1}^{2t} + \delta_{m+1,n+1}^{2t})/4 \right) + h_{m,n} \right]^2 \\
 & \left. \alpha (V_{m,n}^{2t} + V_{m+1,n}^{2t}) (U_{m,n}^t - U_{m+1,n}^t) \left(1/2(\Delta L)^2 \right) \right\}
 \end{aligned}$$

are constants which can be calculated from known information.

Likewise, for the mass balance equation 3.5, simplifying and grouping terms yields

$$A'_m S'_{m-1} + B'_m S'_m + C'_m S'_{m+1} = D'_m,$$

4.5

where

$$A'_m = -\left[(H_{xB}^{2t} U_{m-1,m}^{3t}) (1/4\Delta L) + (H_{xB}^{3t} D_{x,m-1,m}^{3t}) (1/2(\Delta L)^2) \right]$$

$$B'_m = (1/\Delta t) (\bar{h} + \delta_{m,m}^{3t}) + (H_{xF}^{2t} U_{m,m}^{3t} - H_{xB}^{2t} U_{m-1,m}^{3t}) (1/4\Delta L) +$$

$$(H_{xF}^{3t} D_{x,m,m}^{3t} + H_{xB}^{3t} D_{x,m-1,m}^{3t}) (1/2(\Delta L)^2)$$

$$C'_m = (H_{xF}^{2t} U_{m,m}^{3t}) (1/4\Delta L) - (H_{xF}^{3t} D_{x,m,m}^{3t}) (1/2(\Delta L)^2)$$

and

$$D'_m = -\left\{ -(\bar{h} + \delta_{m,m}^{2t}) S_{m,m}^{12t} (1/\Delta t) + [H_{yF}^{2t} V_{m,m-1}^{2t} (S_{m,m-1}^{12t} + S_{m,m}^{12t}) - \right.$$

$$H_{yB}^{2t} V_{m,m}^{2t} (S_{m,m}^{12t} + S_{m,m+1}^{12t})] (1/4\Delta L) - [H_{yF}^{2t} D_{y,m-1}^{2t} (S_{m,m-1}^{12t} - S_{m,m}^{12t}) -$$

$$H_{yB}^{2t} D_{y,m}^{2t} (S_{m,m}^{12t} - S_{m,m+1}^{12t})] (1/2(\Delta L)^2) \left. \right\}$$

are also constants which can be calculated.

Duplicating the same procedure for the y direction gives for the continuity equation

$$A_m V_m + B_m V_{m-1} + C_m V_{m+1} = D_m,$$

4.6

where

$$A_m = A_m = (1/\Delta t)$$

$$B_m = (1/2\Delta L) H_{yF}^{3t}$$

$$C_m = -(1/2\Delta L) H_{yB}^{3t}$$

and

$$D_m = - \left\{ (1/\Delta t) (\delta_{m,m}^{3t}) + (1/2\Delta L) (H_{yF}^{3t} U_{m,m}^{3t} - H_{yB}^{3t} U_{m-1,m}^{3t}) \right\}$$

are constants as for the y direction. The momentum equation 3.4 becomes

$$E_m V_m + F_m \delta_m - F_m \delta_{m+1} = H_m, \quad 4.7$$

where

$$E_m = (1/2\Delta t) + (V_{m,m-1} - V_{m,m+1}) (1/2\Delta L) + \frac{g [(V_{m,m}^{2t})^2 + (U^{3t})^2]^{1/2}}{H_{yB}^{3t} [(C_{m,m+1}^{3t} + C_{m,m}^{3t})/2]^2}$$

$$F_m = F_m = (g/2\Delta L)$$

and

$$\begin{aligned}
H_m = & - \left\{ (1/2\Delta t)(-V_{m,n}^{2t}) + (\bar{U}^{3t})(V_{m+1,m}^{2t} - V_{m-1,m}^{2t})(1/2\Delta L) + \right. \\
& (\delta_{m,n}^{2t} - \delta_{m,n+1}^{2t})(g/2\Delta L) + (\bar{P}_{m,n}^{3t} - \bar{P}_{m,n+1}^{3t}) \left(1/(\bar{P}_{m,n+1}^{3t} + \bar{P}_{m,n}^{3t}) \right) H_{yF}^{3t} (g/2\Delta L) + \\
& f(\bar{U}^{3t}) + \frac{g V_{m,n}^{2t} [(V_{m,n}^{2t})^2 + (\bar{U}^{3t})^2]^{1/2}}{H_{yB}^{3t} [(C_{m,n+1}^{3t} + C_{m,n}^{3t})/2]^2} - (4 \gamma_y^S / (\bar{P}_{m,n+1}^{3t} + \bar{P}_{m,n}^{3t}) H_{yB}^{3t}) - \\
& (2/H_{yB}^{3t}) \left[\left((\delta_{m,n}^{3t} + \delta_{m+1,m}^{3t} + \delta_{m,n+1}^{3t} + \delta_{m+1,m+1}^{3t})/4 \right) + h_{m,m} \right]^2 \alpha (U_{m,n}^{3t} + \\
& U_{m,n+1}^{3t}) \left(V_{m+1,m}^{2t} - V_{m,n}^{2t} \right) - \left((\delta_{m,n}^{3t} + \delta_{m,n+1}^{3t} + \delta_{m-1,n+1}^{3t} + \delta_{m-1,m}^{3t})/4 \right) + \\
& h_{m-1,m} \right]^2 \alpha (U_{m-1,n}^{3t} + U_{m-1,n+1}^{3t}) \left(V_{m,n}^{2t} - V_{m-1,m}^{2t} \right) \left(1/2(\Delta L)^2 \right) - (2/H_{yB}^{3t}) \left[(\bar{h} + \right. \\
& \delta_{m,n}^{3t})^2 \alpha (V_{m,n-1}^{2t} + V_{m,n}^{2t}) \left(V_{m,n-1}^{2t} - V_{m,n}^{2t} \right) - \left((\bar{h}_{m-1,m} + h_{m,n} + h_{m-1,n+1} + \right. \\
& \left. \left. h_{m,n+1} \right)/4 \right) + \delta_{m,n+1}^{3t} \right]^2 \alpha (V_{m,n}^{2t} + V_{m,n+1}^{2t}) \left(V_{m,n}^{2t} - V_{m,n+1}^{2t} \right) \left(1/2(\Delta L)^2 \right) \left. \right\}
\end{aligned}$$

are constants as for the y direction.

Finally, the mass balance equation for the y direction yields

$$A'_m \delta_{n-1} + B'_m \delta_n + C'_m \delta_{n+1} = D'_m, \quad 4.8$$

where

$$A'_m = (H_{yF}^{3t} V_{m,m-1}^{4t}) \left(1/4\Delta L \right) - (H_{yF}^{4t} D_{y,m-1}^{4t}) \left(1/2(\Delta L)^2 \right)$$

$$B'_m = (1/\Delta t)(\bar{h} + \delta_{m,m}^{4t}) + (H_{YF}^{3t} V_{m,m-1}^{4t} - H_{YB}^{3t} V_{m,m}^{4t})(1/4\Delta L) + \\ (H_{YF}^{4t} D_{Y,m,m-1}^{4t} - H_{YB}^{4t} D_{Y,m,m}^{4t})(1/2(\Delta L)^2)$$

$$C'_m = -(H_{YB}^{3t} V_{m,m}^{4t})(1/4\Delta L) - (H_{YB}^{4t} D_{Y,m,m}^{4t})(1/2(\Delta L)^2)$$

and

$$D'_m = - \left\{ -(\bar{h} + \delta_{m,m}^{3t})(1/\Delta t) + [H_{XF}^{3t} U_{m,m}^{3t} (\sum_{m+1,m}^{3t} + \sum_{m,m}^{3t}) - \\ H_{XB}^{3t} U_{m-1,m}^{3t} (\sum_{m,m}^{3t} + \sum_{m-1,m}^{3t})] (1/4\Delta L) - [H_{XF}^{3t} D_{X,m,m}^{3t} (\sum_{m+1,m}^{3t} - \\ \sum_{m,m}^{3t}) - H_{XB}^{3t} D_{X,m-1,m}^{3t} (\sum_{m,m}^{3t} - \sum_{m-1,m}^{3t})] (1/2(\Delta L)^2) \right\}$$

are constants as for the y direction.

Solution - The solution of the recursion equations 4.2, 4.4, and 4.5 through 4.8 is accomplished in the following manner: Starting with the continuity and momentum equations in the x direction (4.2 and 4.4), it can be seen that a total of four unknowns exist between these two equations, requiring two boundary conditions in order to be able to solve this set (A_m , B_m , C_m , D_m , E_m , F_m , and H_m are constants which can be calculated from known information). Recalling the previous discussion on boundary conditions, solutions of these equations are derived assuming a solution of the form

$$\delta_m + P_m U_m = Q_m \quad 4.9$$

and

$$U_m + R_m \delta_{m+1} = T_m, \quad 4.10$$

where P_m , Q_m , R_m , and T_m are constants to be defined.

Backstepping on 4.10 gives

$$U_{m-1} + R_{m-1} \delta_m = T_{m-1}$$

or

$$U_{m-1} = T_{m-1} - R_{m-1} \delta_m. \quad 4.11$$

Substitution of 4.11 into 4.2 and grouping terms to come up with an equation like 4.9 gives the constants

$$P_m = \frac{B_m}{A_m - C_m R_{m-1}} \quad 4.12$$

and

$$Q_m = \frac{D_m - C_m T_{m-1}}{A_m - C_m R_{m-1}}. \quad 4.13$$

Rearranging 4.9 and substituting into 4.4 for δ_m and grouping terms to acquire an equation like 4.10 gives the constants

$$R_m = \frac{F_m}{E_m + P_m F_m} \quad 4.14$$

and

$$T_m = \frac{H_m + F_m Q_m}{E_m + P_m F_m}. \quad 4.15$$

Equations 4.12 through 4.15 are the four constants that are needed for use with 4.9 and 4.10 to calculate δ and U . To

use these new constants at point m , values of the constants at the previous point $m-1$ are needed (4.12 and 4.13). Thus, some starting values are necessary before these equations can be used. If 4.2 is arranged in the form of 4.9, then the constants, for $m = 2$ only, are

$$P_m = \frac{B_m}{A_m} \quad 4.16$$

and

$$Q_m = \frac{D_m - C_m U_{m-1}}{A_m}. \quad 4.17$$

Since the boundary conditions are specified with velocity U (Figure 4) given for all time, 4.16 and 4.17 may be used to calculate P_2 and Q_2 .

The procedure to calculate U and δ is as follows:

Using the boundary conditions given at $m = 1$ for the velocity, Q_2 is calculated by 4.17 and P_2 by 4.16. Proceeding across the row (for the first half time step), the rest of the constants are calculated by 4.12 through 4.15. At $m = m_{\max} - 1$ calculations are terminated for the constants. The boundary conditions at the end of the row (δ in our case here) are used along with the constants at $m = m_{\max} - 1$ and 4.10 to calculate U at $m = m_{\max} - 1$. This value of U is then substituted into 4.9 to calculate δ at $m = m_{\max} - 1$. This value of δ along with the constants at $m = m_{\max} - 2$ is used to calculate U at $m = m_{\max} - 2$, etc until U is calculated

at $m = 2$. Values of δ at $m = 1$ and U at $m = m_{\max}$ are then obtained by extrapolation, if needed, and all values for the row are completed and the next row is then ready to be calculated.

After U and δ have been calculated for all rows for time $(2k+1)\Delta t$, the value of S for all rows at the same time step must be calculated. Recalling the recursion equation 4.5, a solution of the type

$$S_m + E'_m S_{m+1} = F'_m \quad 4.18$$

is desired. Rearranging 4.5 in the form of 4.18 gives the constants (for $m = 2$ only)

$$E'_m = \frac{C'_m}{B'_m} \quad 4.19$$

and

$$F'_m = D'_m - \frac{A'_m S_{m-1}}{B'_m}, \quad 4.20$$

which are the starting values for E'_m and F'_m . Since S_1 is given as a boundary condition, backstepping one space in 4.18, substituting in 4.15 for S_{m-1} , and grouping terms to come up with an equation like 4.18 gives the constants

$$E'_m = \frac{C'_m}{B'_m - A'_m E'_{m-1}} \quad 4.21$$

and

$$F'_m = \frac{D'_{m+1} - A'_{m+1} F'_{m+1}}{B'_m - A'_m E'_{m-1}}. \quad 4.22$$

Since salinity is to be specified as a boundary condition on all four sides, the following procedure is used: Equations 4.19 and 4.20 are used for $m = 2$, using the values of salinity at $m = 1$ as a starting value. The results of this step are then used to start calculating the constants E'_m and F'_m (4.21 and 4.22) which are then calculated progressively until $m = m_{\max} - 1$ is reached. Then equation 4.18 is used along with these constants and boundary conditions to calculate the salinity in the reverse order as was done for δ and U .

The same procedure can be used to derive the recursion equations in the y direction (for either velocity or tidal height as a northern boundary condition), but it will not be repeated here. The results of the derivation of this type for V , δ and S are given below. The technique for calculation of V , δ and S with these equations is essentially the same as has been previously described.

Recursion equations for V and δ , y direction, are:

Starting equations for northern boundary

Velocity as a
Boundary Condition

$$P_2 = \frac{C_2}{A_2}$$

$$Q_2 = \frac{D_2 - B_2 V_1}{A_2}$$

Tidal Height as a
Boundary Condition

$$R_1 = - \frac{F_1}{E_1}$$

$$T_1 = \frac{H_1 - F_1 \delta_1}{E_1}$$

Constant equations

$$P_m = \frac{C_m}{A_m - B_m P_{m-1}}$$

$$Q_m = \frac{D_m - B_m T_{m-1}}{A_m - B_m P_{m-1}}$$

$$R_m = -\frac{F_m}{E_m - P_m F_m}$$

$$T_m = \frac{H_m - F_m Q_m}{E_m - P_m F_m}.$$

Recursion equations for S, y direction, are:

Starting equations

$$E'_2 = \frac{C'_2}{B'_2}$$

$$F'_2 = \frac{D'_2 - A'_2 S'_1}{B'_2}.$$

Constant equations

$$E'_{m+1} = \frac{C'_{m+1}}{B'_{m+1} - A'_{m+1} E'_m}$$

$$F'_{m+1} = \frac{D'_{m+1} - A'_{m+1} F'_m}{B'_{m+1} - A'_{m+1} E'_m}.$$

CHAPTER V

COMPUTER PROGRAM

General

The computer program for the computational scheme outlined in Chapter IV is called COASTAL MODEL and is written in Fortran IV for use on the Control Data Corporation (CDC) Model 6600 or 6700 computer. Both of CDC's scope 3.3 and 3.4 operating systems are compatible with the program. A core size of 75,000 octal is required, and a computation time of about 10 min is necessary for a 30 x 50 grid with 156 iterations covering two 12-hr tidal cycles. A table of equivalent notations between that used in the program and Chapters II through IV is given in Appendix B. Appendix C is a copy of the basic program which is not optimized and was used for Case I of the oscillating jet.

Main and Sub-programs

A general overall flow diagram of the program is given in Figure 5a with a more detailed illustration given in Figures 5b and 5c. It consists of a main driver program and five sub-programs. The main program handles input of

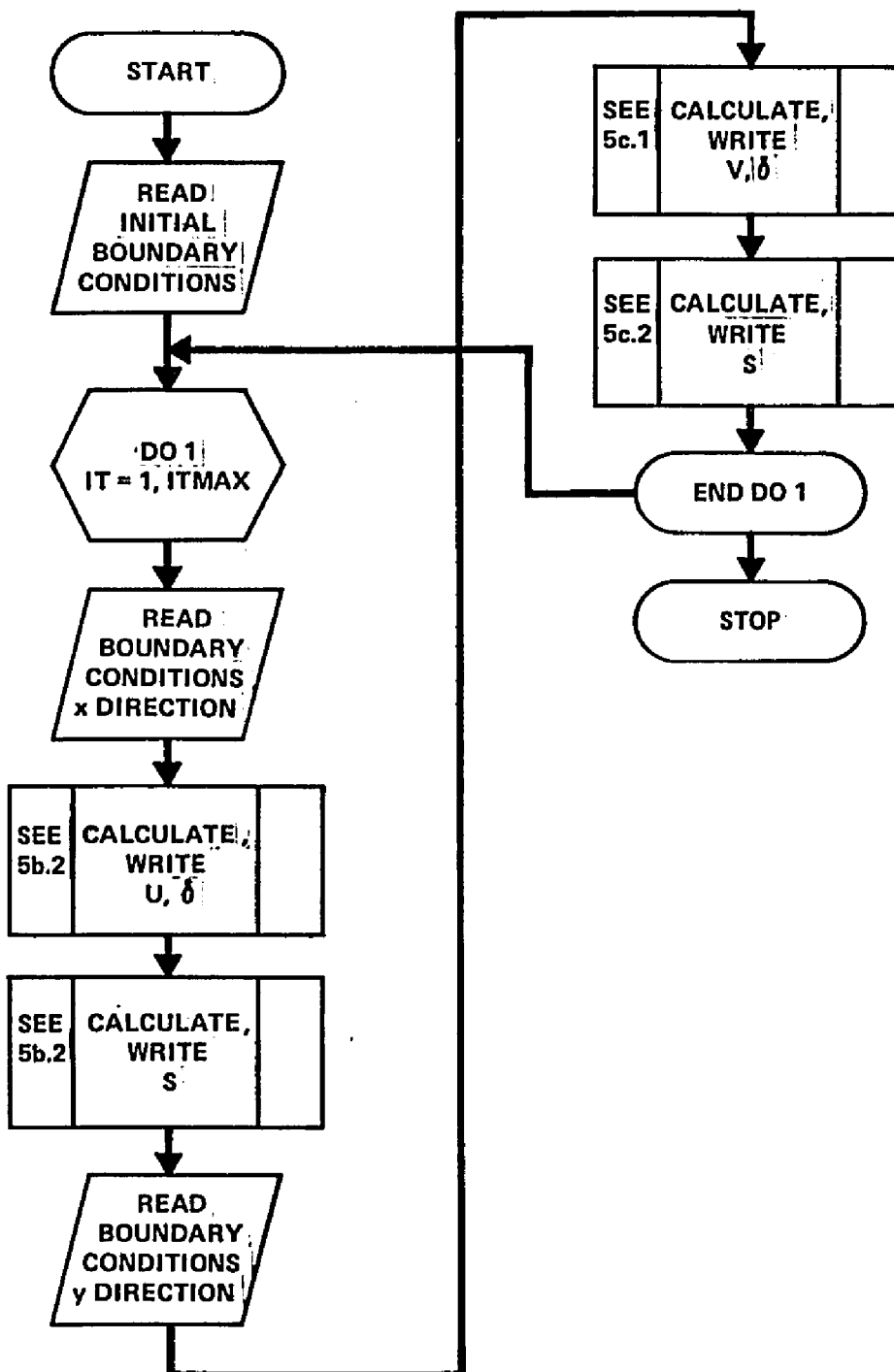
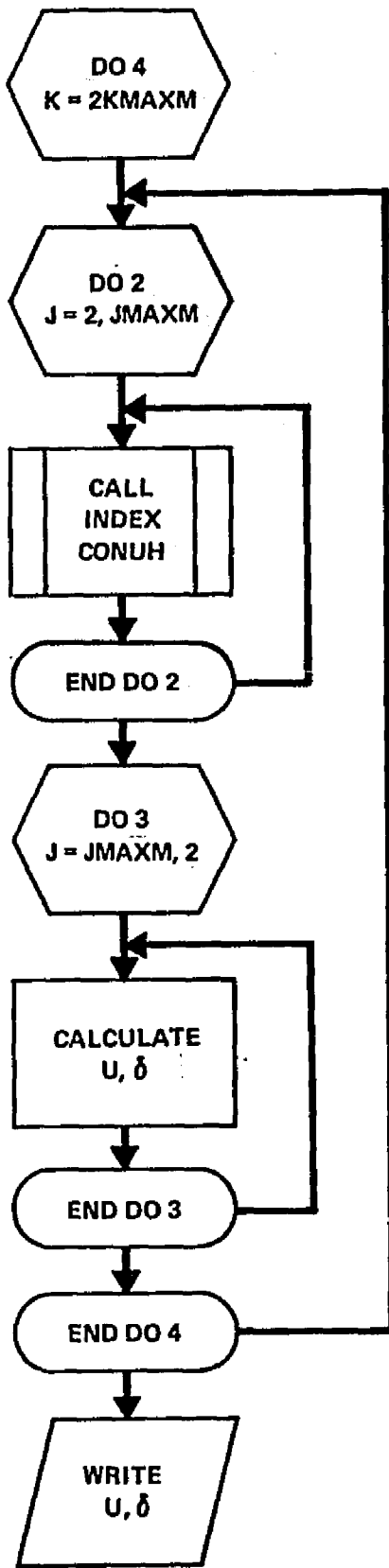
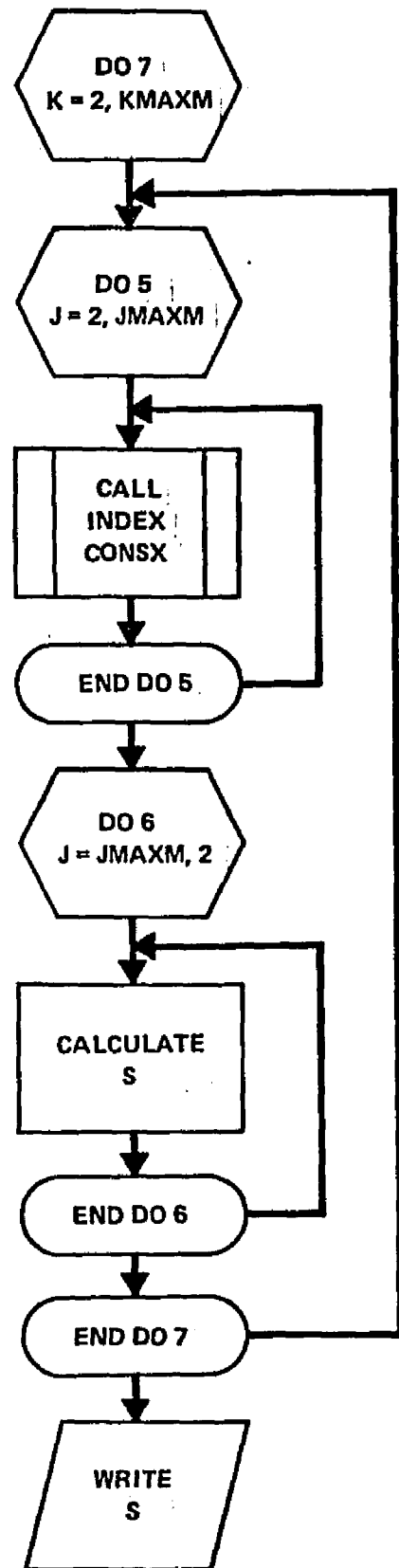


Figure 5a

Figure 5
Computer flow diagram for program COASTAL MODEL

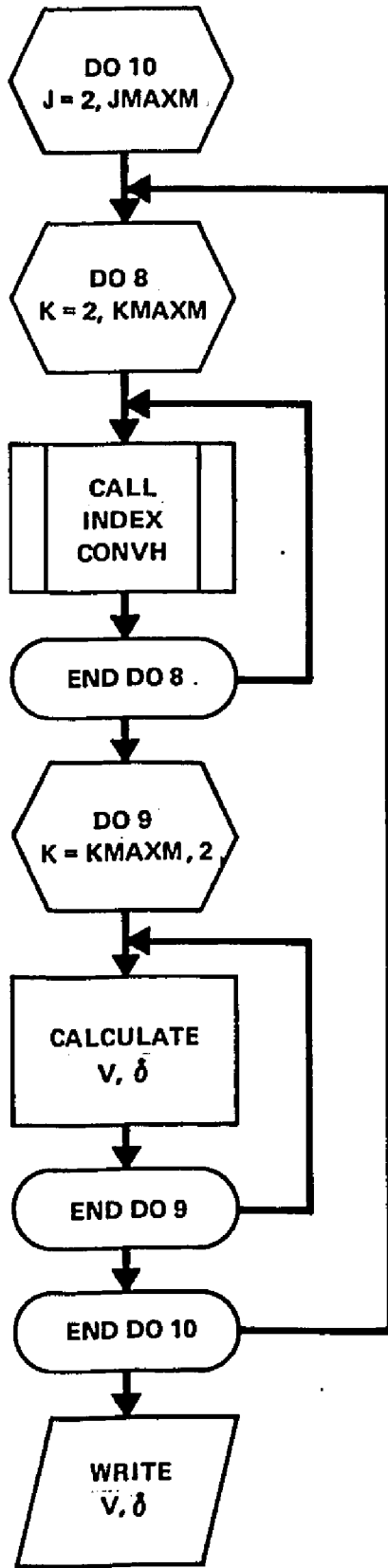


5b.1

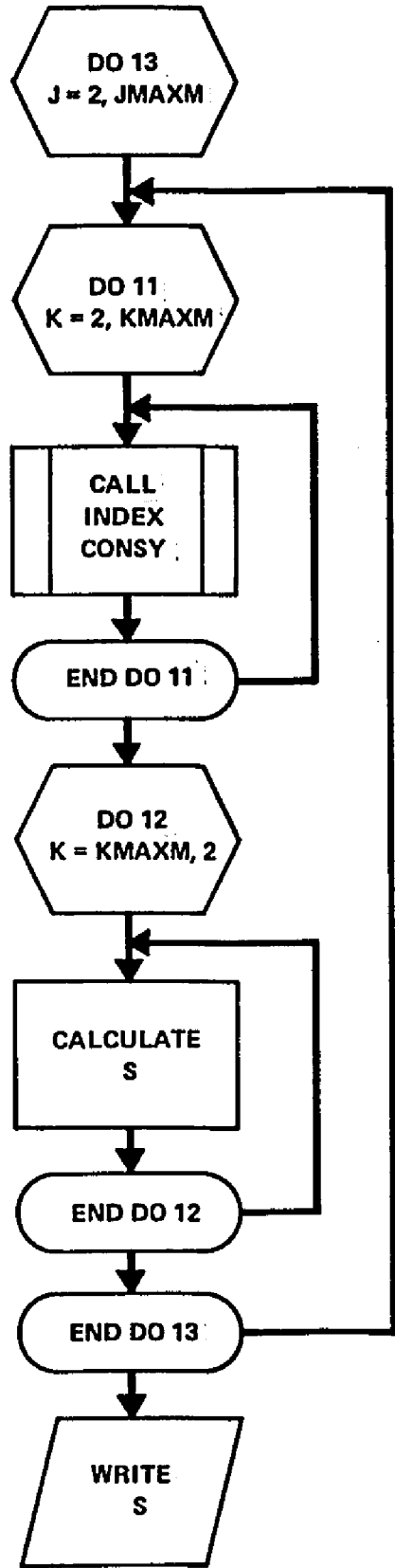


5b.2

Figure 5b



5c.1



5c.2

Figure 5c

initial and boundary conditions, print and write statements, and controls the calculations through the proper sequence.

The sub-programs and their functions are:

INDEX - calculates common parameters which are used repeatedly in the other sub-programs.

CONUH - calculates constants which are used to determine U and δ for the advanced time step from $2k\Delta t$ to $(2k+1)\Delta t$. Calculations are along x axis.

CONSX - calculates constants which are used to determine S for the advance time step from $2k\Delta t$ to $(2k+1)\Delta t$. Calculations are along x axis.

CONVH - calculates constants which are used to determine V and δ for the advanced time step from $(2k+1)\Delta t$ to $(2k+2)\Delta t$. Calculations are along y axis.

CONSY - calculates constants which are used to determine S for the advanced time step from $(2k+1)\Delta t$ to $(2k+2)\Delta t$. Calculations are along y axis.

Calculations were initiated by calling up the basic programs from disk, correcting, and compiling using CDC's optimum compiler. In executing the main program, data that were required but never changed, such as water depth h and gravitational acceleration g , were stored in the main program. Other information needed, such as grid spacing time step, wind stress, number of grid points in the x and y

directions, and number of iterations, was read in from cards. Before starting the calculations of U and δ , initial and boundary conditions were either read in or calculated from the program.

Next, the sub-routines for INDEX and CONUH were called and executed, calculating along and m or x axis (J in computer notation) from $m = 2$ to $m = m_{\max} - 1$. U and δ were then calculated, moving from $m = m_{\max} - 1$ to $m = 2$.

This procedure was used for each row from $n = 2$ to $n_{\max} - 1$. Finally, values of U and δ were extrapolated linearly where needed to fill in the grid. Linear extrapolation was used because it was more accurate and provided less fluctuation at the boundary. The same procedure was followed for S , where the previously determined values of U and δ were used to calculate the constants in CONSX.

Calculations of V , δ , and S were performed in the same manner as described above, except that the time step was at $(2k+2)\Delta t$ and the constants were calculated along each column from $n = 2$ to $n_{\max} - 1$ using CONVH or CONSY. V and δ were then calculated in decreasing order until $n = 2$. This was repeated for each column from $m = 2$ to $m = m_{\max} - 1$. The salinity calculation was then performed in the same manner as described above.

Plot

The data resulting from COASTAL MODEL were stored as a printed format and on magnetic tape. Since the velocity data were not a vector but components of a vector, a program was devised to read U, V, and δ from the magnetic tape, compute a current vector, plot the vector, and contour the tidal height data. This was done by a program called MODPLOT on the CDC 6600 or 6700 computer. MODPLOT read the tape data generated by COASTAL MODEL, called up the proper Calcomp sub-routines, performed the calculations, and put all information on a separate tape which was then run on a Calcomp 936 plotted to generate the displays desired. The program MODPLOT is not in Appendix C.

The vector part of MODPLOT did not plot all the data available, only those from $m = 1$ to 15 and $n = 15$ to 37, i.e., the area centered around the Bay mouth. The program read the data desired, plotted a coastline, and calculated the vector centered at the + point of the computation grid. The technique of calculation consisted of taking the U and V components on either side of the + point, averaging to get a U and V at this point, and then calculating a vector.

Next, the tidal heights desired were read from the magnetic tape, and an in-house developed algorithm was used to contour the data. All tidal data points for the grid were used in this program.

CHAPTER VI
RESULTS AND DISCUSSION

Basic Concepts

Three physical situations were studied. The first was a tidal or long period wave reflecting from a wall. This situation was used to verify the accuracy and completeness of the finite difference formulations previously described and to correct any program problems.

The steady-state jet was used as an intermediate step between the wave reflection from a wall and an oscillating jet. This case was run to better understand the computational stability problem, determine techniques to handle open boundary conditions, compute data which could be directly compared to the steady-state jet data in the literature, and determine if there would be anything unique about this case which corresponds to time averaged flow for a river or estuary emptying onto a continental shelf.

The final situation represented a tidal estuary discharging onto a continental shelf. An oscillating jet was used to drive the flow and simulate a tide rather than having a tidal wave progressing shoreward and reacting with

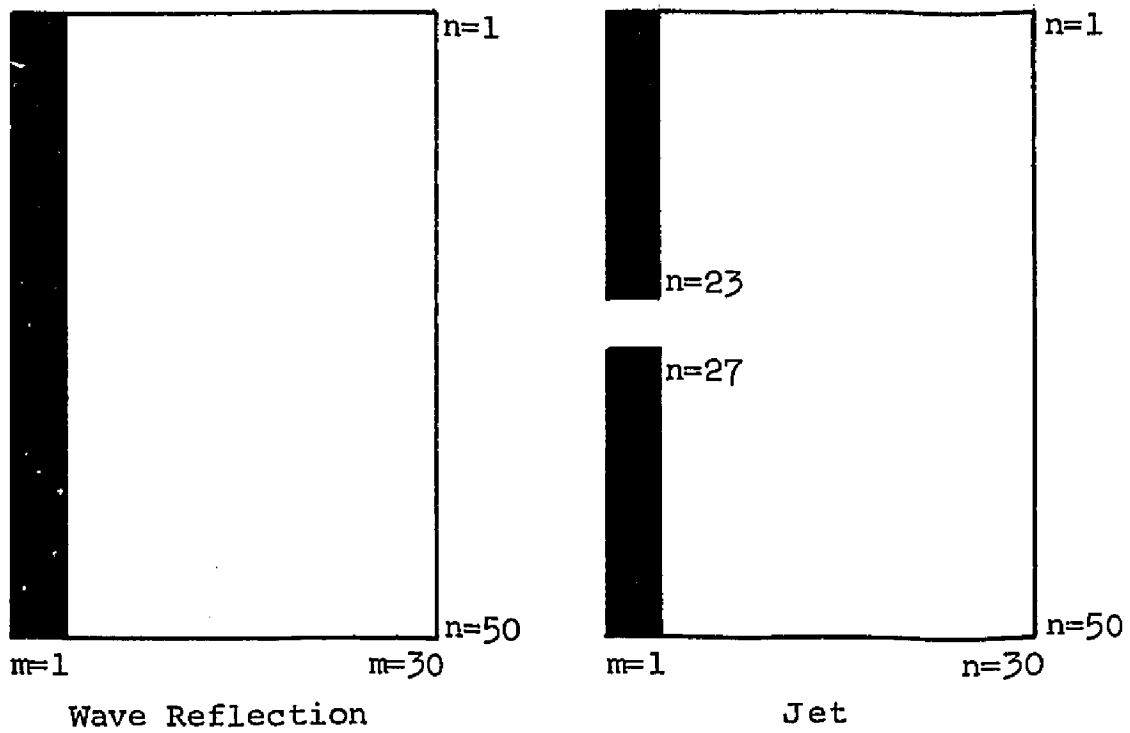
a steady jet. This allowed a simplification of boundary conditions by eliminating the need to try to determine the interrelationship between tidal and jet velocity at the Bay entrance.

The inputs and boundary conditions for each case are summarized in Table 1, and Figure 6 gives a physical picture of the computational domain and grid setup.

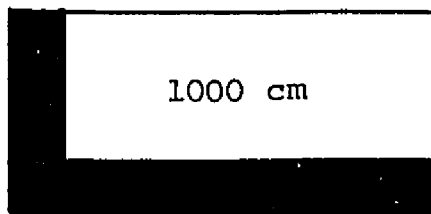
TABLE 1
EXPERIMENTAL PARAMETERS

	<u>Reflection</u>	<u>Steady- State Jet</u>	<u>Oscil- lating Jet</u>
Number of Grid Points			
x-direction	30	30	30
y-direction	50	50	50
Grid Spacing (ΔL), cm	179,640	359,280	359,280
Time Step (Δt), sec	150	300	300
Initial Conditions at t=0	U=0 V=0 $\delta=f(x)$	U=0 V=0 $\delta=0$	U=0 V=0 $\delta=f(y)$, or 0
Boundary Conditions for Grid			
Left Side	U=0, S=30.0	U=f(y)	U=f(t,y)
Right Side	$\delta=f(t)$, S=30.0	$\delta=0$	$\delta=0, f(y)$
Top	V=0, S=30.0	V=0, -4	$\delta=0, 5, 10$
Bottom	$\delta=f(x, t)$, S=30.0	$\delta=0$	$\delta=0$
Chézy Coefficient, $\text{cm}^{1/2} \text{sec}^{-1}$	0	400	400
Turbulent Eddy Viscosity Coefficient, $\text{cm}^2 \text{sec}^{-1}$ (horizontal)	0	10^8	0
Coriolis Parameter (f), sec^{-1}	0	8×10^{-5}	8×10^{-5}
Bottom Slope	0	0	1/1354
Wind Stress (τ), $\text{gm cm}^{-1} \text{sec}^{-2}$	0	0	0, 1.9
Depth, cm	1000	1000	f(x) 1000

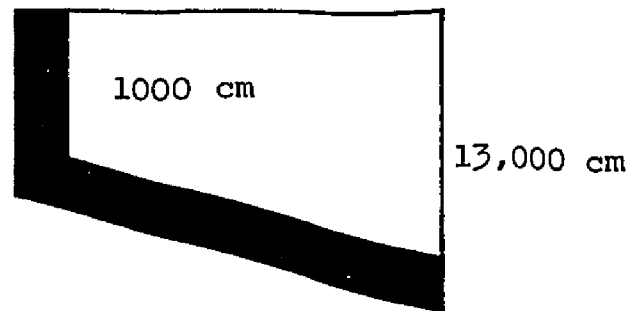
GRID OUTLINE



BOTTOM PROFILES



Wave Reflection and
Jet Cases



Oscillating Jet
Case III

Figure 6

Grid outline and bottom profiles

Wave Reflection from a Wall

For this case a 30 x 50 point grid (30 points in the x direction, 50 points in the y direction) with a spacing $\Delta x = \Delta y = 179,640$ cm (0.97 nm) and a time step $\Delta t = 150$ sec was chosen. Water depth was 1000 cm, and no bottom friction, side friction, force of Coriolis, or wind stress was used. Initial conditions for time $t = 0$ were $U = V = 0$ and $\delta = f(x)$ or $\delta = \text{constant}$. For the initial boundary condition δ , two cases were run: $\delta = 50$ cm (δ uniform over the grid) and $\delta = a_0 \cos kx$ (tidal height decreasing as a function of distance from the coast). Results from all cases were the same, the only difference being the time required for the solution to reach a steady state. Results from the case $\delta = a_0 \cos kx$ are discussed below. The wall was established on the left or western side of the grid, and the open sea constituted the northern, southern, and eastern boundaries, Figure 6. Boundary conditions for the x direction were velocity at the wall, $U = 0$, and tidal height in the open sea, $\delta = a_0 \cos \sigma t \cos kx$, where $k = 2\pi/L$, $\sigma = 2\pi/T$, $a_0 = \text{wave amplitude}$, and x is some fixed value. For the y direction velocity, $V = 0$ was used on the northern edge and tidal height, $\delta = a_0 \cos \sigma t \cos kx$, on the southern edge. Salinity values of 30‰ were used on all boundaries. The value of 0.97 nm for the grid spacing

was chosen so that the width of the Bay mouth (about 9.7 nm) would contain 10 grid points for the x velocity to be used later. A wave period of 12.42 hours (semi-diurnal tide) was used which gave a wave length of 4.4×10^7 cm for a depth of water of 1000 cm. The grid spacing was therefore adequate (Leendertse (1970)) to describe the wave and not generate stability problems. All runs were for a wave propagating in a direction normal to the wall.

Results of the computation are given in Figures 7, 8, and 9. Figure 7 is a plot of tidal height and velocity versus time for a point in the middle of the grid ($m = 15$, $n = 25$, Figure 6). Data from the calculations were plotted for only a half tidal cycle in order to amplify the results. The results of the computation are compared with the classical solution of a wave reflected from a wall (solid line, Figure 7) using equations from Ippen (1966) to calculate the data at the same point. It can be seen from this figure that there is good agreement between the theoretical and computed data.

Figure 8 is a plot of the theoretical and computed velocity profiles along the center of the computational grid (in an east-west direction, $n = 25$, $m = 1, 2, \dots, 30$) at maximum flood velocity. Agreement here is also good. Figure 9 is a plot of the theoretical and computed tidal

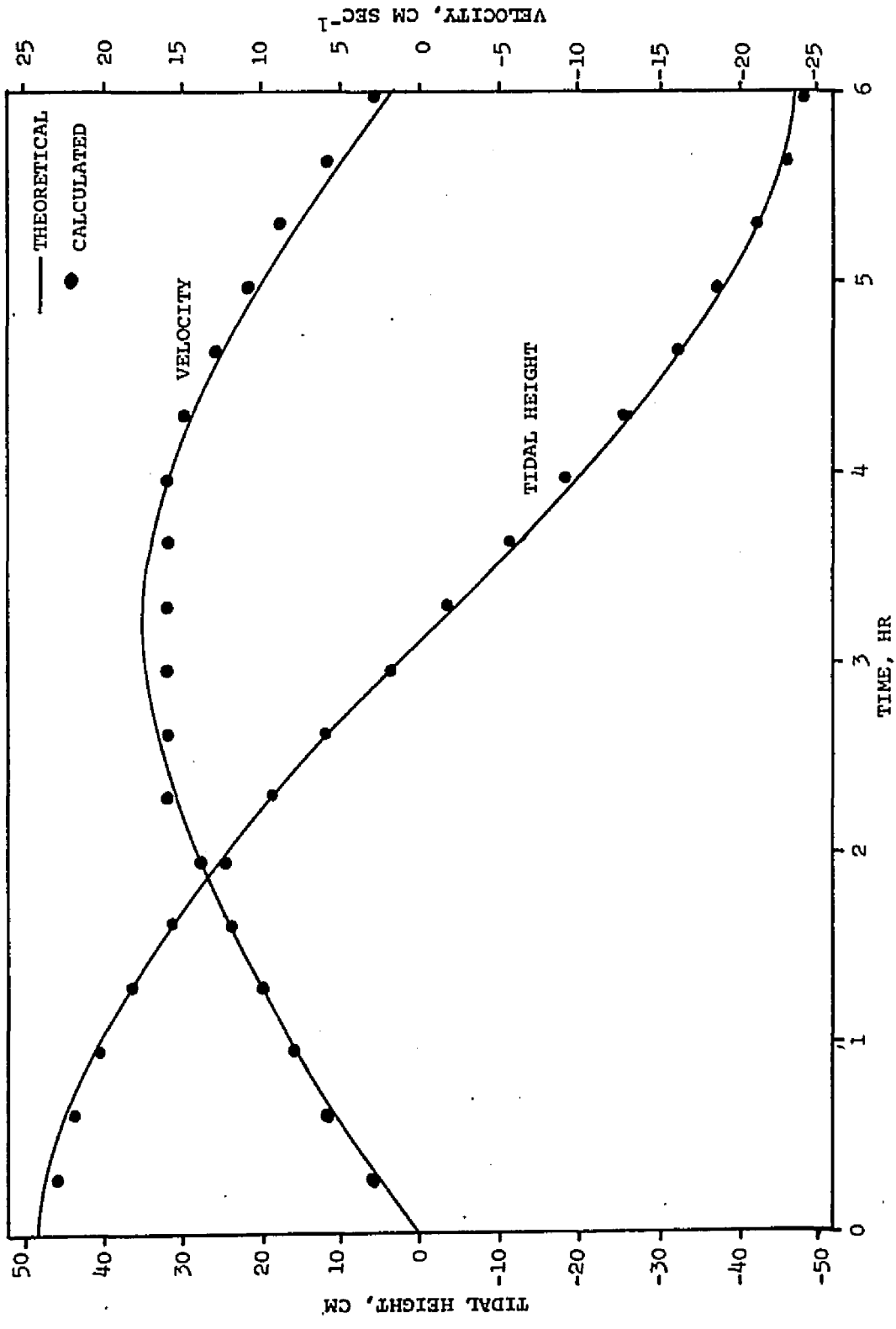


Figure 7
Tidal height as a function of time for grid point
($m = 15, n = 25$)

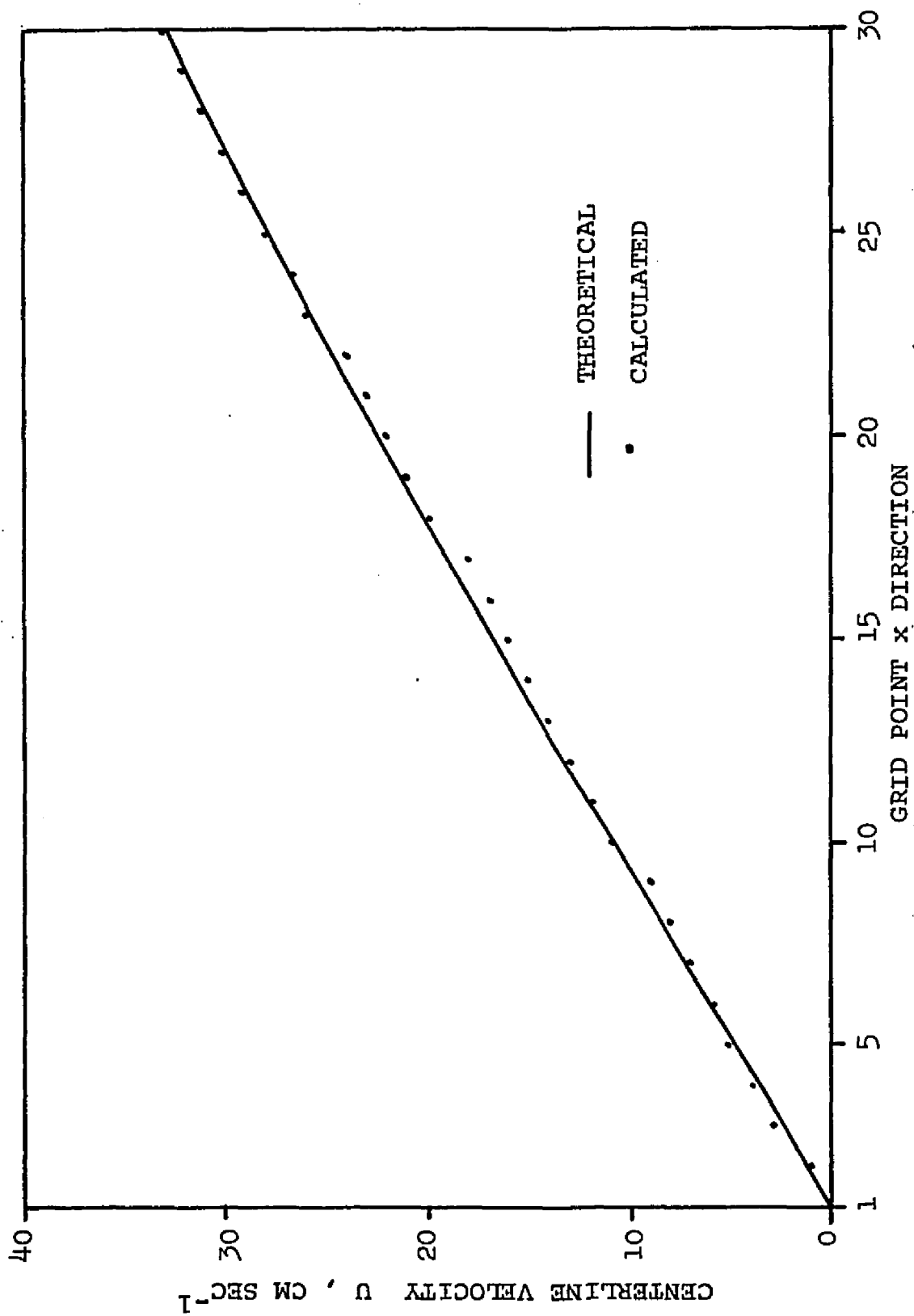


Figure 8 - Maximum theoretical and computed velocity as a function of distance in x direction, wave reflection

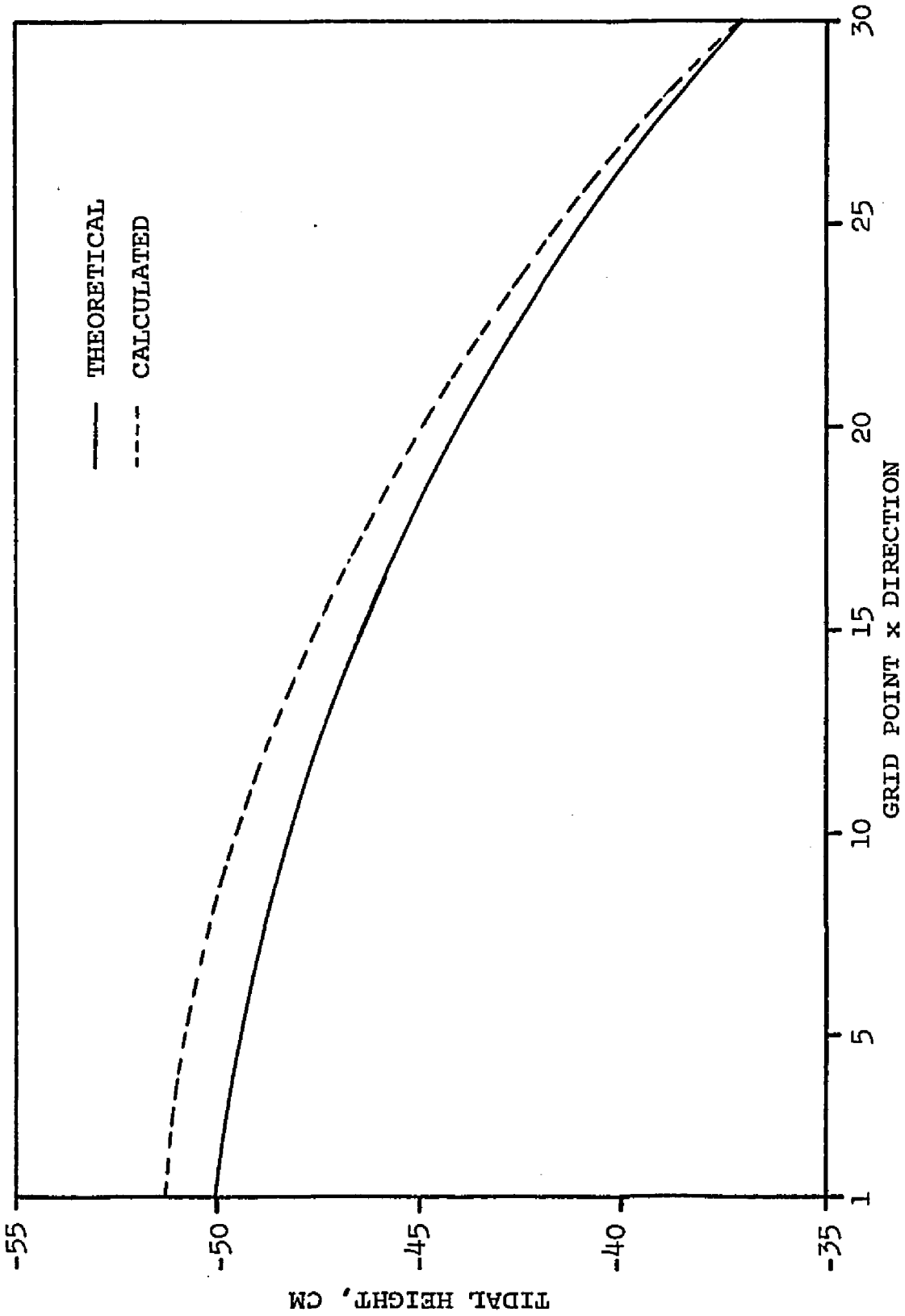


Figure 9 - Maximum theoretical and computed tidal height as a function of distance in x direction, wave reflection

height (below MSL) along the same centerline used in Figure 8. In Figure 9 there is a maximum difference of slightly more than 1 cm at the wall which decreases to 0 at the open eastern boundary.

Results from the salinity calculations were not plotted since the values remained constant at all times and at all points within the flow field.

For stability, the Courant-Friedricks-Lewy criteria for a two-dimensional explicit scheme $\Delta t = \Delta L / \sqrt{2gh}$ gives a value of 128.3 sec for a grid spacing of $\Delta L = 179,640$ cm. The solutions were found to be stable with a half time step of $\Delta t = 150$ sec used here.

Steady-State Jet

General - For this physical situation a 30 x 50 point grid was used as before, but the grid spacing was increased to $\Delta L = 359,280$ cm (approximately 2 nm). The Courant-Friedricks-Lewy criteria for this grid spacing gave $\Delta t = 256$ sec. A value of 300 sec for each half time step was chosen so that a total time step of $\Delta t = 600$ sec, or 10 min, covered a complete iteration. No stability problems arose with this particular time step and grid spacing. Salinity was not calculated since it was held constant over the grid for all cases. Holding the salinity constant generated a situation in which the density was homogeneous both vertically and horizontally. Water depth was 1000 cm, and no wind stress was assumed. Bottom friction was used in all cases with a Chézy coefficient of $400 \text{ cm}^{1/2} \text{ sec}^{-1}$. This Chézy coefficient corresponded to a Manning coefficient of 0.036 and is similar to those used by Leendertse (1971) and Dronkers (1964).

Initial conditions were $U = V = \delta = 0$. A coastline was established at the left side of the grid, with an opening representing a Bay mouth 17.9 km (~ 10 nm) wide centered in the middle of the coast at $n = 25$, Figure 6. Boundary conditions for the x direction were velocity at the coast, $U = 0$, except at the Bay opening or jet where $U = f(y)$ and

$\delta = 0$ on the eastern boundary. The jet started at $U = 0$ and built to a maximum in 16 iterations (160 min) and then remained steady for 10 iterations (100 min). The jet was given a parabolic profile with a maximum centerline velocity (velocity integrated with respect to depth) of 25 cm sec^{-1} . Boundary conditions for the y direction were velocity for the northern edge of the grid, $V = 0$, or a linear variation from 0 at the wall to a maximum of -4 cm sec^{-1} and tidal height $\delta = 0$ for the southern edge. Using velocity as an open boundary condition on the top of the grid created no problems because the boundary was far enough from the Bay mouth so no complications arose. If the northern (velocity) boundary was moved close to the Bay entrance, the boundary acted as a wall and there was a deflection of the outflow.

Four cases for the steady-state jet with bottom friction were run: Case I, steady-state jet as described above; Case II, steady-state jet with side friction; Case III, steady-state jet with Coriolis force; and Case IV, steady-state jet with an ambient velocity. Vector plots (velocity vectors) and tidal height contours are for a time of 260 min after starting when the jet has reached a steady state.

Case I - Figures 10 and 11 show the vector plots and tidal height contours for the steady-state jet. Four distinguishing features can be seen in the vector plot:

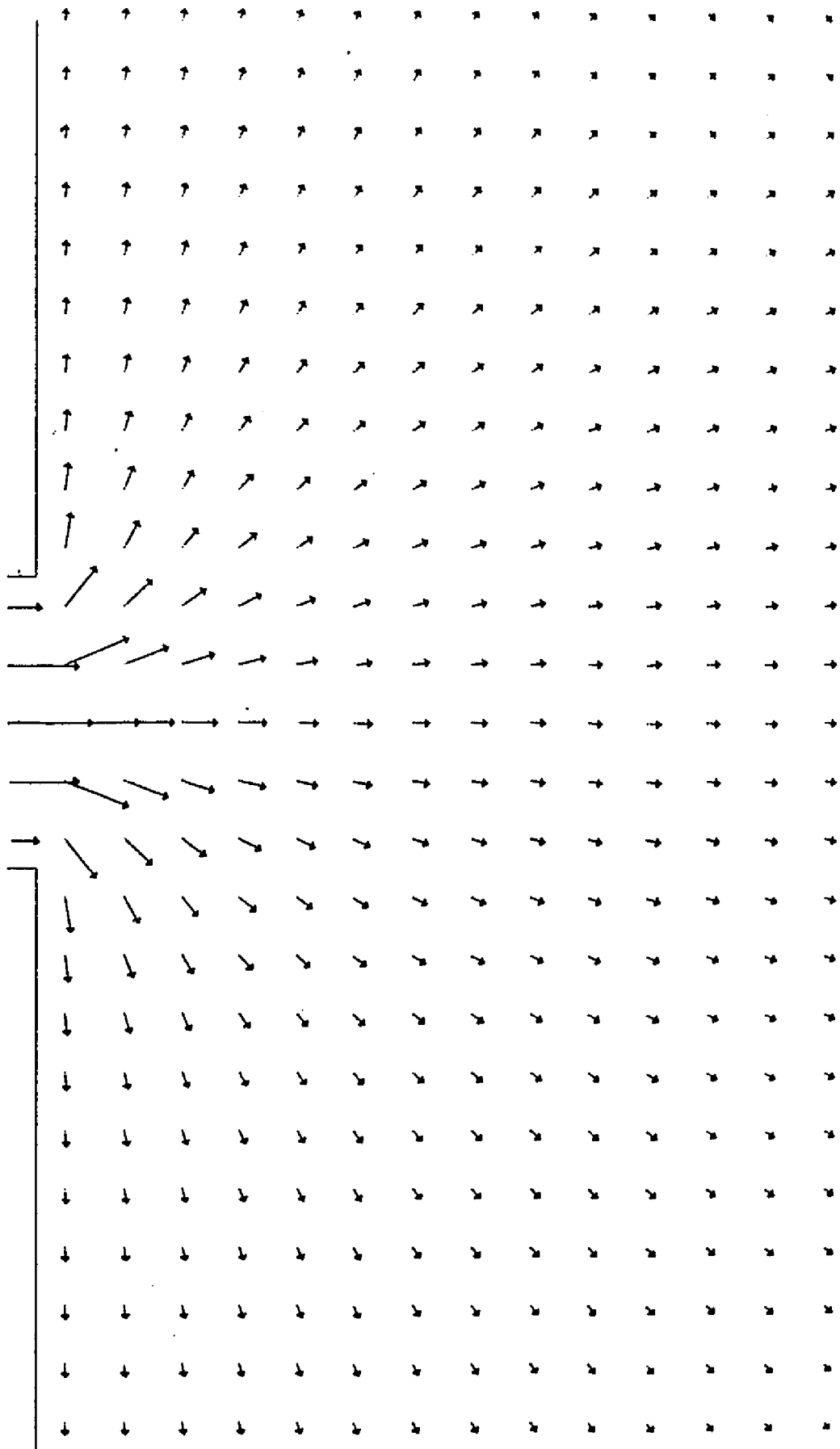


Figure 10 - Velocity vector plot, steady-state jet

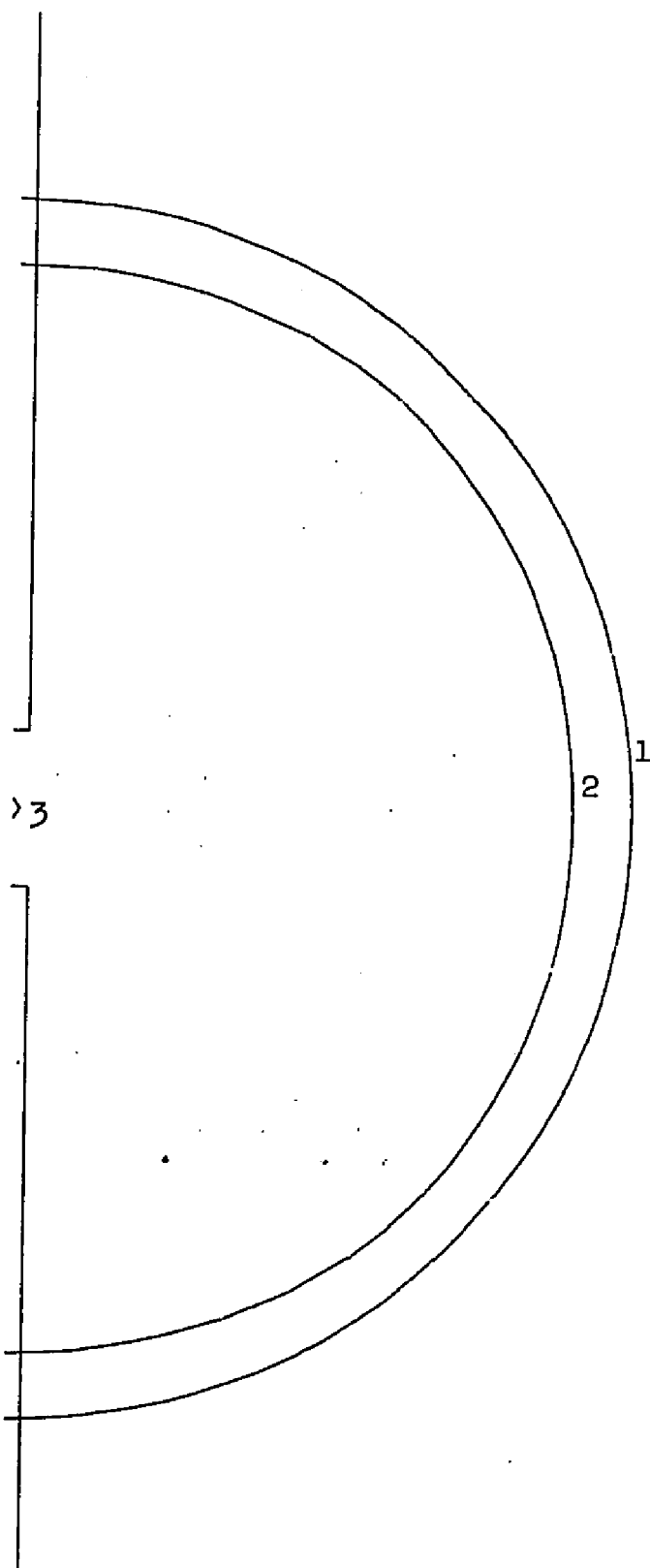


Figure 11 - Water level plot, steady-state jet, cm

first, the jet is dispersive (i.e., the velocity vectors diverge from the jet centerline) and not entraining (vectors converge toward the jet centerline); second, the centerline velocity U decreases sharply as a function of distance along the axis of the jet; third, there is a northern current along the coast above the jet and a southern current below it; and fourth, there are no eddies formed above or below the jet.

The dispersion of the jet is believed to be caused by a buildup of water (and therefore pressure gradient) around the Bay entrance and is shown by the plot of tidal height, Figure 11.¹ As the height of water above MSL is increased, a pressure gradient or head is generated in the x and y directions. This head causes the dispersion, since the water level at the boundaries, by virtue of the boundary conditions, does not go above datum (i.e., $\delta = 0$). Because of the above restriction, the water level inside the boundaries is an unknown and is allowed to fluctuate.

¹In the derivations of Chapters II through IV, tidal height has been the term used to refer to the time-dependent level of the water above or below datum (MSL). In the steady-state case since there are no tides, the tidal height is really a water level (relative to mean sea level) that generates a pressure gradient and will be referred to as a water level in the following discussion.

The cause of the diverging flow in this case is similar to that reported by Bondar (1970) and Engelund and Pedersen (1973). Bondar (1970) reasoned that the river flow which was fresh and less dense was atop a more dense, saline wedge. This lens of less dense water created a hydraulic head, causing divergence or spreading of the flow of the surface layer. Bondar quotes angles of divergence of 40° or more for rivers emptying into the Black Sea and develops equations to predict the spread. Engelund and Pedersen (1973) take the same approach in studying the divergence of warm water jets emptying into a cooler body of water.

If the bottom friction is increased, the velocity in both the x and y directions decreases, causing the jet to shrink in size and the water level to increase, with the maximum increase at the Bay mouth. Figure 12 shows a plot of the centerline velocity U as a function of distance for three values of bottom friction. A decrease in C from 400 to 100 (increase in bottom friction) generated a small change in velocity at the same value of x/y , while a decrease in C from 100 to 5 caused a sharp change. Figure 12 indicates that bottom friction, while having some effect on the velocity, would have to be unreasonably large to cause a drastic change at a given point. Also, it shows

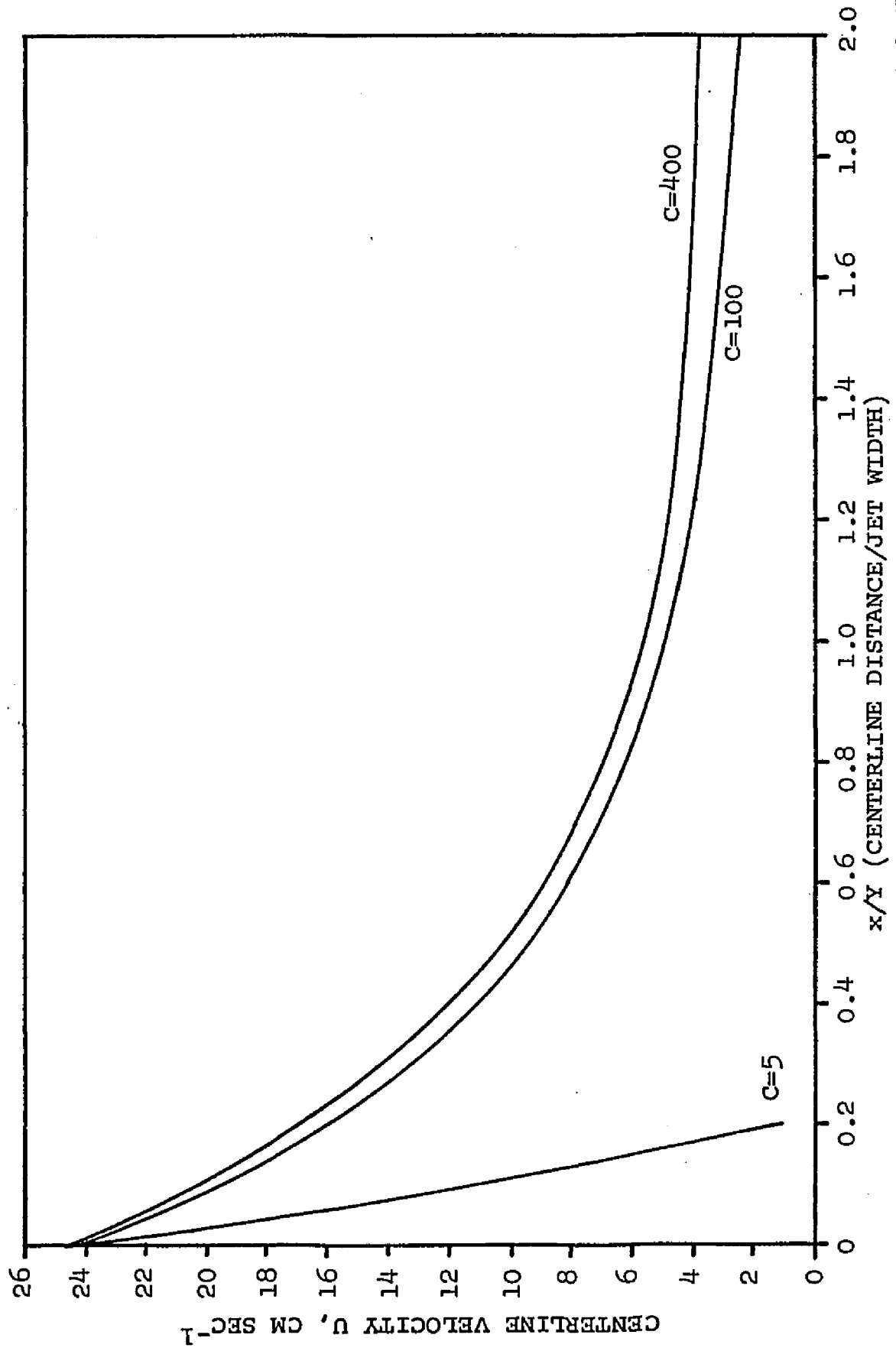


Figure 12 - Centerline velocity distribution resulting from different values of bottom friction, steady-state jet

that changes in C from 400 to 100 can cause the location (x/y) of velocities of 5 cm sec^{-1} or less to change rapidly. To try to understand how important friction is in this case, the jet was allowed to reach maximum velocity (25 cm sec^{-1}) after 160 min of buildup and was then cut off and the computations continued for 100 min. Upon termination of the jet, the remaining fluid that was in motion moved through the computational area, decreasing in velocity with time. The maximum positive velocity in the flow field as a function of time (after termination of the jet) is shown in Figure 13. The velocity decreases from a maximum of 25 cm sec^{-1} to $1/10$ this amount in 100 min. By extrapolation (dashed line) velocities of 1 cm sec^{-1} should be reached in about 4 hr. This decrease in velocity suggests that bottom friction is dominant over rotation since the velocity decreases to near 0 in a time less than the inertial period for this latitude (19.9 hr).

Before comparing further the results of Case I with the classical plane jet, the results from Case II will be examined.

Case II - This case consisted of the steady-state jet used above, but with side as well as bottom friction. Here, α (equations 2.37 and 2.38) was given a value of 10,000, resulting in an eddy viscosity value of about

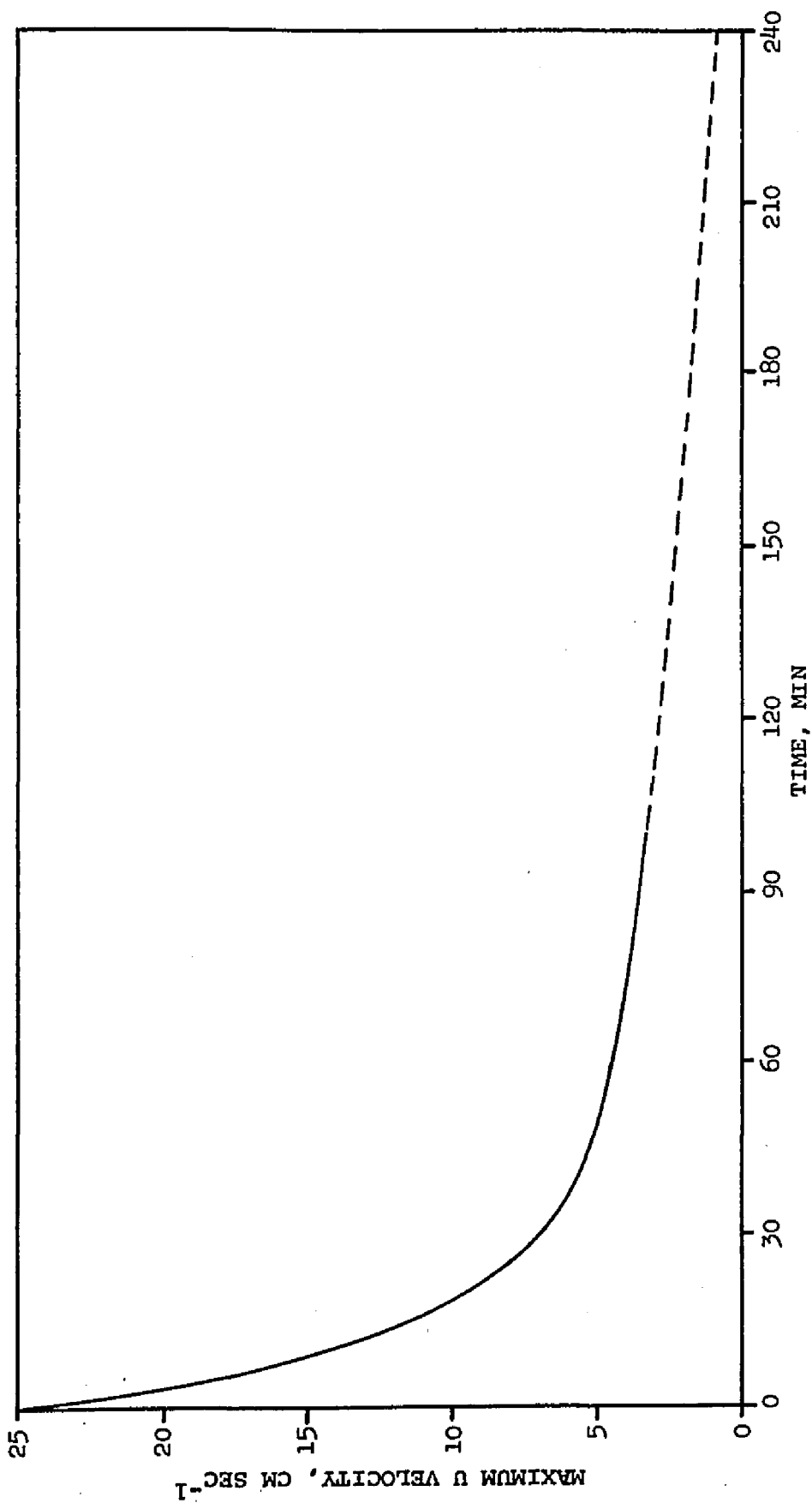


Figure 13
Decay time, steady-state jet

$10^8 \text{ cm}^2 \text{ sec}^{-1}$. Values in the literature vary from 10^5 to 10^8 (Sverdrup, et al (1941)). The results for the vector plot are shown in Figure 14. Four features are apparent: the jet is not as dispersive or does not spread laterally as much as in Case I; there is a decrease in the centerline velocity as a function of distance along the jet; the magnitude of velocity vectors adjacent to the coast above and below the jet, when compared to Case I, has decreased; and there are no eddies formed.

Figure 15 shows an x,y plot of the location of $U_0/2$ (half the centerline velocity) for Cases I and II. This figure verifies the decrease in lateral spread caused by the addition of side friction.

A comparison of the velocity as a function of distance in the x direction for Cases I and II is shown in Figure 16 by curves a and b (other parts of this figure will be discussed later). The velocity drops from a maximum of 25 cm sec^{-1} to less than 5 cm sec^{-1} in 30 km for both the bottom and side friction cases.

Bickley (1937) in his expansion of Schlichting's (1933) work derived the exact solution for the two-dimensional motion of an incompressible viscous fluid due to a side friction jet issuing from a long, narrow orifice. Albertson, et al (1950), summarized experimental data to determine

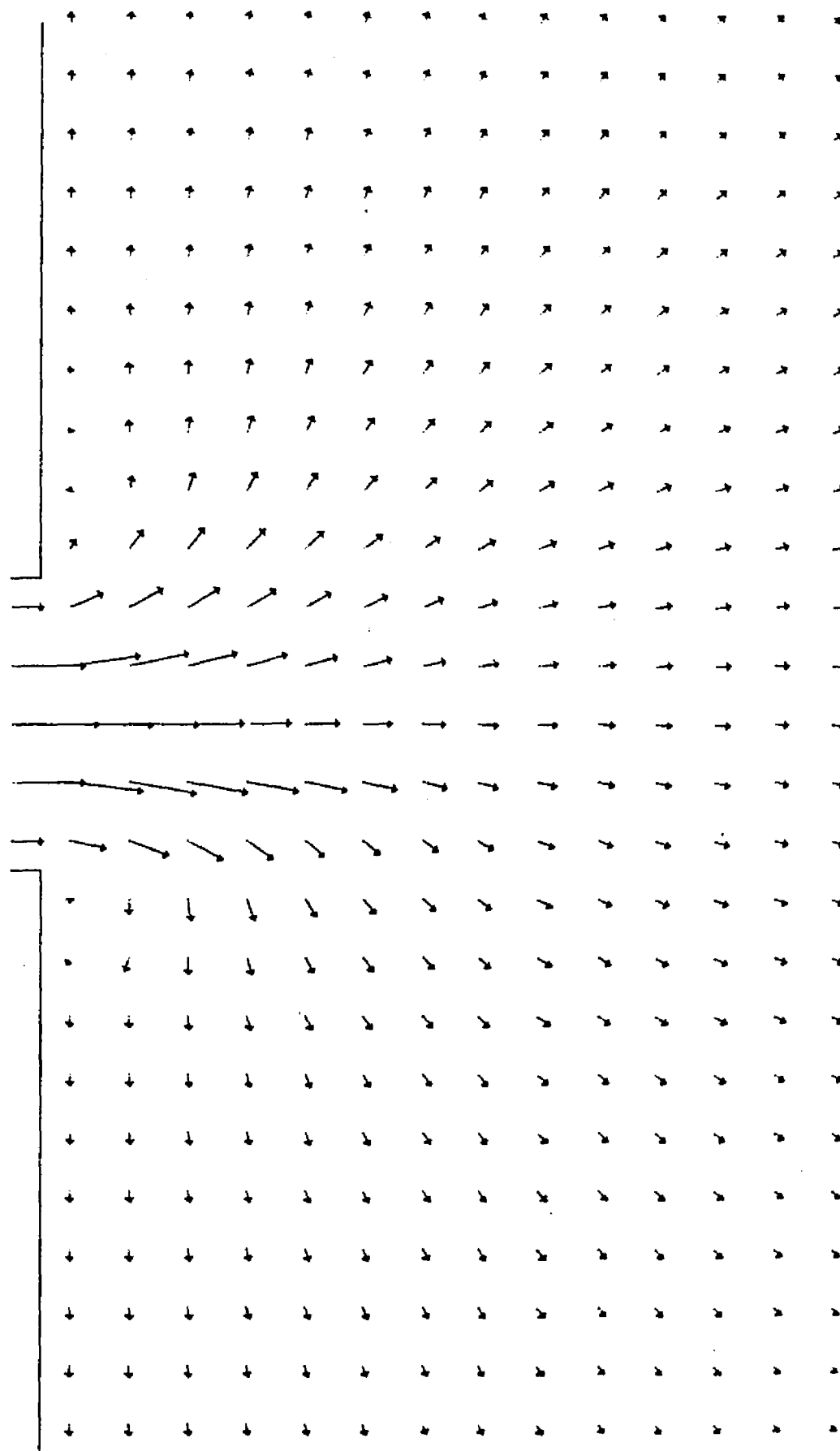


Figure 14 - Velocity vector plot
steady-state jet with side friction

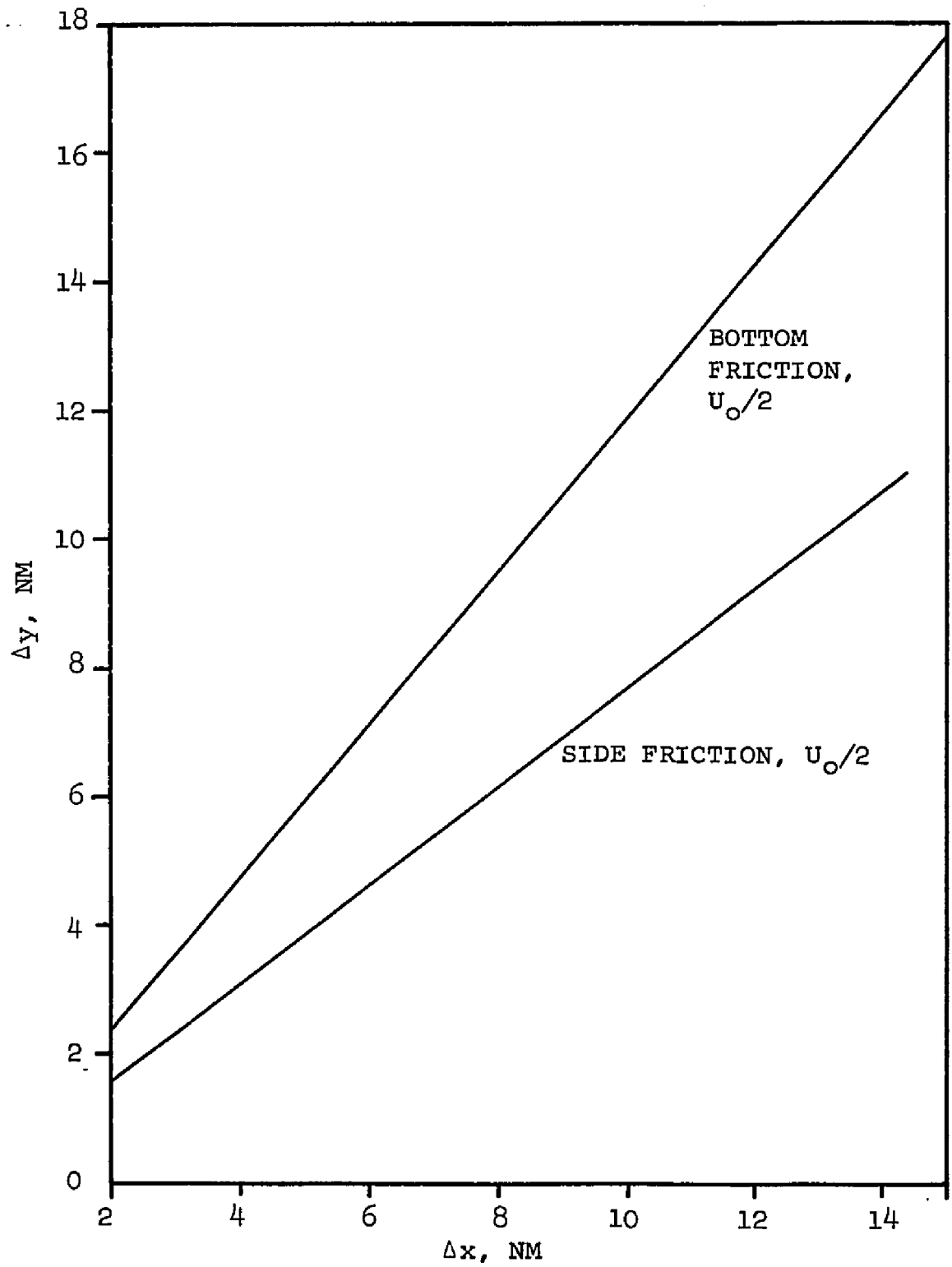


Figure 15 - $U_o/2$ as a function of x and y for side and bottom friction case steady-state jet

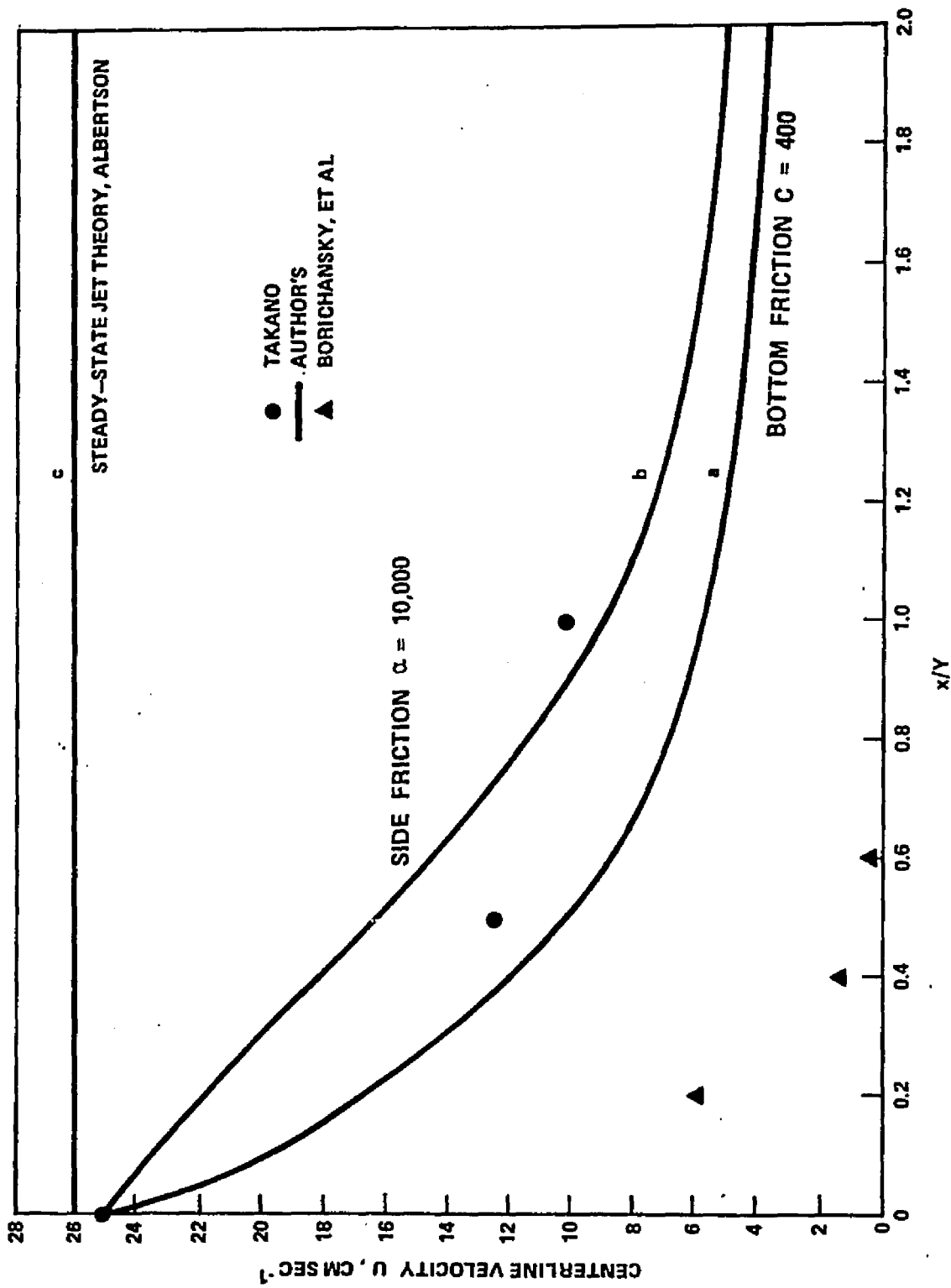


Figure 16 - Centerline velocity distribution for side and bottom friction case, steady-state jet

the velocity distribution and character of a side friction jet and to formulate empirical equations to predict the velocity distribution of a jet issuing from an orifice or slot. Albertson's (1950) summary of the side friction plane jet shows an entraining flow and a centerline velocity which begin to decrease only after a distance of six jet diameters. This would mean that, if a side friction plane jet theory were directly applicable to an estuary like Chesapeake Bay and the Bay flow were not tidal or deflected by the earth's rotation or other causes, the maximum centerline velocity would be detected unchanged up to a distance of 108 km from shore and the flow would be entraining.

Recent works by Takano (1954a) and Borichansky and Mikhailov (1966) have attempted to evaluate the velocity distribution off the mouth of an estuary or river. Takano (1954a) derives the velocity distribution by not considering the inertia terms and by using only the side friction and pressure gradient terms. He assumes a thin layer of river water which is homogeneous and 1 or 2 meters thick resting on a more saline ocean wedge. In contrast, Borichansky and Mikhailov consider the inertia and side and bottom friction terms only. The results of both these investigations show a centerline velocity decreasing

rapidly as a function of distance. Their velocity predictions for selected centerline points for an estuary of the type used in Case I are plotted as individual points in Figure 16 along with the prediction for a side friction jet (curve c) given by Albertson (1950). It can be seen that the centerline velocity results of Cases I and II agree in trend with the results of Takano (1954a) and Borichansky and Midhailov (1966) and not with the predictions of Albertson, et al (1950).

Gadgil (1971) was the first to make an attempt to look at both bottom (Case II) and side (Case III) frictions together. She used a laminar steady-state jet in a rotating container which had a rigid top and bottom. The rotation was used to generate an Ekman layer and, thus, bottom friction. While this is different from the steady-state jet considered here, bottom friction can exist without rotation (Case I), the results of her investigation are interesting to examine for similarities. Her results showed that if the rotation was strong, bottom friction dominated, the jet was dispersive, vorticity was decaying but not diffusing laterally, and momentum decreased with downstream distance. If there was little or no rotation and side friction dominated, the jet entrained fluid, vorticity was conserved but diffused laterally, and the

momentum flux across the jet remained constant. Gadgil (1971) also was able to predict the distance it would take the velocity of a side or bottom friction jet to decrease to zero. In general, the distance required for her jet to decrease to zero was greater for a side friction case than for a bottom friction case.

Gadgil also points out that, in cases where bottom friction dominates, if side friction is considered it will control the flow pattern near the mouth of the jet and give way to a bottom friction velocity distribution as the distance from the jet entrance increases. This could be an explanation for the flow pattern observed in Figure 14.

In summary, for the velocity along the centerline it can be concluded that the distribution for an estuary or river discharging into a continental sea will decrease rapidly, in a form similar to that shown in Figure 15, if the jet is considered a bottom friction type. For this type of jet the flow will be dispersive (i.e., velocity vectors diverge away from the jet centerline). If the jet is dominated by side friction, it will follow a distribution along the centerline similar to that described by Albertson (1950) and the flow will be entraining (velocity vectors converging toward jet centerline). For a case in

which side and bottom frictions exist, the flow pattern will be a combination of the two as described by Gadgil (1971).

Another interesting comparison of the U component of velocity is in the transverse direction. Bickley (1937) in his solution found the transverse distribution of the U component of velocity was a function of the hyperbolic secant squared ($U = f(\text{sech}^2 y)$). Albertson, et al (1950), in their work assumed that the transverse distribution of the component of velocity was Gaussian. The normalized transverse velocity distribution U/U_0 (U component of velocity located at distance y from centerline/centerline velocity) was plotted against y/b (distance from centerline of U/distance from centerline of $1/2 U_0$) for Case I, Figure 17. It can be seen from this figure that the data indeed follow a $\text{sech}^2 y$ curve.

As mentioned, the velocity vectors along the shore above and below the jet have decreased in intensity. It should be noted that a shoreward movement of water near the coast both above and below the jet has been generated.

Case III - This case consisted of the addition of the Coriolis force for a jet of the type in Case I. The Coriolis parameter was for a latitude of 37° and was calculated to be 0.00008 sec^{-1} . The computational results

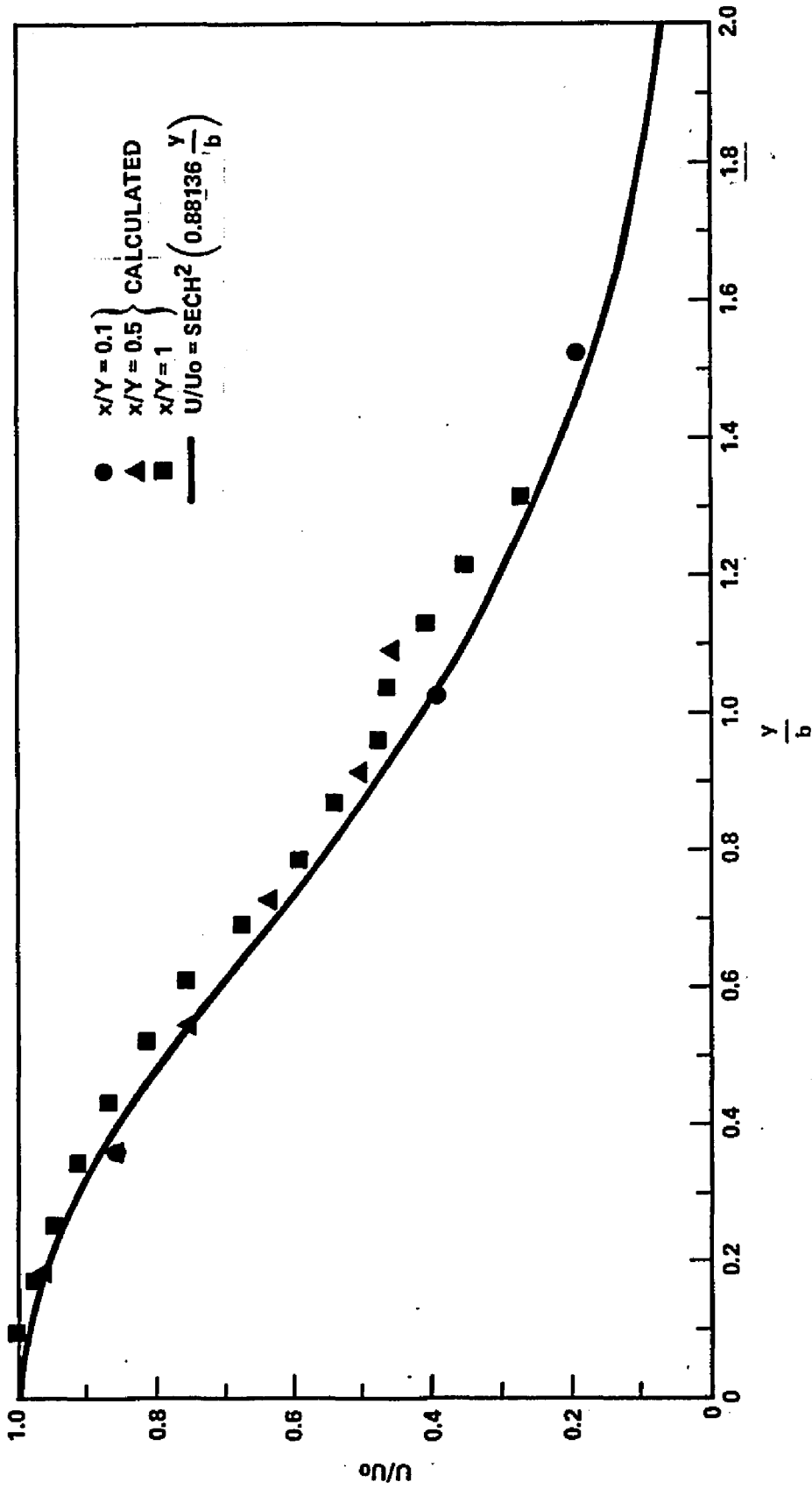


Figure 17
 Cross-stream velocity distribution
 steady-state jet

for the vector plot are shown in Figure 18, and the water level contours are shown in Figure 19. The same four features recognized and described for the vector plot of Case I are apparent here. Comparing Figure 18 with the vector plot of Case I, Figure 10, shows no major differences. There is a slight rotation of the vectors to the southern half of the plot, but nothing that is very noticeable. Plots of the centerline velocity for this case are the same as those of Case I and are not shown. The plot of water level, Figure 19, when compared with the water levels of Case I, Figure 11, also shows a slight difference, with some water being piled up to the south.

At this point it is helpful to consider two dimensionless quantities, the Ekman and Rossby numbers. The Ekman number is used to determine the relative importance of friction and rotation and is defined as $A_z/\Omega H^2$, where A_z is the vertical eddy viscosity. An A_z corresponding to a Chézy coefficient of $400 \text{ cm}^{-1/2} \text{ sec}$ can vary from about 76.5 to $133.9 \text{ cm}^2 \text{ sec}^{-1}$, depending on the type of vertical velocity profile assumed. (See Appendix D.) These values of vertical eddy viscosity are in the range of those quoted by Sverdrup, et al (1942), Neumann and Pierson (1966), and Dyer (1973). The corresponding Ekman number for the above range of turbulent eddy viscosity varies from 1.05 to 1.83.

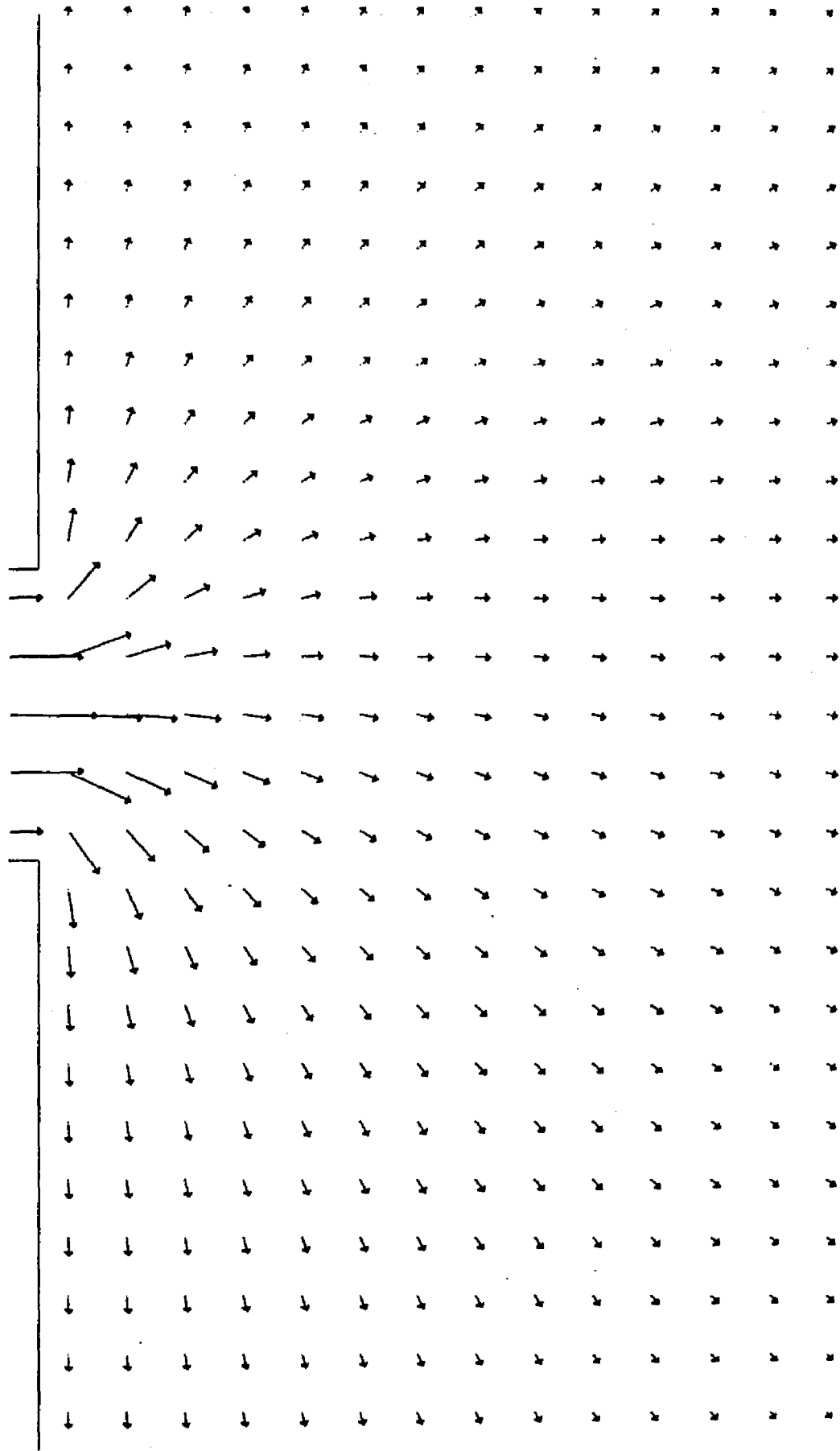


Figure 18 - Velocity vector plot
steady-state jet with Coriolis force

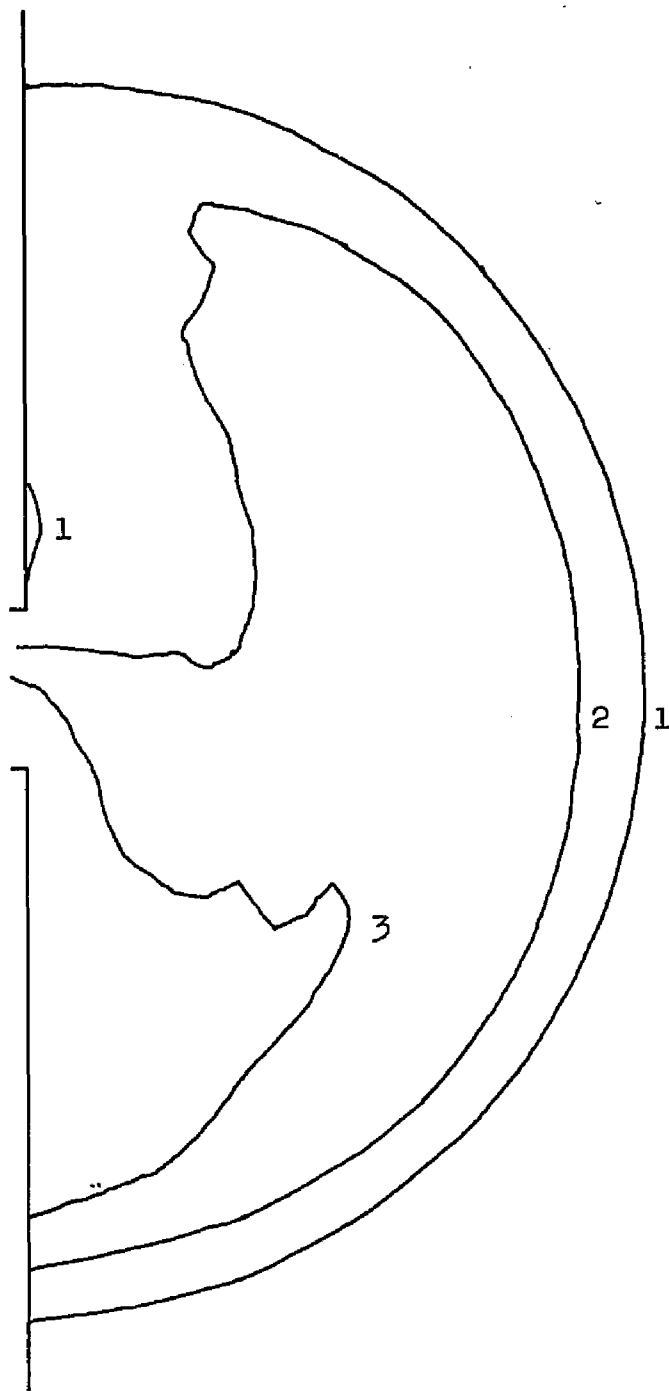


Figure 19
Water level plot
steady-state jet with Coriolis force, cm

It can be considered that in this case the flow is frictionally dominated for the higher values of the Ekman number, i.e., >1 .

The Rossby number, $R_o = U/\Omega L$, is used to determine the relative importance of the inertial terms to those of rotation. For a characteristic length $L = 359,280$ cm (one-grid spacing) and velocity change of 25 cm sec^{-1} over this distance, the Rossby number is 0.9 . This is a maximum value. While not one, it is much larger than the Rossby numbers usually found in laboratory experiments where rotation is considered dominant and shows that the inertial terms have increased in importance but are still not controlling. Takano (1955), when investigating the effect of the seaward flow off a river mouth, concluded that for his analytical equations, the Coriolis term could be insignificant if the inertial terms were large (i.e., large Rossby number).

Thus, for this case the friction terms can dominate those of rotation, while the inertial terms might not. This should help to explain the lack of a significant deflection of the outflow due to rotation and verifies the results of the jet decay experiment in Case I.

Case IV - This case consists of the addition of a southward flowing velocity to the situation of Case I.

Surface velocities in the Chesapeake Bight region are highly variable and depend on distance from shore and on season. Values in the literature range from 1.2 cm sec^{-1} to 32.4 cm sec^{-1} (Harrison, et al (1967)). A value of 4 cm sec^{-1} to the south was chosen and varied linearly from 0 at the coast to a maximum of -4 cm sec^{-1} at the right side of the computational grid. The results of the computation are shown as a vector plot in Figure 20. Here the northern flow along the coast decreased, and the jet was deflected and turned south as a wide band of flow. Again, there are no visible eddies. This case suggests that, for a frictionally dominant flow, an ambient southern velocity is more important in the turning of the Bay effluent to the south than the Coriolis force.

The northern flow along the coast above the Bay mouth still persists, as seen in Figure 19. Bumpus (1969) has described reversals or northern flow in the surface waters in the Mid-Atlantic Bight. His results are derived from surface drifters, and the reversals described exist at several locations on the coast and mainly during the summer. These reversals occur during a season of light winds so that the flow patterns established by a layer of lighter water on a more dense saline wedge, along with an imposed ambient current, could cause the time averaged surface flow described by Bumpus and shown by Figure 20.

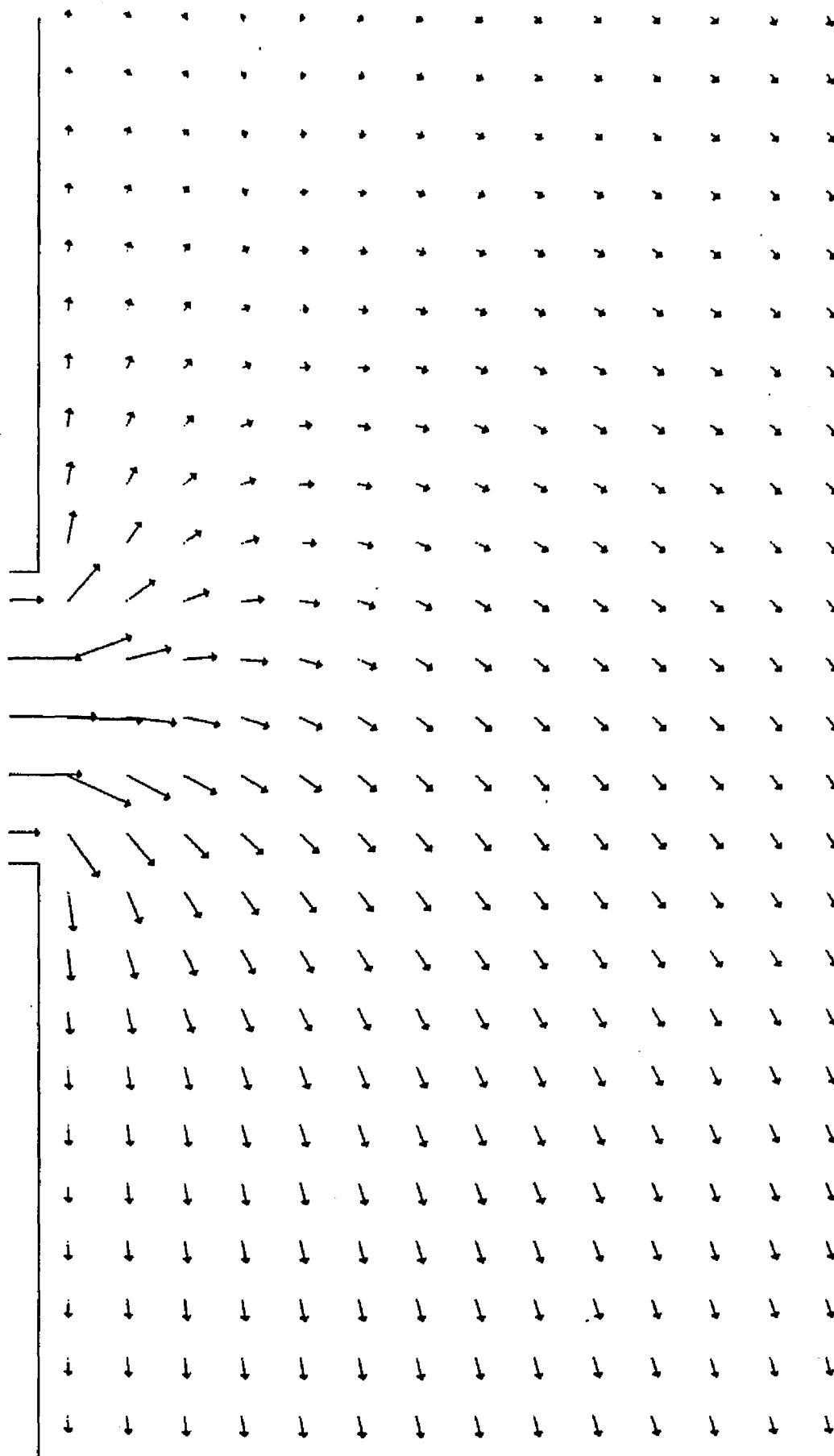


Figure 20 - Velocity vector plot, steady-state jet with southerly ambient velocity.

Oscillating Jet

General - For this physical situation, grid size, time step, grid spacing, Bay entrance, coastline, and bottom friction were the same as those for the steady-state jet. The Courant-Friedricks-Lewy stability criterion was also the same, and no problems were encountered in using an oscillating jet as a boundary condition. Salinity was not calculated, as for the steady-state jet, since it was held constant over the grid for all cases.

The initial conditions for the grid were the same as for a steady jet, but the boundary conditions were changed. In the east-west direction, velocity and tidal height were the boundary conditions as before, with the only change being at the Bay mouth. Here, the jet was made to oscillate sinusoidally with a period of 12.42 hr (semi-diurnal tide) and a maximum centerline velocity (integrated with respect to depth) of 25 cm sec^{-1} . The velocity profile across the Bay mouth remained parabolic. Boundary conditions in the north-south direction were changed, due to the problem of reflection from the northern boundary, so that tidal height was used on both boundaries. For all cases, except that of an ambient southward flowing velocity, the tidal height on the northern and southern boundaries remained zero.

Six different cases for an oscillating jet with bottom friction were run: Case I, oscillating jet; Case II, oscillating jet with Coriolis force; Case III, oscillating jet with sloping bottom; Case IV, oscillating jet with wind from east; Case V, oscillating jet with wind from north; and Case VI, oscillating jet with ambient velocity from the north.

In computing data for all the above cases, the program was run through two complete tidal cycles, with data for the vector plots and water level contours taken from the last tidal cycle. The term water level is used here as in the steady-state case because, although the velocity varies with a period equal to that of a semi-diurnal tide, the tidal height on the open boundaries is not fluctuating with time.

Case I - Figure 21 shows a plot of the water level and velocity as a function of time through both tidal cycles for two points on the grid ($m = 1, n = 25$ and $m = 6, n = 25$). In one tidal cycle the velocity and water level adjust so that they are out of phase by about 90° and remain this way throughout the second tidal cycle. The velocity and water level can be seen to decrease as a function of distance from the Bay mouth, when like curves in Figure 21 are compared. This figure suggests that the data taken during

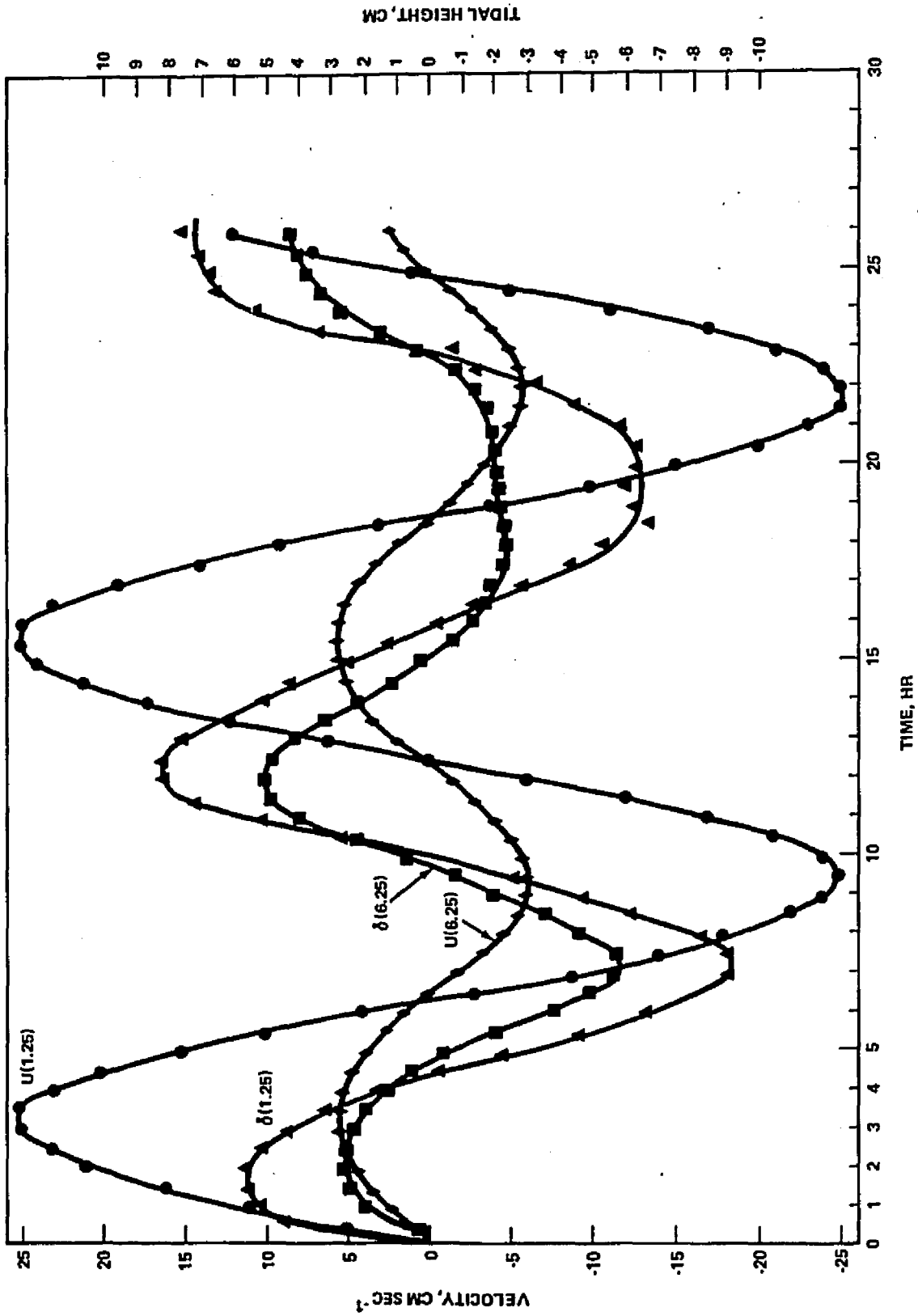


Figure 21 - Velocity and water level as a function of time at two grid points, oscillating jet

the second tidal cycle are for a jet which has reached equilibrium.

Figures 22 through 26 show the vector and water level plots for an oscillating jet during the second tidal cycle. Figures 22 and 25 are the plots of the water level at slack before ebb and at slack before flood, respectively. The contours show symmetry around the Bay entrance, as did Figure 11 for the steady-state jet. The height of the water is referenced to datum, and the effect of a head or pressure gradient caused by the height of the water above and below datum can be seen. The vector plots are given in Figures 23, 24, and 26. Figure 23 is a vector plot of the flow at maximum ebb, and Figure 24 is a vector plot for the time when the centerline jet velocity at the Bay mouth is 12 cm sec^{-1} . Figure 26 shows the vector plot at maximum flood. The main features of the flow in these figures are: the flow is dispersive for an ebb tide and convergent toward the Bay entrance for a flood tide, the velocity decreases as a function of distance along the centerline, there is a strong flow along the coast above and below the jet for both flood and ebb tides, and there are no eddies in these figures (which are instantaneous pictures). To further check for eddies, the flow was averaged over a tidal cycle to remove the tidal component for

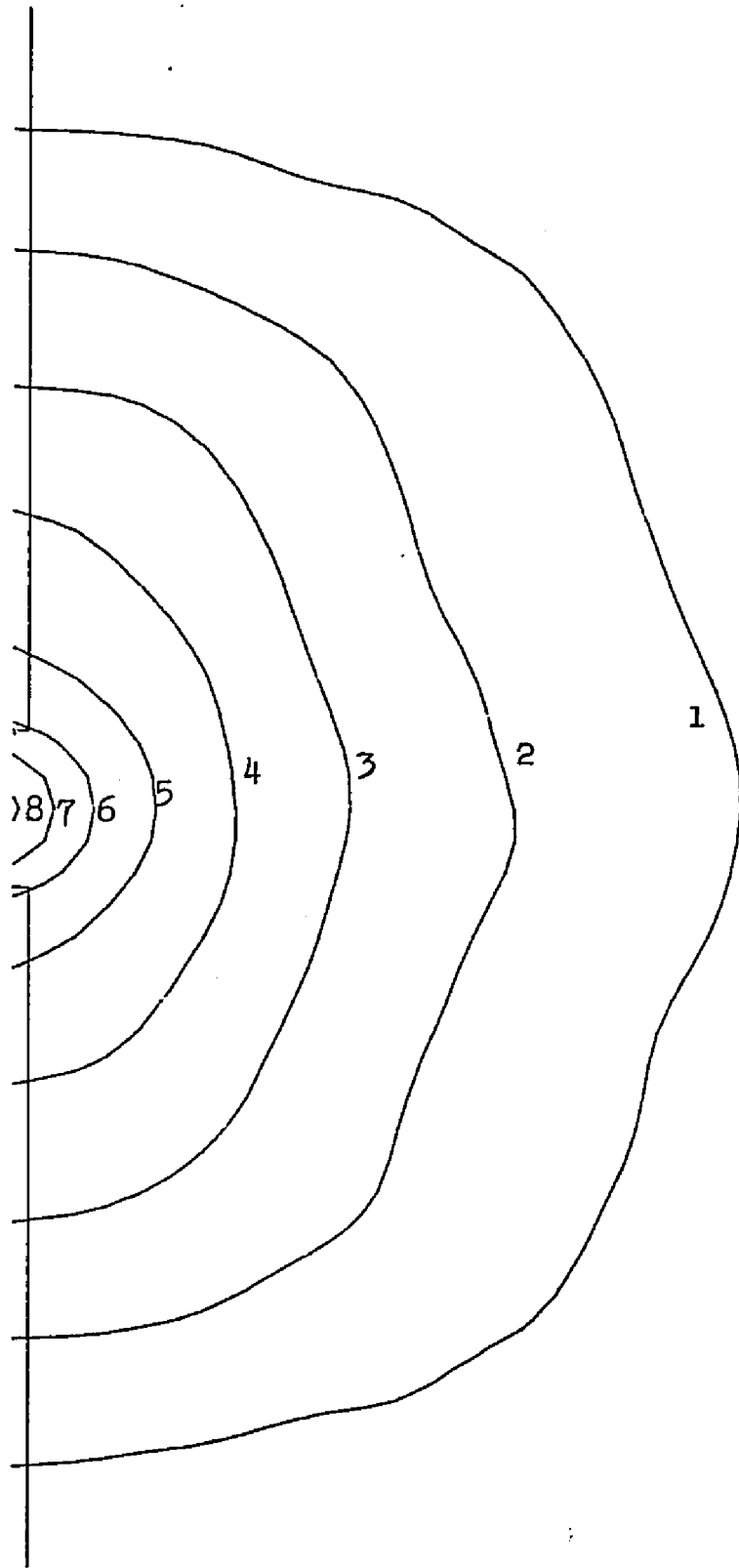


Figure 22
Water level plot
oscillating jet at slack before ebb, cm

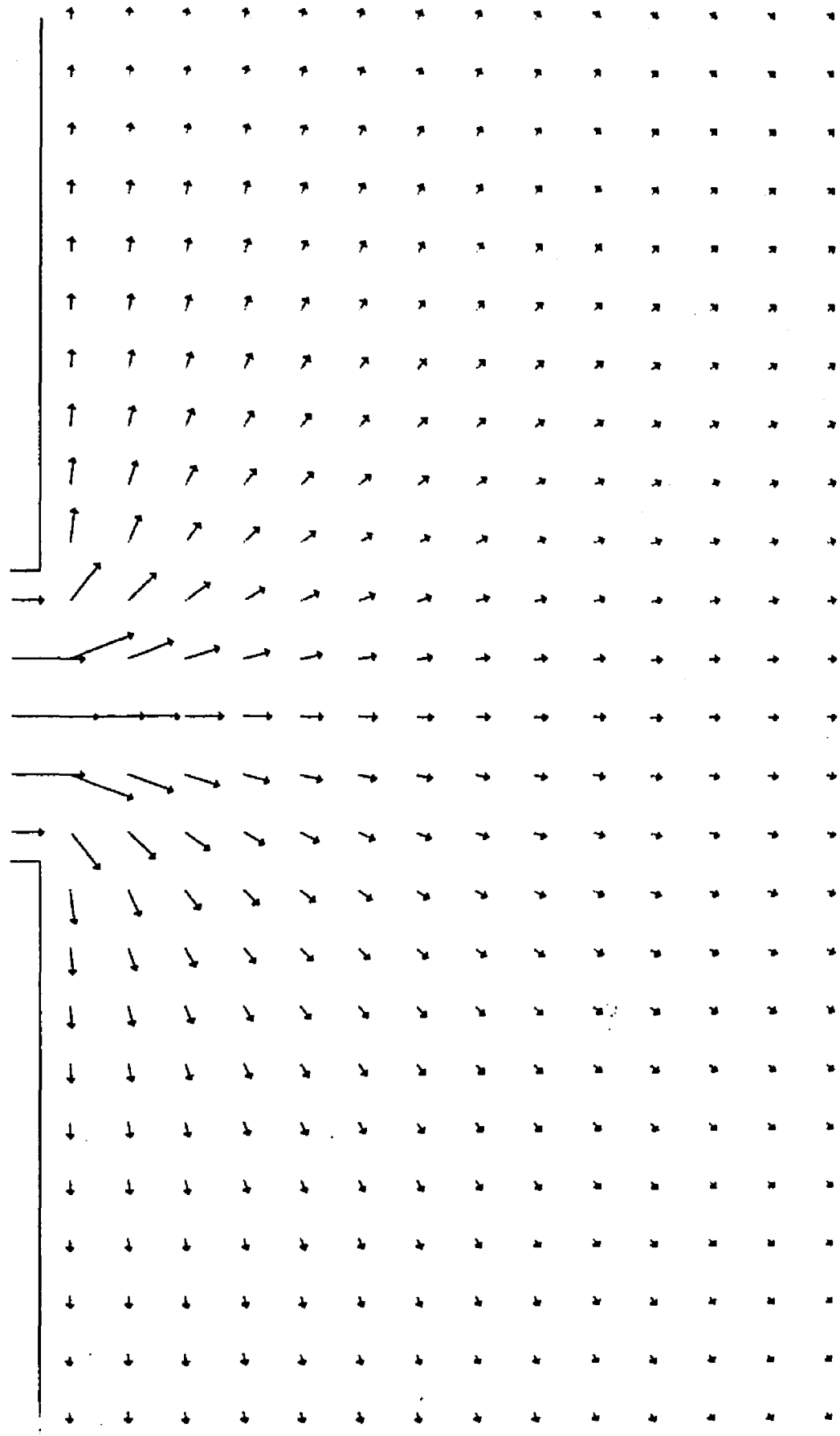


Figure 23 - Velocity vector plot
oscillating jet at maximum ebb

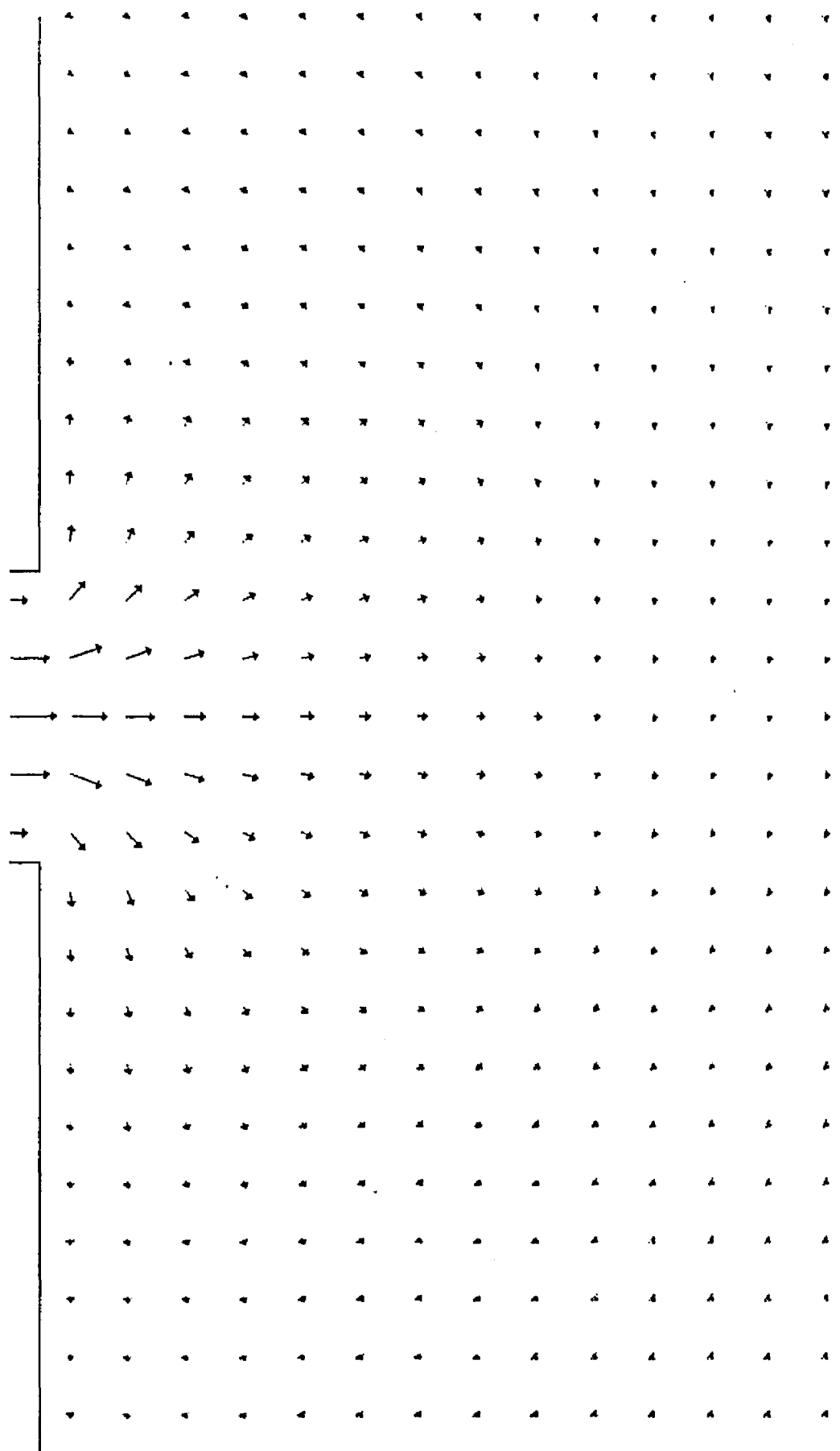


Figure 24 - Velocity vector plot, oscillating jet at a maximum centerline velocity of 12 cm sec⁻¹

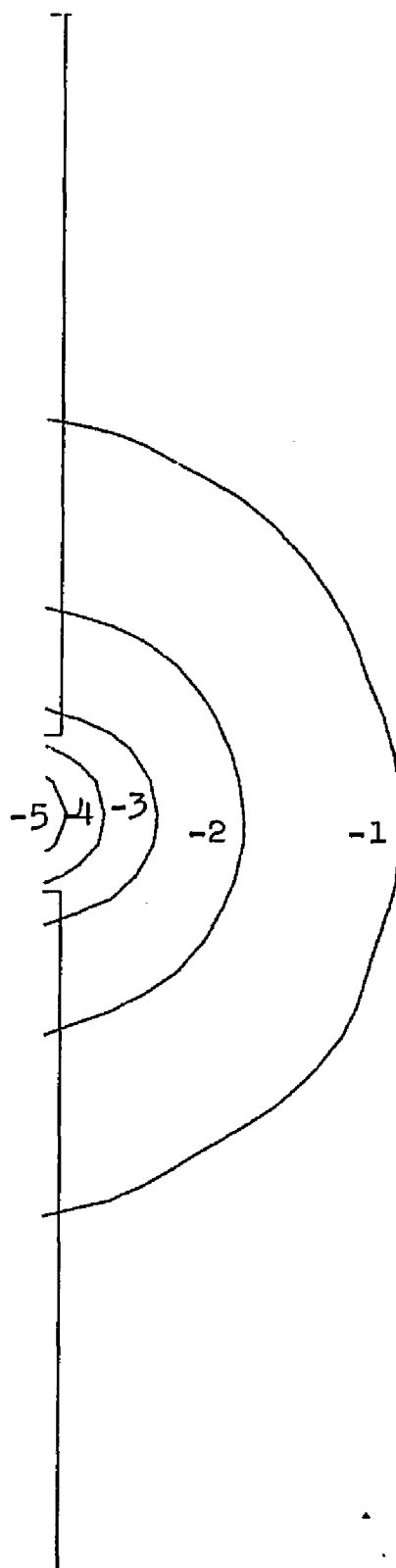


Figure 25
Water level plot
oscillating jet at slack before flood, cm

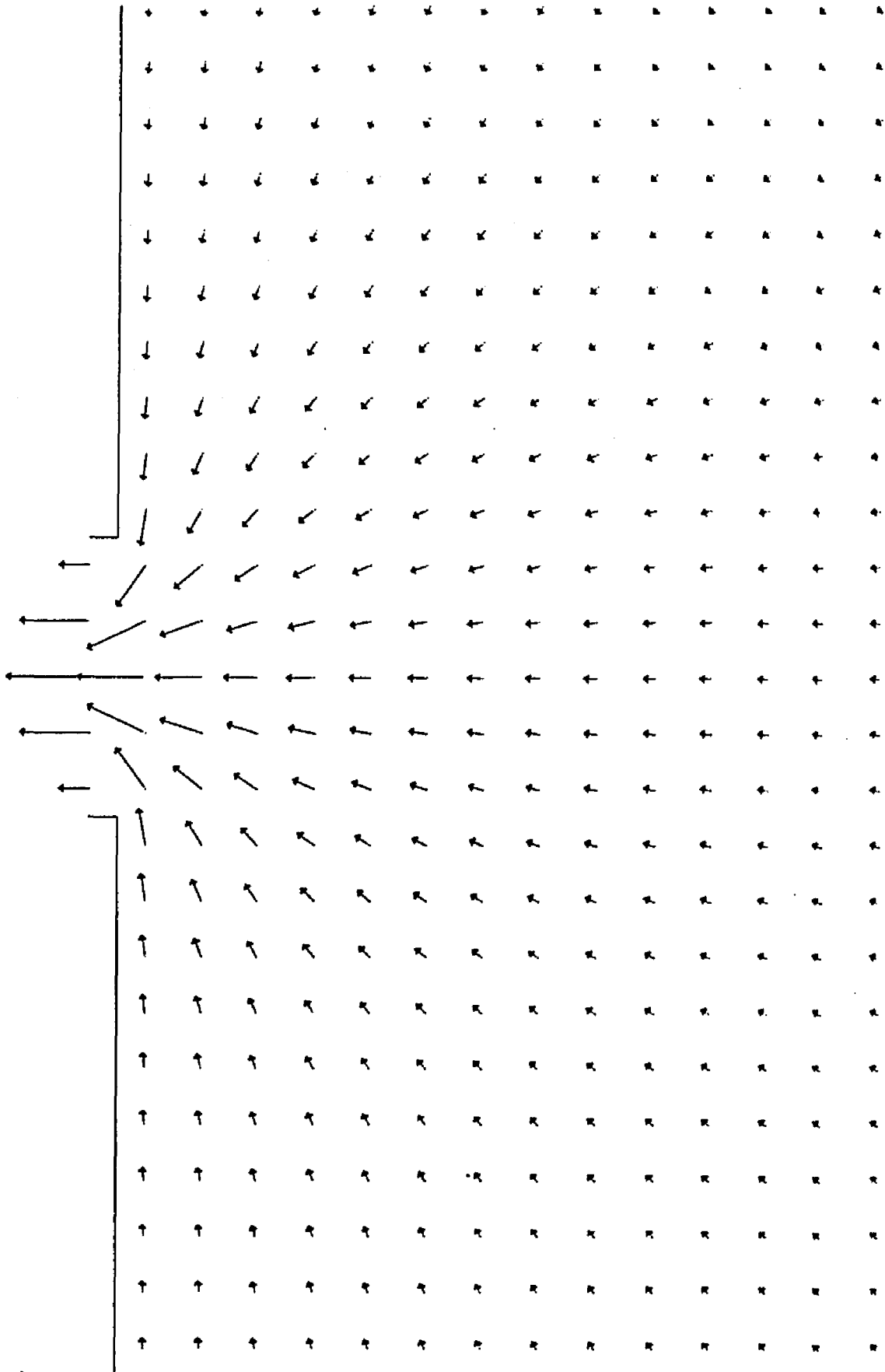


Figure 26 - Velocity vector plot
oscillating jet at maximum flood

the grid points in the vicinity of the Bay mouth. Only the southern portion of the Bay entrance was examined since the flow is symmetrical. The results of this summation are shown in Figure 27. Here it can be seen that, from an Eulerian point of view, there is a weak residual clockwise circulation. This corresponds to the results of Harrison, et al (1962), in their measurement and inference of an eddy south of the Bay entrance near Virginia Beach, Virginia. It is believed this net circulation is the result of the non-linear terms, in the equations of motion, on the tidal velocity fluctuation.

The dispersion and convergence characteristics of the oscillating jet are believed to be caused by a pressure gradient. This gradient is generated by the water level varying above and below datum, as shown in Figures 22 and 26, and is the same mechanism that causes the dispersion of the steady-state jet.

The centerline velocity behaves in the same manner as described for the steady-state jet, in that it decreases as a function of distance from the Bay mouth. This condition holds for both flood and ebb and can be seen in Figures 23, 24, and 26; it is shown as velocity versus distance in Figure 28 for the ebb condition only.

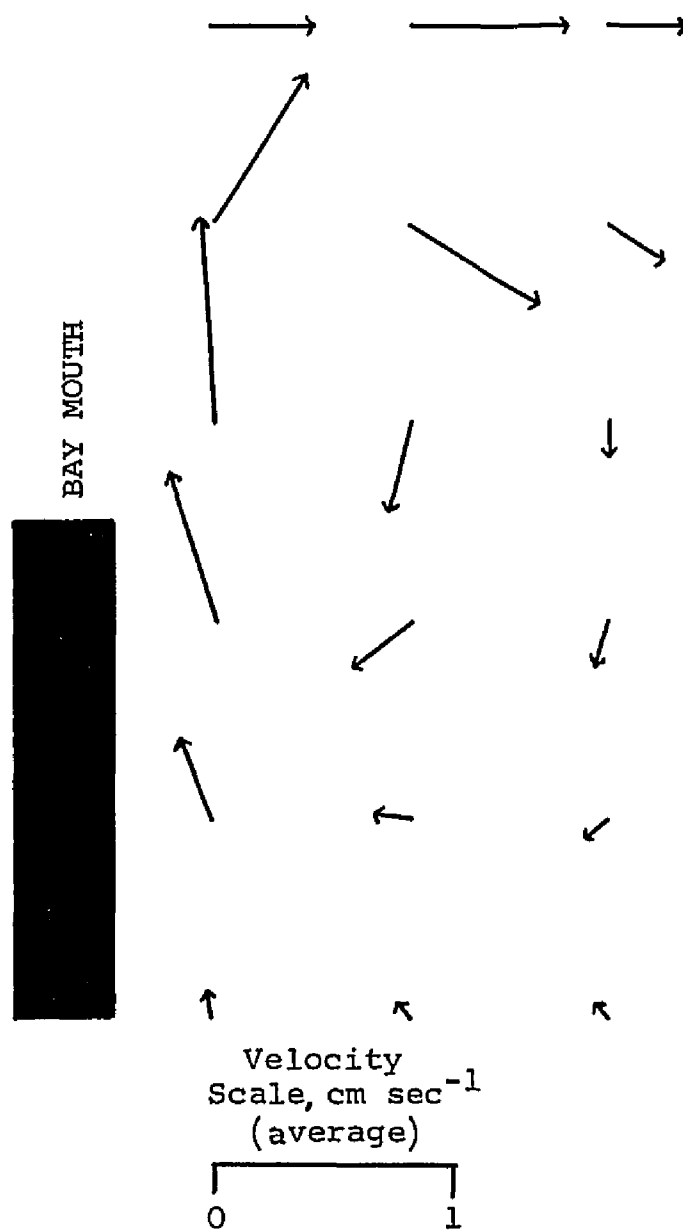


Figure 27
Tidal averaged flow, oscillating jet

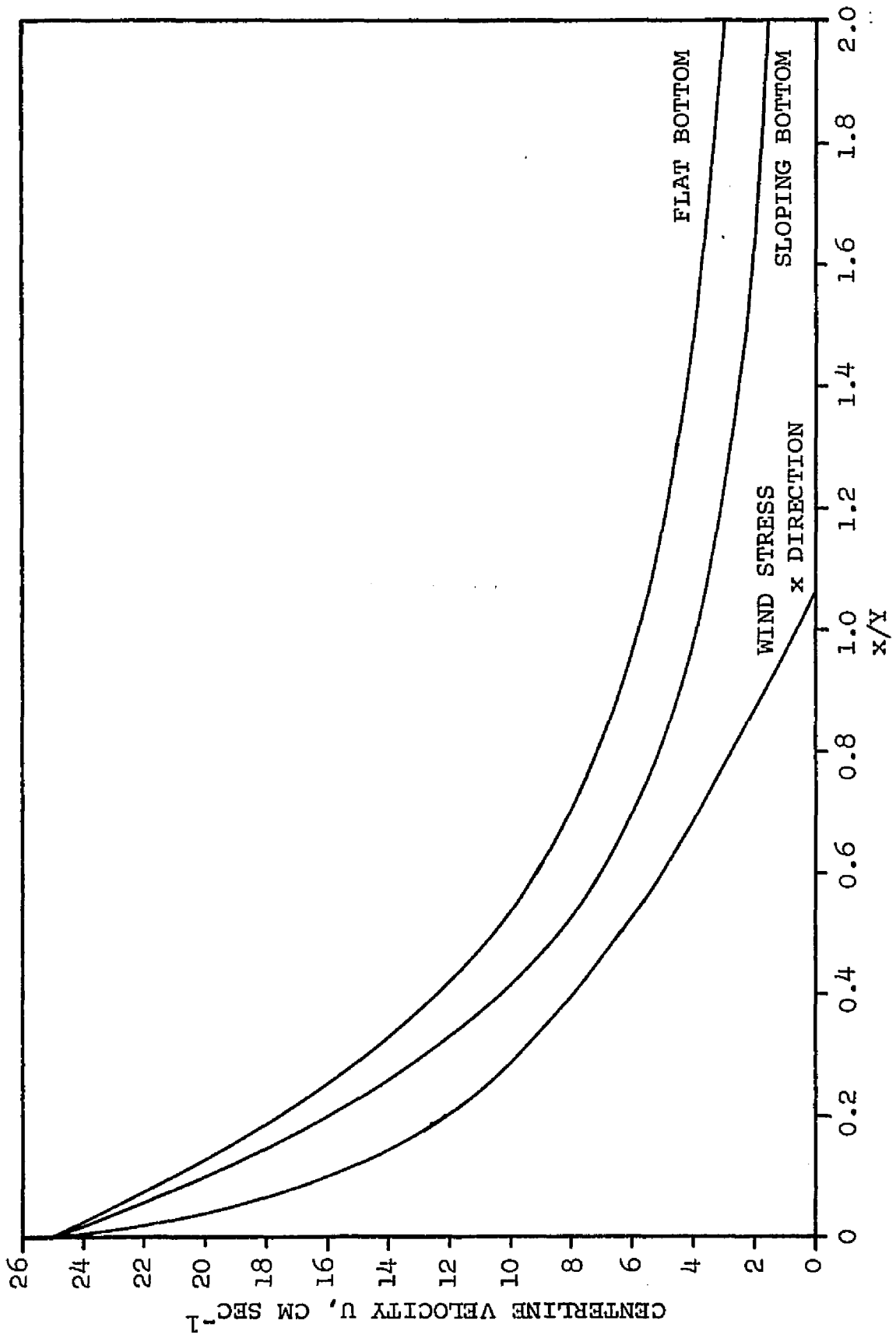


Figure 28 - Centerline velocity distribution for flat and sloping bottom, oscillating jet

The strong coastal flow away from the jet above and below the Bay entrance for the ebb flow reverses itself during the flood stage. In both cases a strong coastal current is apparent.

One final interesting aspect can be discussed in this case. The Amazon River has flow features that are very similar to this case. These features are: (1) There is no Coriolis effect since the Amazon is located on the equator; (2) the Amazon is unique in that it has no salt wedge; and (3) it is tidal and the width of the mouth reported by Gibbs (1970) is between 10 and 20 km, similar to the 17.9 km for the Chesapeake Bay. However, there are some differences worth noting: (1) The depth at the mouth of the Amazon is 2 to 4.5 times that used here; (2) the tidal range is 5 times that of the Chesapeake Bay; and (2) the volume of discharge is 100 times that of the Chesapeake Bay.

If Figures 2 and 3 of Gibbs (1970) are examined, with attention paid to the 20 ‰ isohaline, and compared with Figures 10 and 11 for the steady-state jet and Figures 22 and 25 for the oscillating jet, the similarities in the fan-like spread of the Amazon effluent can be seen.

Case II - This case consisted of the addition of the Coriolis force to an oscillating jet of the type in Case I. The same value of the Coriolis parameter, f , applied in

Case III of the steady-state jet was used. The results of the calculations are given in the vector plots, Figure 29 for maximum ebb and Figure 30 for maximum flood. The four main features seen and described for the vector plots of the previous case apply here with little difference seen between Figures 23 and 29 and between Figures 26 and 30.

As for Case I, the tidal component was averaged out to observe the eddy effect. This is shown in Figure 31. Here it can be seen that the Coriolis effect strengthens the northern and weakens the southern flow of the eddies.

Case III - This case is different from any described thus far. In this run the shape of the bottom was changed from flat to gently sloping for the Case I oscillating jet. The bottom varied from 1000 cm in depth (~ 32 ft) at the coast to 13,000 cm in depth (~ 425 ft) 10⁴ km from the coast, giving a slope of $1/1354$. Bottom friction was held constant and not allowed to vary with depth, and the Coriolis force was not considered.

Figures 32 and 33 show the vector plots at maximum ebb and flood for the second tidal cycle. The same four general features recognized for the vector plot of Case I of the oscillating jet are again seen here. However, there are some differences: First, the gradual sloping of the bottom

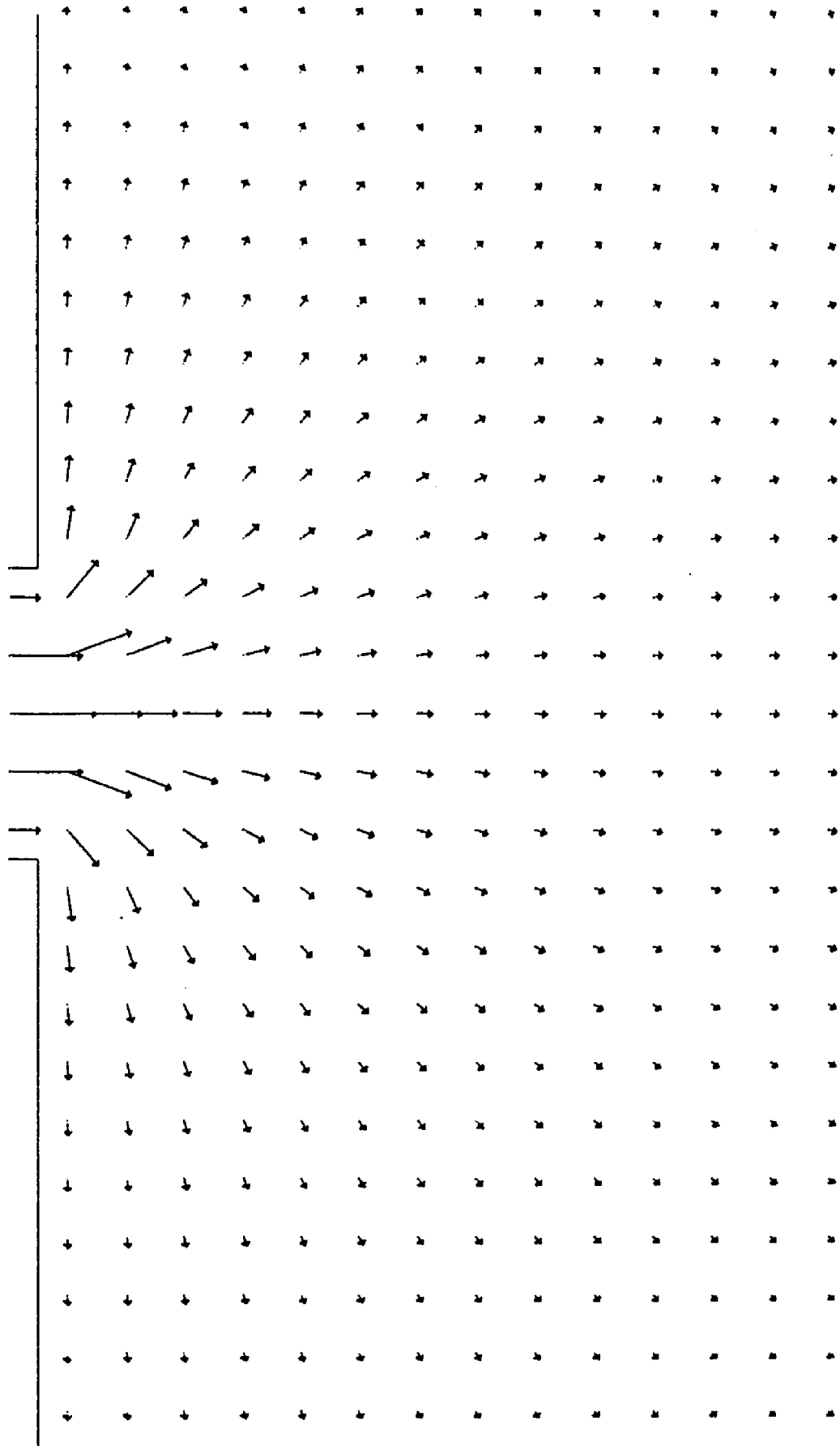


Figure 29 - Velocity vector plot, oscillating jet at maximum ebb and with Coriolis force

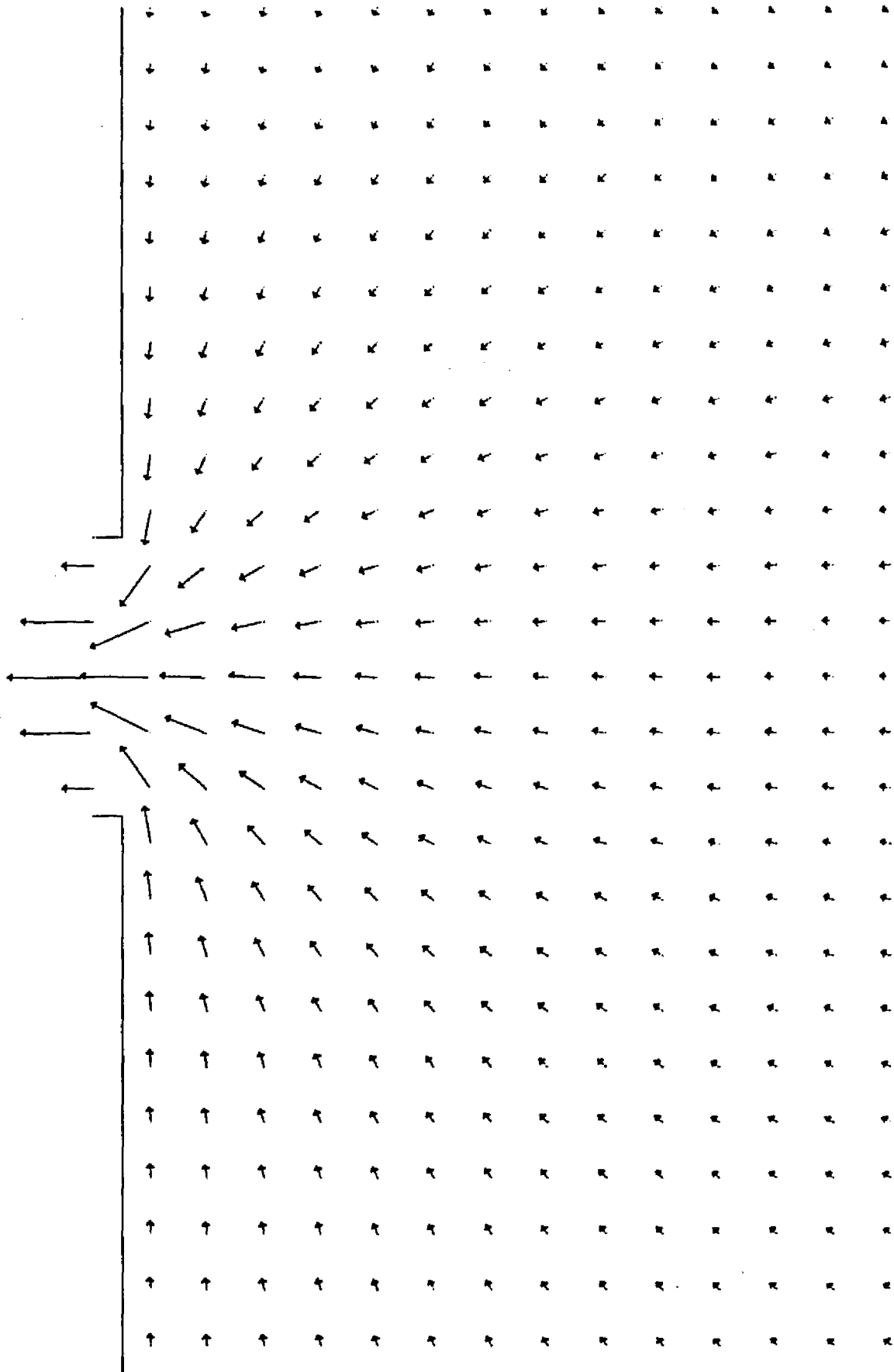


Figure 30 - Velocity vector plot, oscillating jet at maximum flood and with Coriolis force

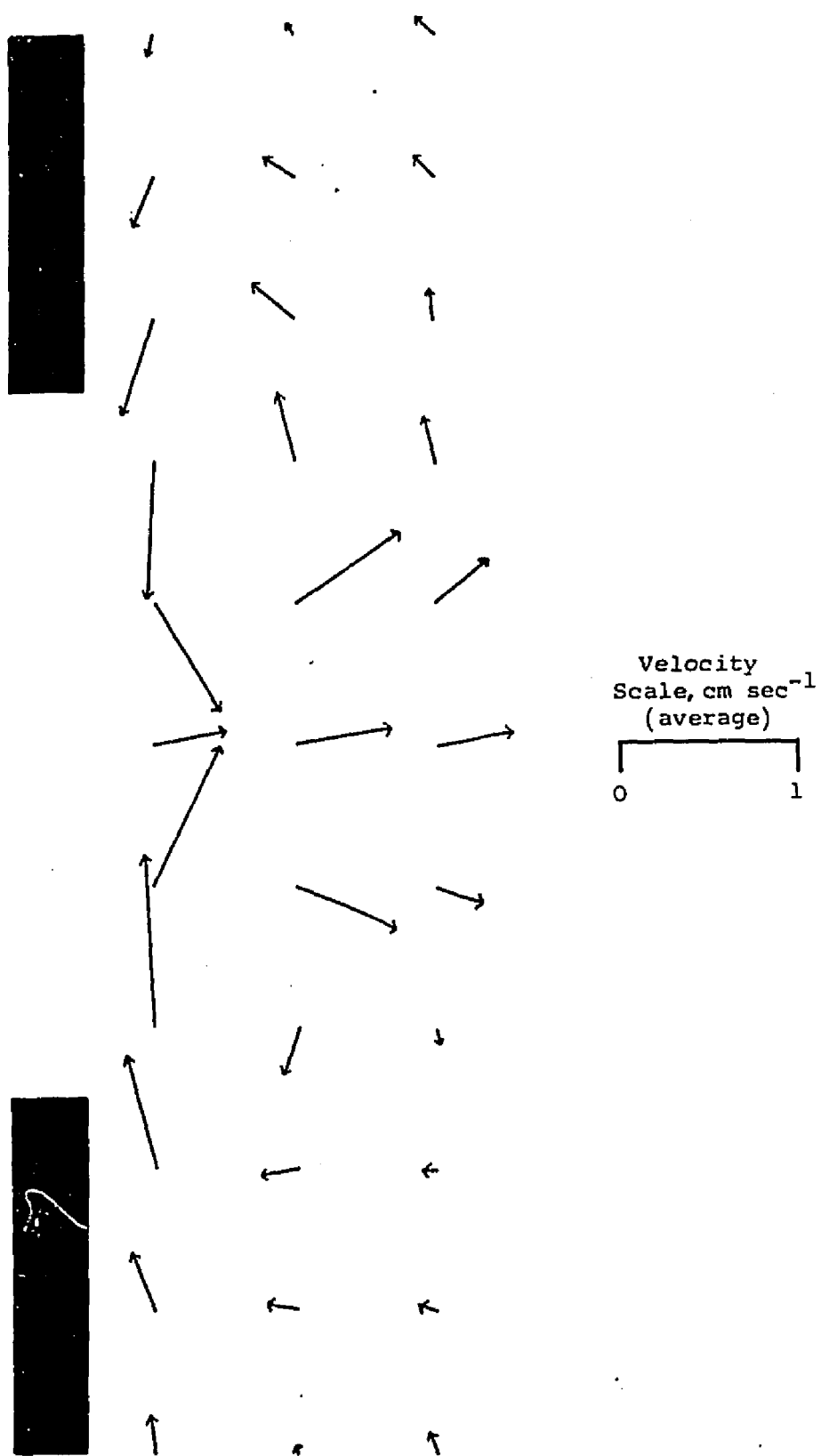


Figure 31
Tidal average flow, oscillating jet with Coriolis force

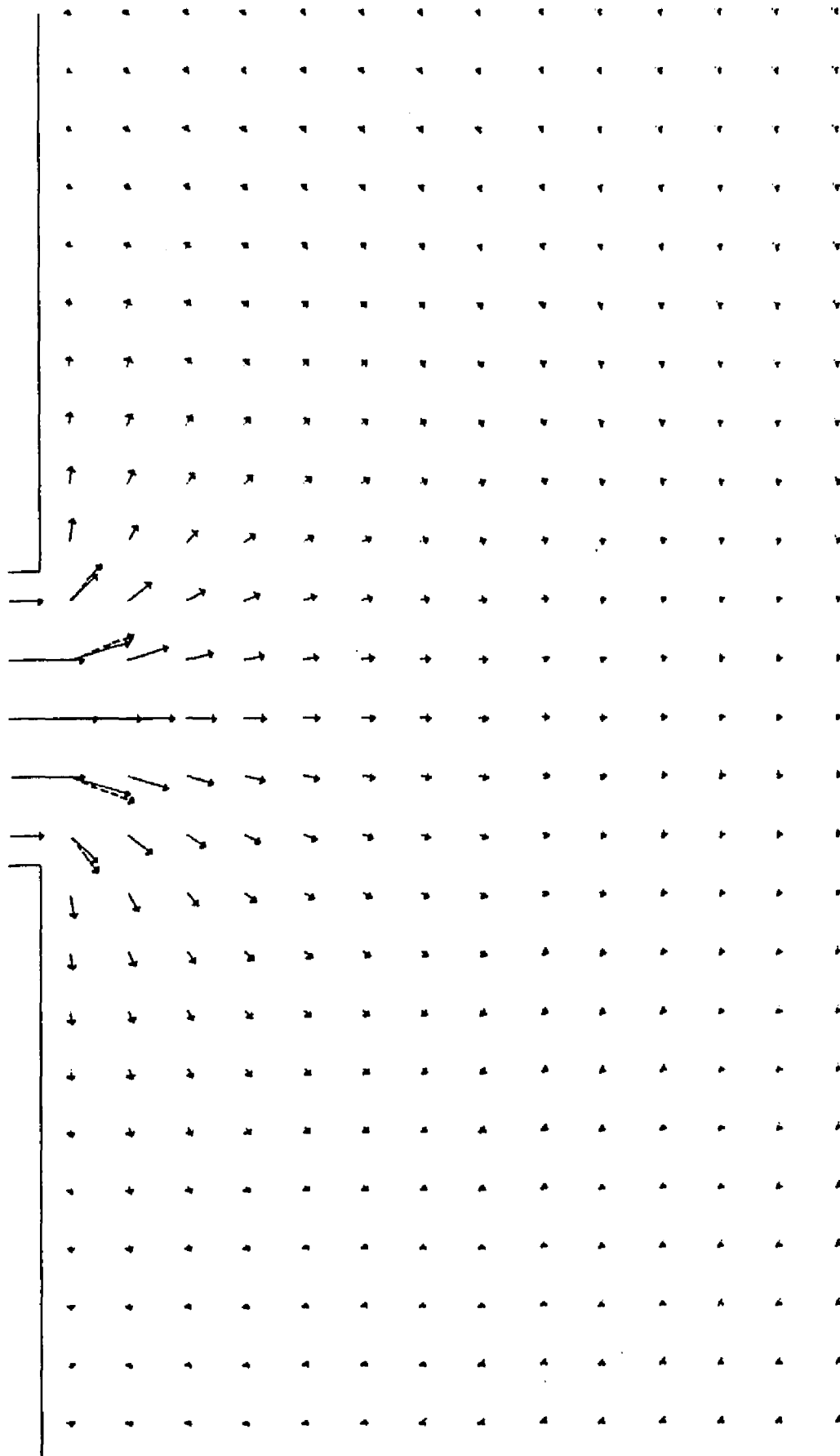


Figure 32 - Velocity vector plot, oscillating jet
at maximum ebb and with sloping bottom

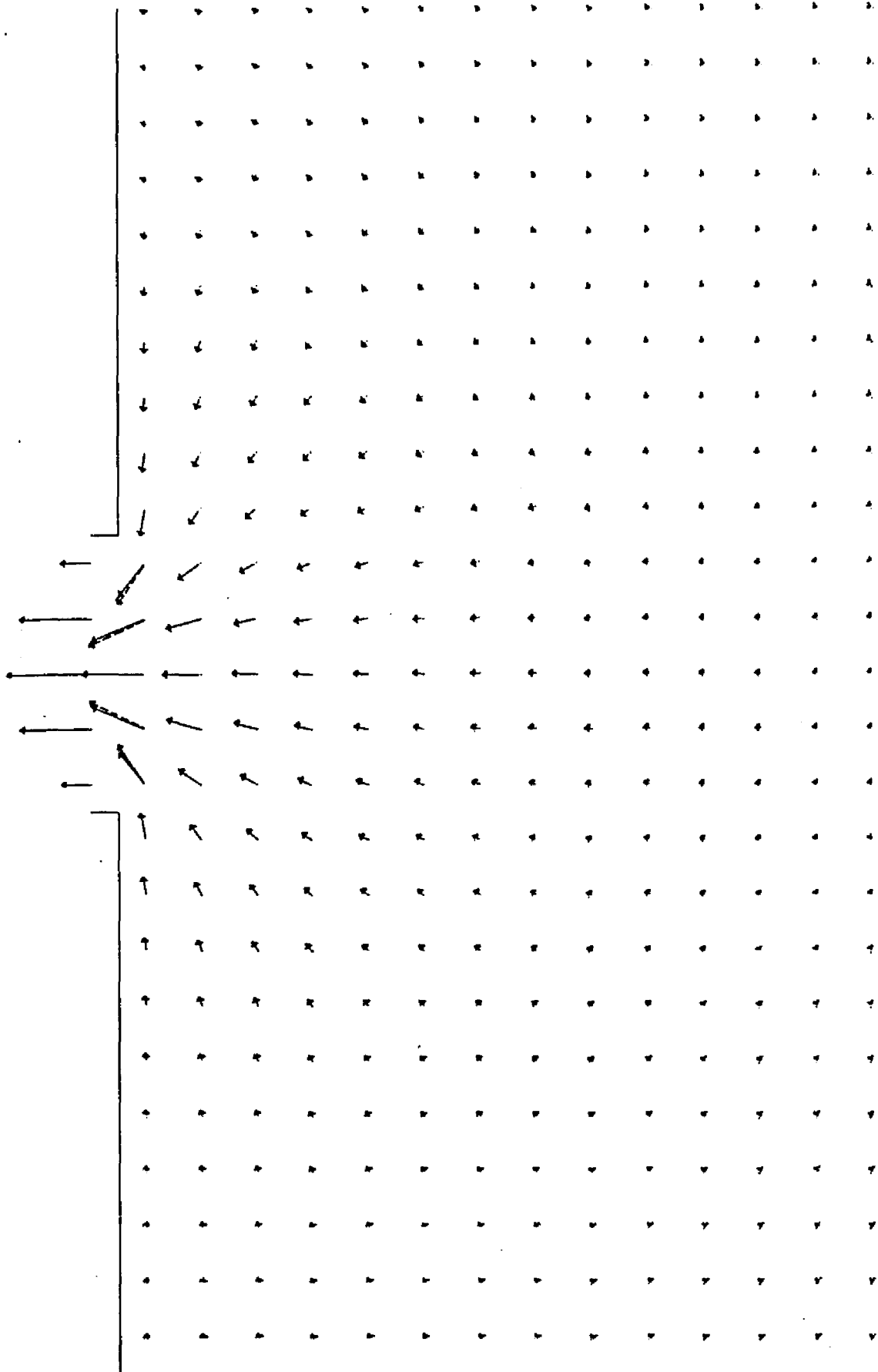


Figure 33 - Velocity vector plot, oscillating jet at maximum flood and with sloping bottom

causes the jet to change slightly in shape. This is illustrated by the dashed vector lines in Figures 32 and 33. The dashed lines located near the mouth of the Bay are the vectors for the Case I oscillating jet at the same grid point and time. From the comparison of the dashed and solid vector lines in Figures 32 and 33, it can be concluded that the sloping bottom causes the jet to be less dispersive during the ebb and less convergent during the flood in the vicinity of the Bay entrance. This result for the ebb case agrees with the laboratory modeling results of Borichansky and Mikhailov (1966), in their work on the interaction of river and seawater in the absence of tides. Further, if the lengths of the vectors are compared for the two cases, it will be seen that generally the magnitudes of the vectors for the flat bottom case are larger than those for the sloping bottom. This is illustrated by the centerline velocity during ebb, Figure 28.

Finally, it is believed that the causes of the dispersive and convergent characteristics of the jet are the same as those described for Case I of the oscillating and Case I of the steady-state jets.

Cases IV and V - These cases are for the effect of wind stress and are discussed below. The value of the wind stress τ^s used was for a wind of 15 knots. The wind stress

is defined as $\tau^s = 2.6 \times 10^{-3} \rho_a' (W')^2$, where ρ_a is the density of air in gm cm^{-3} and W' is the wind speed in cm sec^{-1} at a height of 15 meters above the sea surface. This gave a value of τ^s of 1.9 dyne cm^{-2} for a wind speed of 15 knots (750 cm sec^{-1}). Two cases were run: Case IV, where the wind was on-shore, and Case V, for a northerly wind. The results are shown in Figures 34 through 37.

Case IV - Figures 34 and 35 show the vector plots at maximum ebb and flood, respectively. During maximum ebb, the outflow along the center of the jet is retarded and the jet is split and deflected, symmetrically, north and south. A plot of the centerline velocity as a function of distance for maximum ebb is shown in Figure 28. This type of situation creates an area of minimum velocity where the centerline velocity goes to zero. Also, the jet when split is driven parallel and close to the shore.

For the maximum flood case the wind stress drives water toward the Bay and shore, causing two areas of zero velocity above and below the jet.

These two plots are somewhat representative of the flow features for an on-shore wind but must be interpreted with caution. The major difference between the representation in these figures and that which exists in nature is that here the jet mass transport does not change with an on-shore

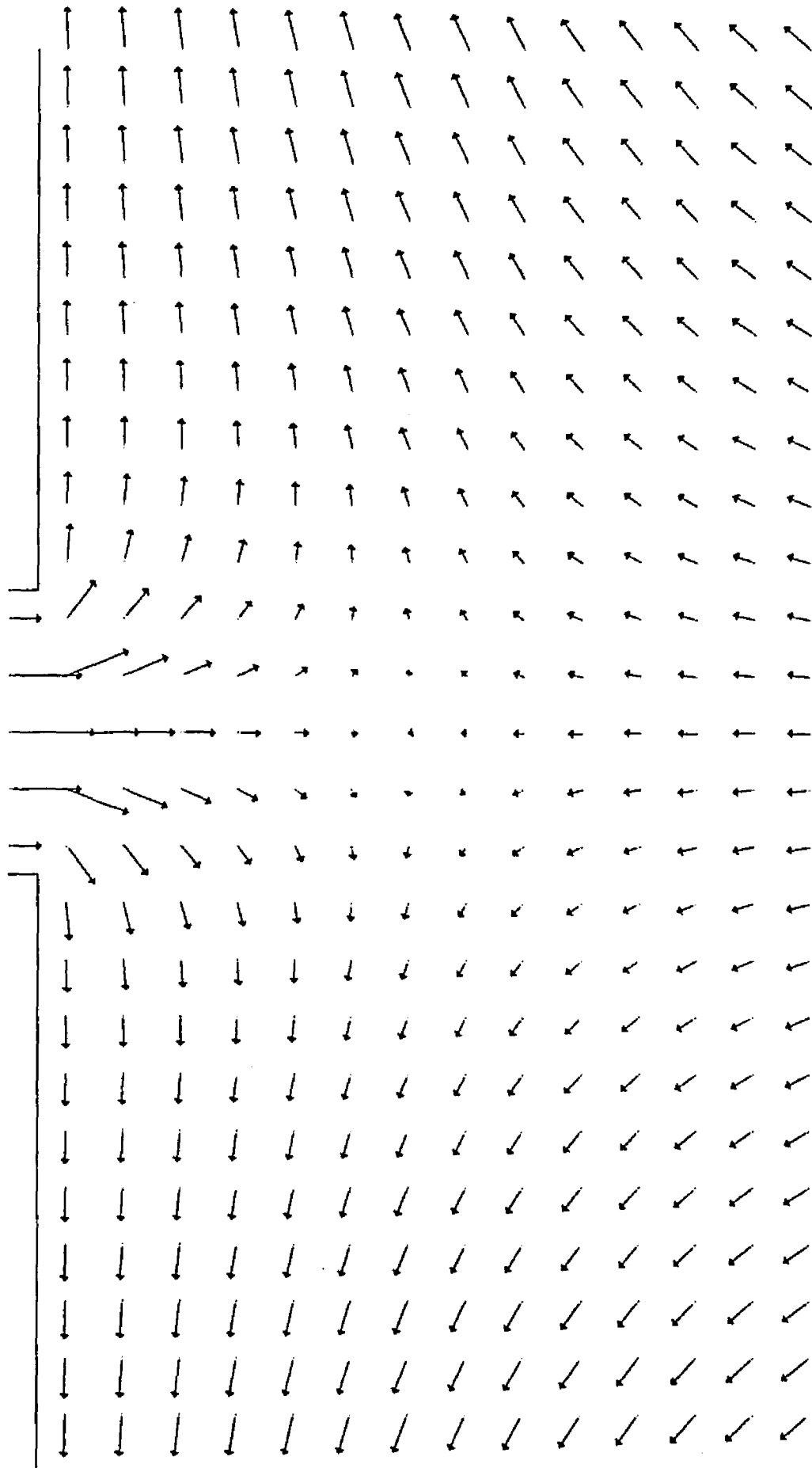


Figure 34 - Velocity vector plot, oscillating jet at maximum ebb and with onshore wind

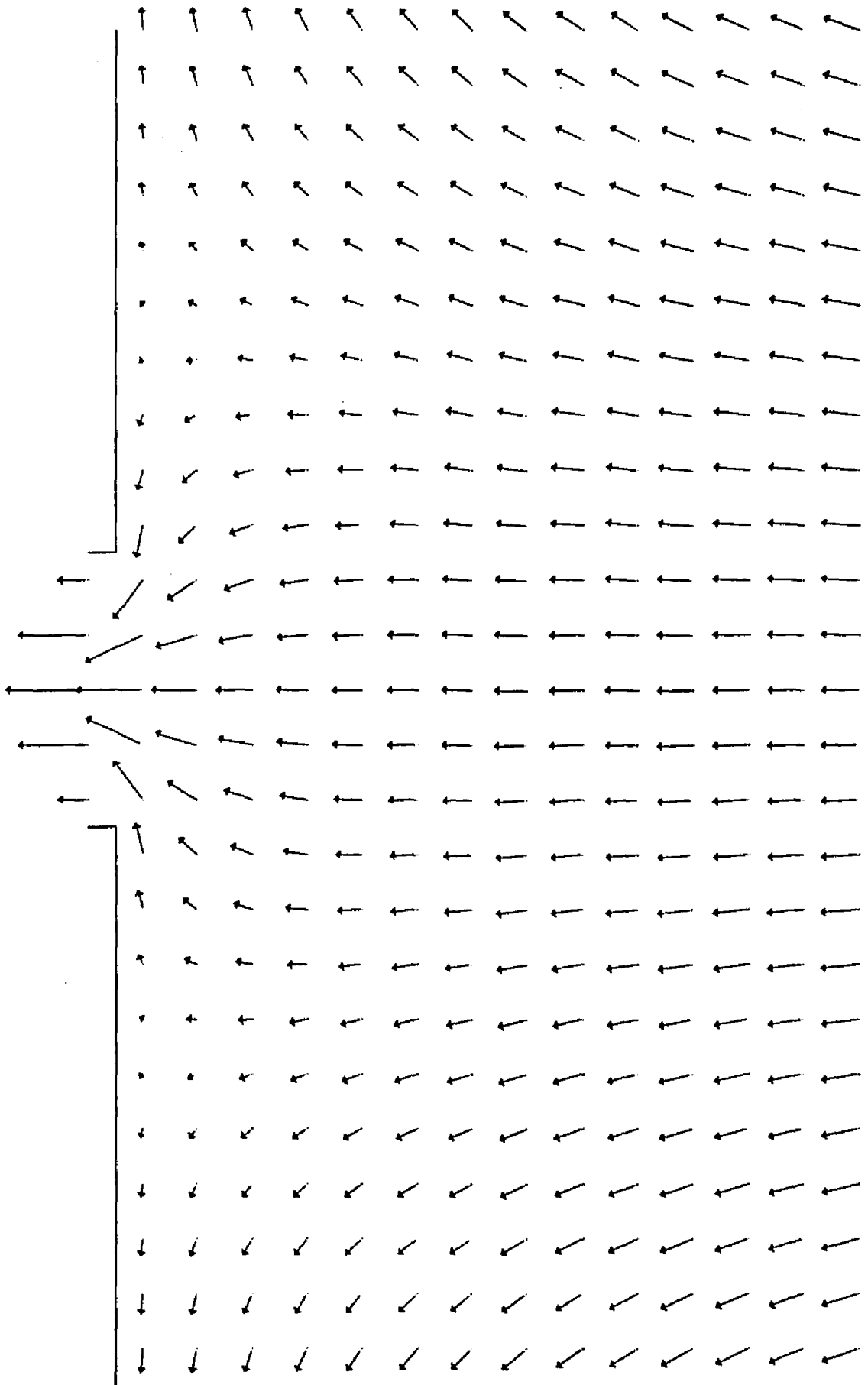


Figure 35 - Velocity vector plot, oscillating jet at maximum flood and with onshore wind

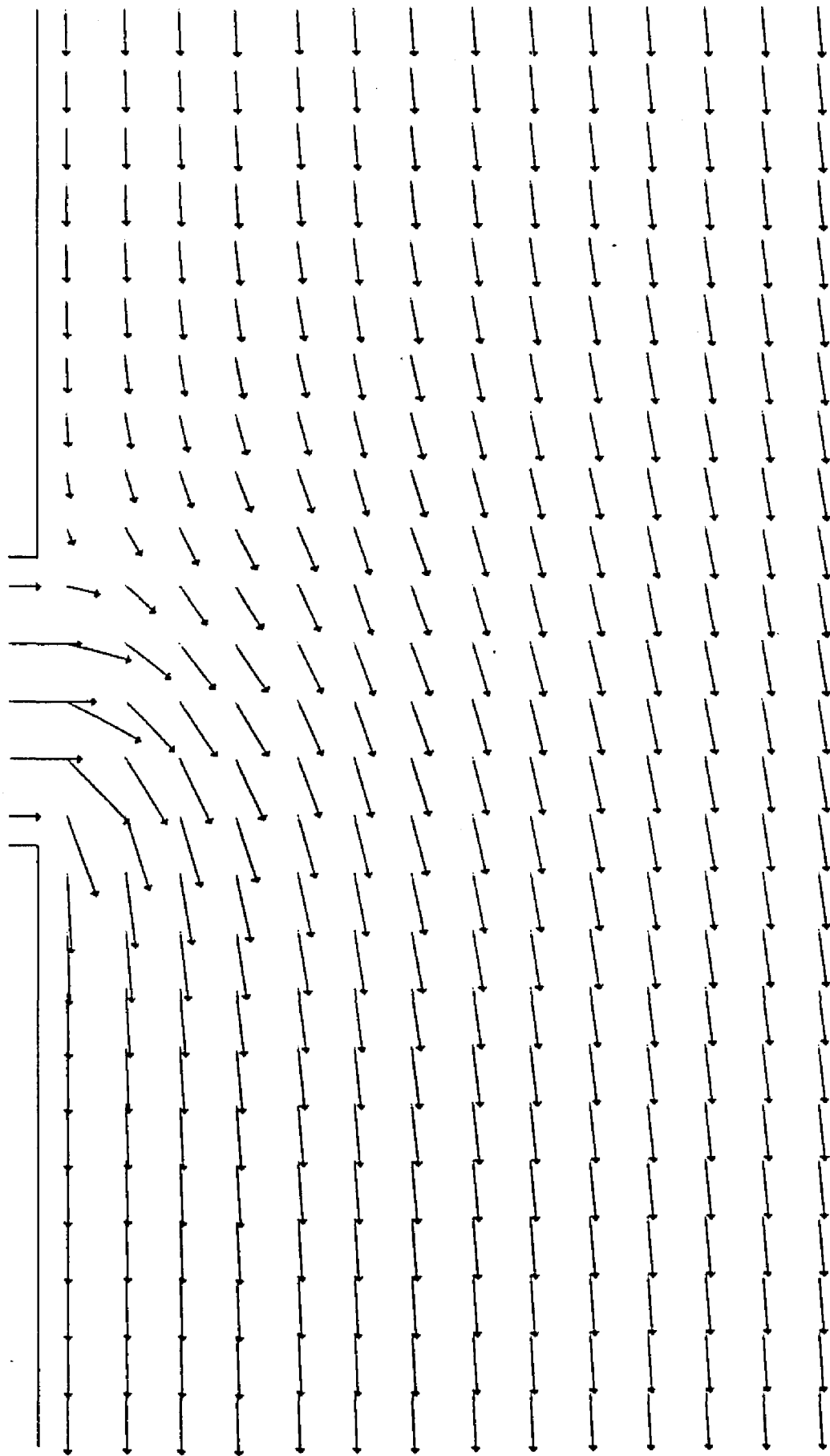


Figure 36 - Velocity vector plot, oscillating jet
at maximum ebb and with northerly wind

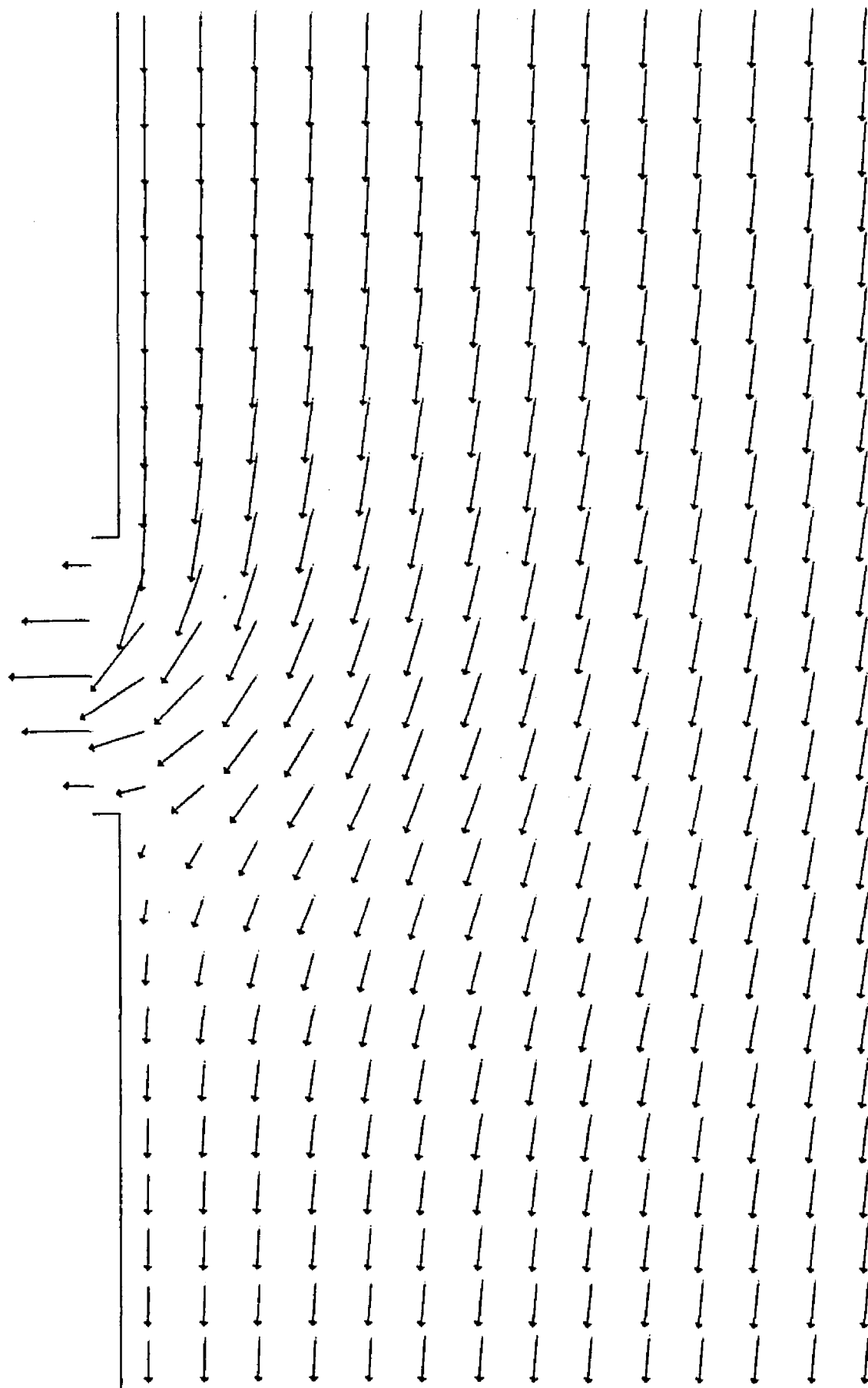


Figure 37 - Velocity vector plot, oscillating jet
at maximum flood and with northerly wind

wind. Stated another way, there is no provision made for mass movement into the Bay, caused by the wind, using the velocity as a boundary condition. Therefore, the plots as shown in Figures 34 and 35 probably have features which would not be seen in a true coastal situation. The important conclusion from studying these two figures is that an on-shore wind can be very effective in changing the flow pattern, and the features given by Figures 34 and 35 are a very general representation of what probably takes place with an on-shore wind.

Case V - Figures 36 and 37 show the results of a north wind blowing over the shallow continental sea. Here the flow is deflected south on the ebb and deflected into the Bay on the flood. There seems to be a point of low velocity during the flood stage south of the jet and also a deflection of the vectors toward shore.

Boicourt (1973) and Stommel and Leetmaa (1972), in their studies of the circulation of the water on the continental shelf, pointed out the importance of wind in driving the shelf circulation. Boicourt (1973) and others have noted that a strong west wind will drive water out of the Bay, while a strong on-shore wind will cause an increase in water level in the Bay. While the results of Case IV do not show the mass flux into the Bay by an on-shore wind due to

the oscillating jet boundary condition, the flow patterns generated do indicate that, if a mass flow across the boundary were allowed, there would be a net flow into the Bay.

The effect of the wind parallel to shore has also been noted in the literature. Budringer, et al (1964), and Duxbury, et al (1966), as quoted by Boicourt (1973), in their description of the Columbia River outflow, assign the cause of outflow deflection to the north in the summer and to the south during the winter to the prevailing winds present during these seasons.

The results from Case V indeed suggest that the stress caused by the wind is a much more dominant force than the Coriolis force and is just as effective as an ambient velocity in deflecting the outflow.

Finally, it will be noted that eddies were not generated in either Case IV or Case V.

Case VI - The final case is one with an ambient velocity imposed upon the situation of Case I. Because the north-south boundary conditions for an oscillating jet are tidal heights, the initial and boundary conditions had to be changed from those of Cases I through IV. The ambient velocity was generated by raising the northern boundary either 5 or 11 cm above datum to give a velocity flowing

south of approximately 5 and 10 cm sec⁻¹, respectively, across the shelf.

This slope is not a unique condition. Stommel and Leetmaa (1972) in their model of the shelf circulation pointed out the importance of the sea surface slope in their coastal model. Sturges (1974) has discussed the slope of the sea surface in this region and described the seasonal variation of sea level at Norfolk, Virginia. Sturges (1974) estimates the slope of the sea surface in the region being modeled as 2.0 ± 0.4 cm/degree or 0.023 to 0.04 cm/nm. For the grid used here the slope was 0.052 and 0.104 cm/nm. It is recognized that most reported shelf velocities for this region are estimated to be 5 cm sec⁻¹ or less; thus, a slope of 0.052 cm/nm approaches a more realistic situation. The importance of small changes in water level here and in the previous cases for both the steady-state and oscillating jets illustrates the need for a good understanding of the permanent, seasonal, and daily variations of the sea surface in order to accurately predict the flow.

Initial conditions for the run were $U = V = 0, \delta = f(y)$. Boundary conditions for the western boundary remained the same, while for the eastern boundary $\delta = f(y)$. For the northern boundary $\delta = 5$ or 11, and for the southern boundary

$\delta = 0$. The results of the computations are shown in Figures 38 through 41 for the maximum ebb and flood of the second tidal cycle with a northern boundary of $\delta = 5$ and 11, respectively.

For Figures 38 and 40 several features can be noted: a quicker turning of the jet by the ambient current than for Case IV of the steady-state jet, a northern velocity which goes to zero along the coast and above the jet, and a confinement of the jet closer to shore.

The rapid turning of the flow by the ambient velocity once it leaves the Bay (Figures 38 and 40) is caused by three factors. First, the ambient velocity is almost constant across the shelf and, therefore, its value near shore is not zero as in the case for the steady-state jet. Second, the magnitudes of the ambient currents used are greater than the 4 cm sec^{-1} used for the steady-state case. Third, the jet velocity is not maintained constant at maximum ebb speed.

Thus, the ambient velocity in these two cases is a more effective factor for the deflection of the jet than the Coriolis force.

The northern velocity along the coast above the Bay entrance has been verified by several observers, Harrison, et al (1967), Bumpus (1969), and discussed in Case IV of

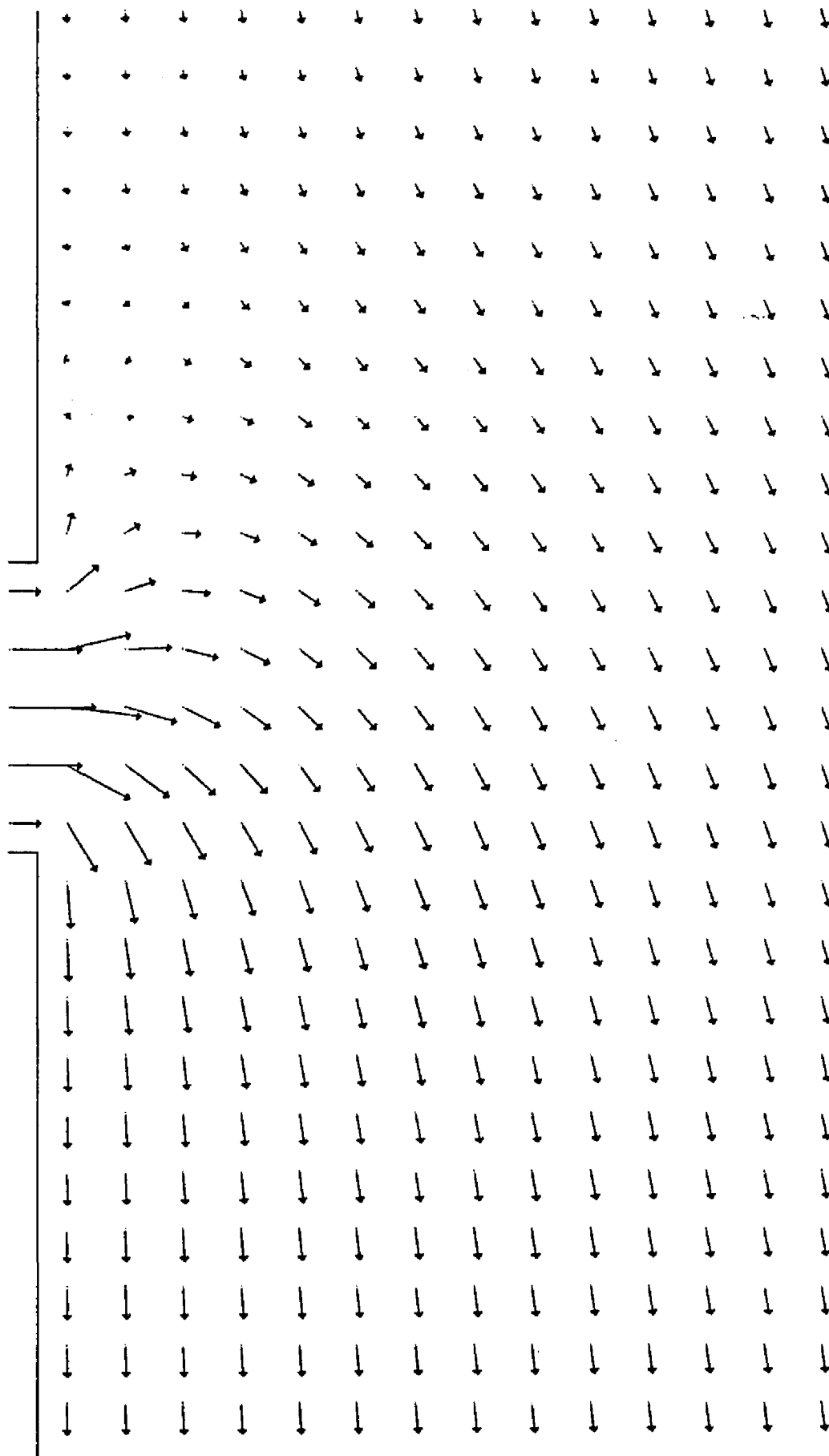


Figure 38 - Velocity vector plot, oscillating jet at maximum ebb and with a southerly ambient velocity of 5 cm sec^{-1}

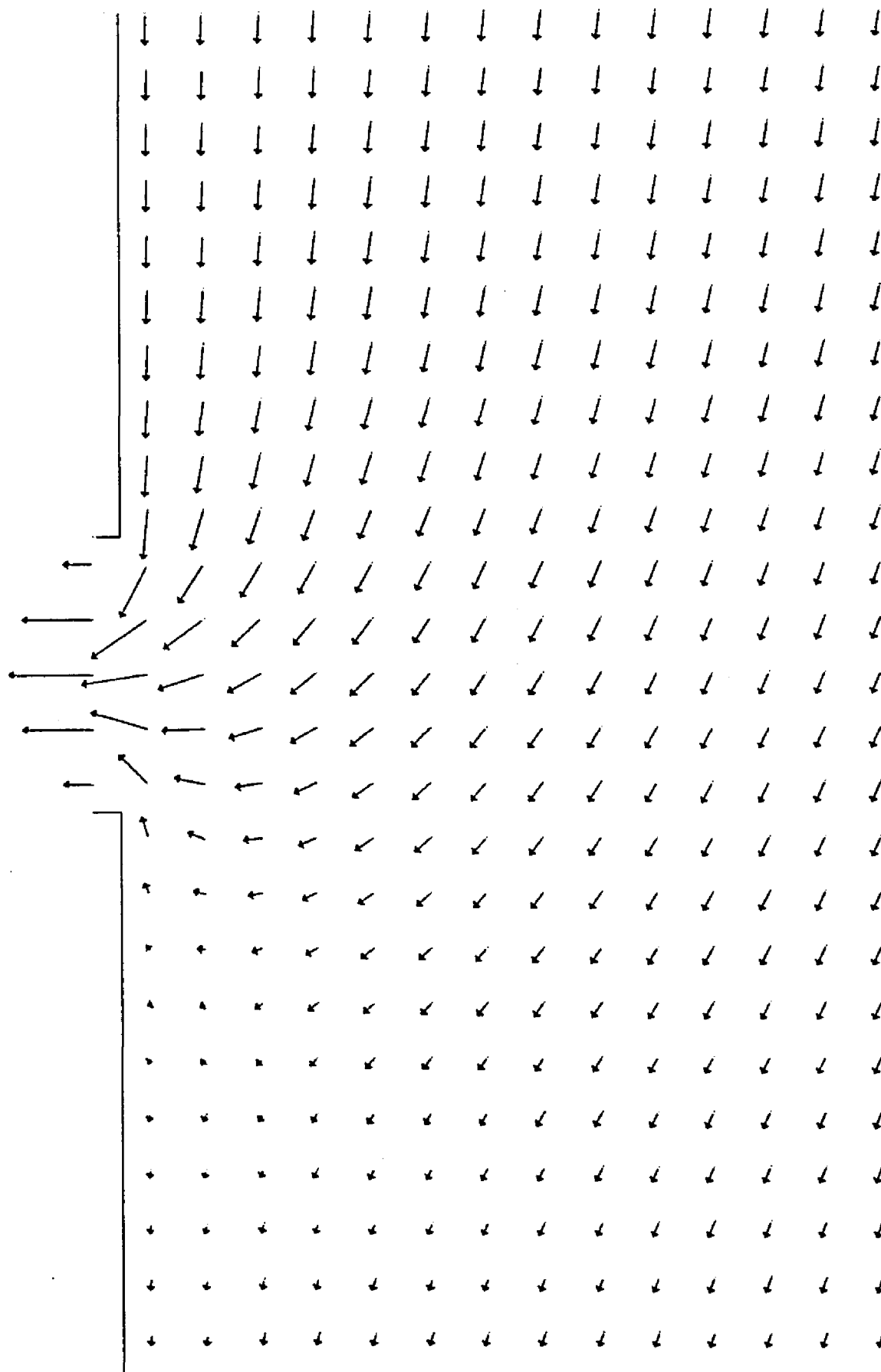


Figure 39 - Velocity vector plot, oscillating jet at maximum flood and with a southerly ambient velocity of 5 cm sec^{-1}

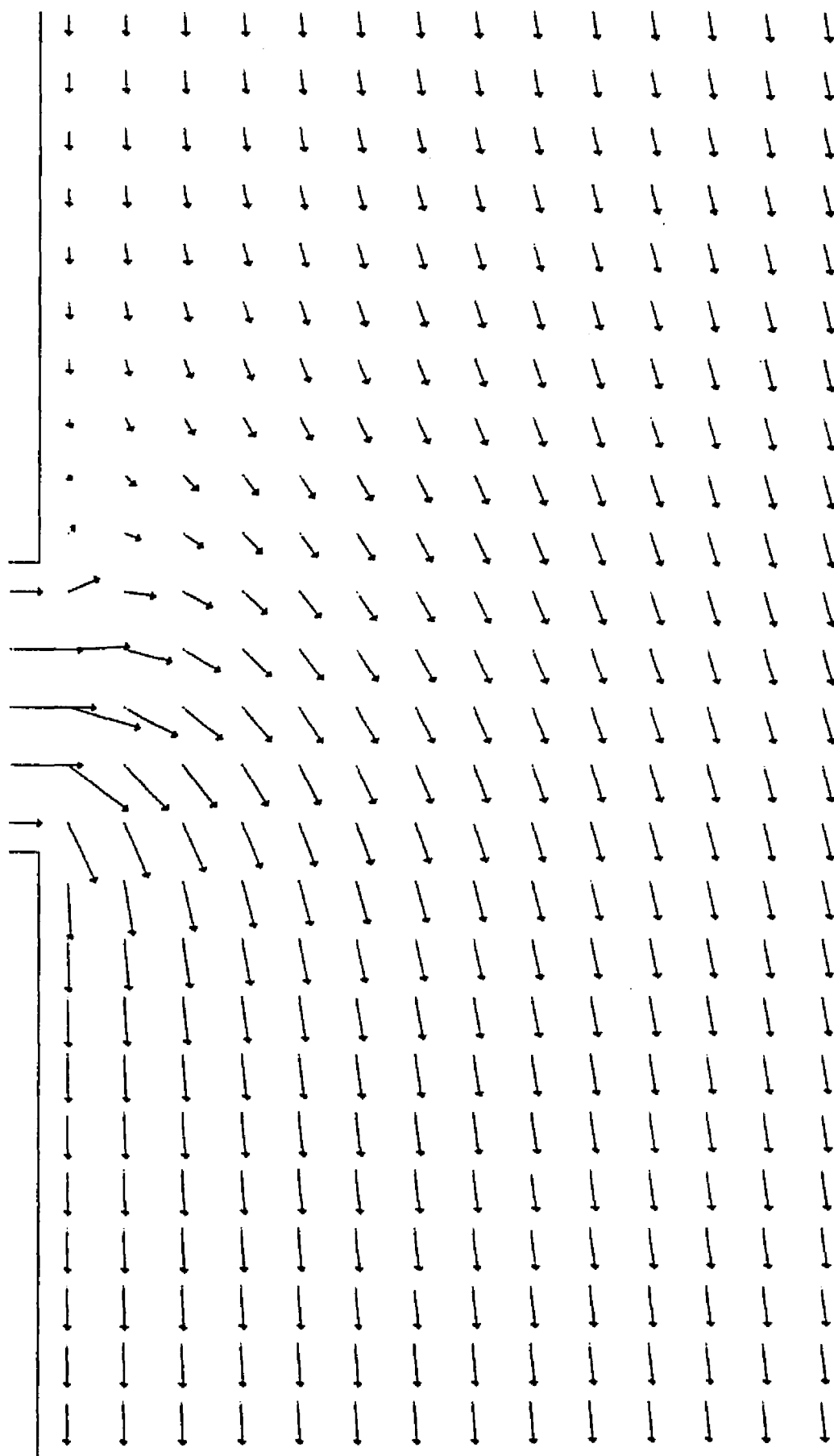


Figure 40 - Velocity vector plot, oscillating jet at maximum ebb and with a southerly ambient velocity of 10 cm sec^{-1}

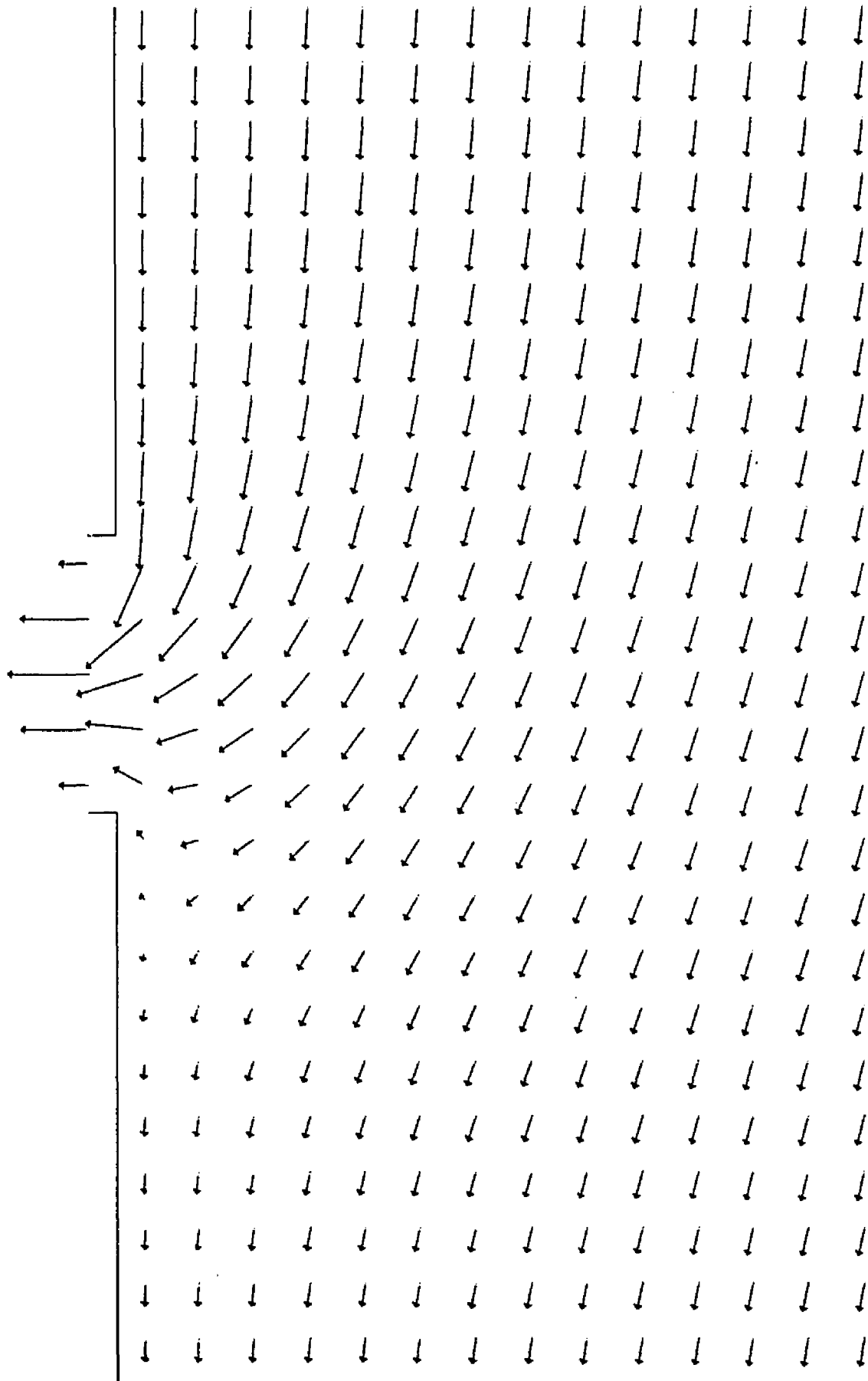


Figure 41 - Velocity vector plot, oscillating jet at maximum flood and with a southerly ambient velocity of 10 cm sec^{-1}

the steady-state jet. Figures 38 and 40 show the way this feature could be limited to an area of coastline just above the Bay entrance and how it can vary with strength of the wind and outflow from the Bay.

Figure 42 is a plot of the salinity distribution on the continental shelf for the month of July 1972. This figure outlines the direction of flow from the Chesapeake Bay when it leaves the entrance. The similarity of the flow pattern of Figure 42 when compared with Figures 38 and 40 is apparent. However, there are some differences which should be noted.

Boicourt (1973) points out that the isohalines leave the Bay entrance at an angle. Current meter observations of Boicourt (1973) and Kuo (Virginia Institute of Marine Sciences, private communication) indeed show that the currents at places in the Bay entrance exit in a direction more southeasterly than due east. This is probably caused by the main channel which also exits in a southeast direction. This fact, along with the ambient southern velocity, probably causes the current to be confined along the coast in a more narrow band than is shown in Figures 38 and 40. Boicourt (1973) has also pointed out that the salinity pattern off the Bay entrance will be a function of the wind and volume of flow out of the Bay. Thus, while the salinity

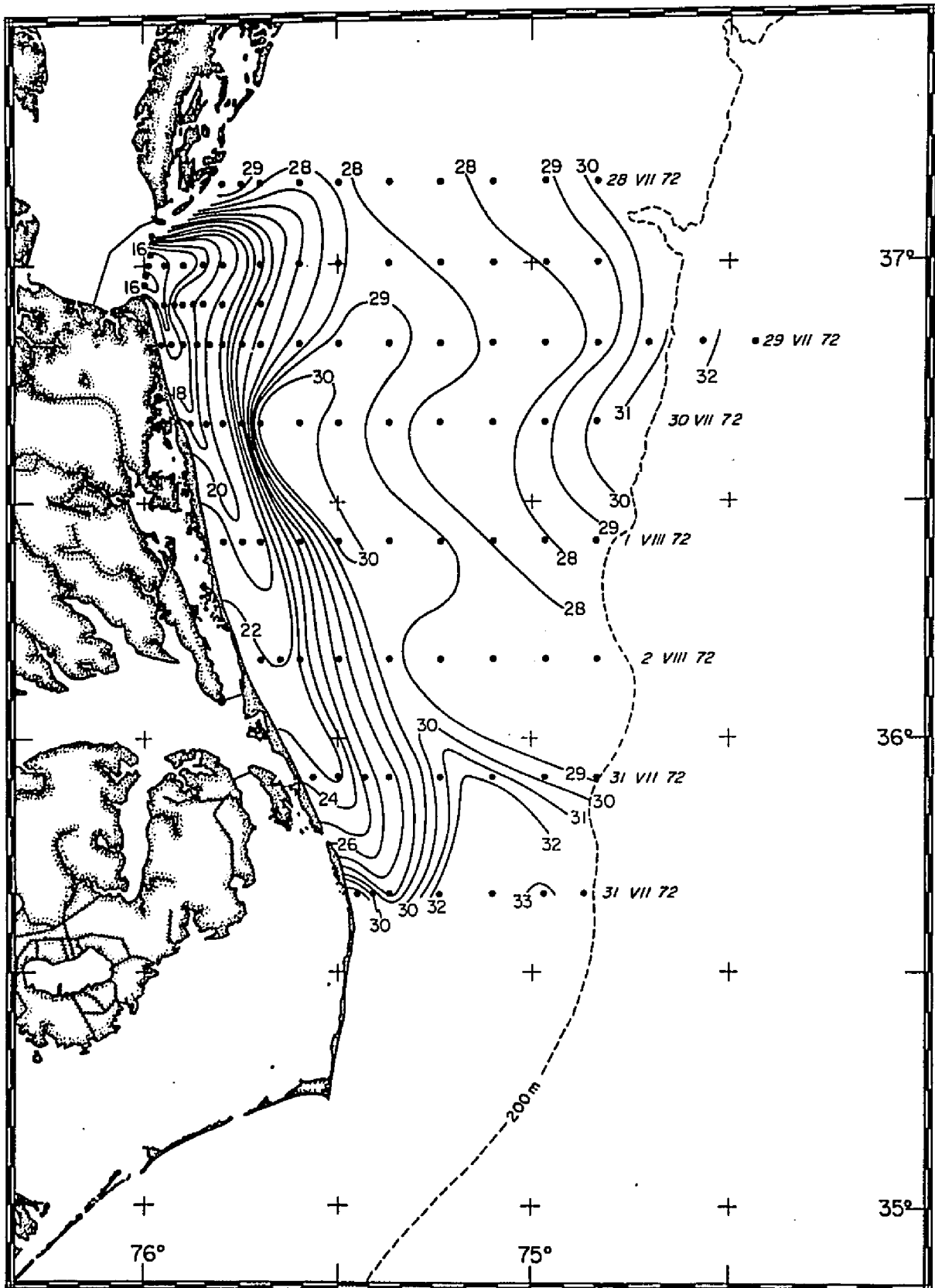


Figure 42
Chesapeake Bight surface salinity distribution
July-August 1972

pattern of Figure 42 verifies in a general way the flow pattern of Figures 38 and 40, the final results will be functions of many variables, some not considered in the discussion of this case.

The flow patterns for the flood tide, Figures 39 and 41, also show three prominent characteristics: a turning of the southerly flow into the Bay, a point of minimal velocity south of the Bay entrance where the flow seems to split, and a weakness of the southerly flow below the Bay entrance. Figures 39 and 41 compare well with the flow patterns into the Bay composed by Boicourt (1973) and described by Harrison, et al (1967).

The flow was averaged over a tidal cycle (for the same points used in Cases I and II) to see if there was an eddy present. The southward, 5 cm sec^{-1} , flowing ambient velocity wiped out the eddy so that no traces of it were found. From an Eulerian standpoint, the eddy has been destroyed.

Finally, Figure 43 shows a series of vector plots for selected points and conditions over a complete tidal cycle. Figure 43a shows for comparison the vectors for Case I at the point $m = 3$ and $n = 22$ (above the Bay mouth). This figure shows a slight rotary characteristic for the tide. Figure 43b is for the same point but with an ambient velocity of 5 cm sec^{-1} south. Figure 43c is for the point

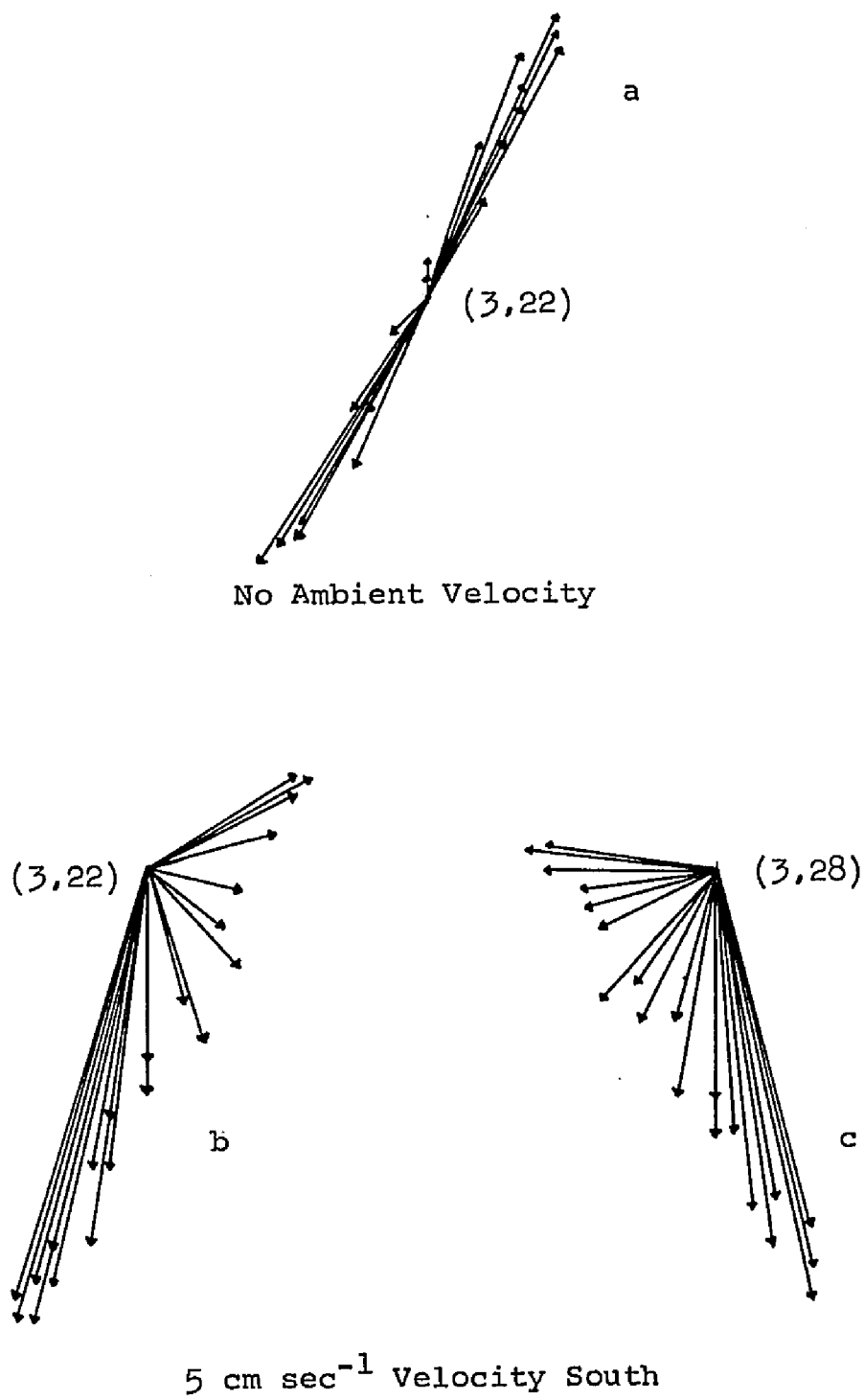


Figure 43
Velocity vector roses at two grid points

$m = 3$, $n = 28$ (below the Bay mouth) and with an ambient current of 5 cm sec^{-1} . Both of these figures show a more diversive spread of the vectors due to the ambient current.

CHAPTER VII
CONCLUSIONS AND RECOMMENDATIONS

The intent of this investigation was to discern the resultant flow fields arising from the discharge of a tidal estuary or river onto the continental shelf using the continuity, momentum, and mass balance equations. The approach was to numerically model the area, simplify the geometry and physical situation where possible, and determine the relative effect of different physical factors on the flow. The model developed in Chapters II through V and the results of its application given in Chapter VI have accomplished this. The results, while for much simpler cases than arise in nature, nevertheless are useful and applicable toward understanding natural situations.

Conclusions

From the results and discussion of Chapter VI it can be concluded that the outflow from a tidal or non-tidal estuary or river onto a continental shelf can be broken into three types: dispersive, in which the velocity vectors diverge from the centerline; entraining, in which the velocity vectors converge toward the centerline; or a combination of the two. The final type will be governed by the degree

of bottom and side frictions, the bottom slope, and the level of the water above datum at the Bay entrance.

The centerline velocity of the bottom friction steady-state jet studied was found to decrease much more rapidly than the side friction cases reported in the literature. Cross-stream U velocities for the same bottom friction case were a function of $\text{sech}^2 y$. For a steady-state jet which considers both side and bottom friction, the centerline velocity profile was found to be a combination of the pure side and bottom friction cases.

For the model case of the Chesapeake Bay, it was determined that the outflow is dispersive, with a centerline velocity decreasing to less than half its maximum velocity in one jet width. Field observations of estuaries other than the Chesapeake Bay verify the rapid velocity decrease along the centerline, but no information was found on the characteristics of the cross-stream velocity distribution. The velocity distribution both along the centerline and laterally will be affected by the wind and ambient currents in the vicinity of the discharge so that field verification of these profiles will be difficult.

From the results of all the cases studied, the slope of the sea surface relative to mean sea level is very important in controlling the movement of the shelf waters, as previously mentioned. For the area studied (Chesapeake Bight) the sea surface slope needed to generate an ambient current, corresponding to currents found by field measurements, agreed with leveling observations by a factor less than two. Small value of the sea surface slope needed and the sensitivity of the model to it suggest that in a natural environment both the permanent sea level height and the seasonal and tidal variations should be accurately known in order to model and predict the shelf circulation, particularly if tidal heights are used as a boundary condition. For modeling purposes it is estimated that this water level should be known to within at least 1-2 cm.

The Coriolis force has often been considered to be the most important factor for generating the turning of an estuary or river (in nature) as it empties onto a shelf. In contrast, for the cases studied, the Coriolis force was not found to be a controlling factor in the turning of the outflow. This turning is believed to be masked by the effect of bottom friction and is illustrated by the large values of the Ekman number (≥ 1) for the cases used.

Thus, the cases studied suggest that, if in nature the bottom friction and the inertial terms are dominant, the wind and ambient current are more important factors in the deflection of the outflow than the Coriolis force.

For the steady-state jet no eddies were found in all four cases investigated. For the oscillating jet eddies were found for Cases I and II after the tidal component was averaged out. The effect of the Coriolis force in Case II was to decrease the strength of the southern flow of the eddies and increase the strength of the northern flow. This also confirms the results reported by other investigators.

This study substantiates the reversal of flow in the circulation pattern above the Bay entrance that has been reported by other investigators both for the Chesapeake Bay and other areas in the Mid-Atlantic Bight. From the model studies, the strength of this reversal will be a function of the strength of the ambient current, dispersion of the outflow from the Bay or river entrance, and wind. The flow can also be tidal dependent.

Results from the modeling efforts show that tidal height or velocity can be used for an open boundary condition. However, if velocity is used, care must be taken to assure that reflection from the boundary does not occur.

This problem can be eliminated by the use of tidal heights for the open boundary conditions, which most investigators use in a model of this type.

The multi-operational techniques used here have proven to be stable and fast. The technique is a more economical way to calculate data than a purely explicit scheme.

Recommendations

Recommendations for future work in the use of this or other models in studying the coastal flow in the vicinity of the Chesapeake Bay entrance can be divided into two general categories: intermediate and advanced.

For the intermediate step, several features and/or factors which were not included in this study should be examined. These are: (1) a more detailed evaluation of the mass conservation of the numerical scheme to verify Leendertse's work; (2) incorporation and use of the mass transport equation to study the effect of simple salinity and density variations on the flow patterns; (3) altering the Bay's discharge to the southeast to observe the difference in flow characteristics above and below the Bay entrance; (4) sloping the bottom to approach a depth of zero near the coast and varying the bottom friction terms to more accurately represent the near shore circulation; (5) development and use of the side friction terms; and (6) use of a jet (to

simulate the Bay discharge) interacting with a tidal wave propagating normal to the coast to more nearly approximate the true environmental situation in the Chesapeake Bight.

For the advanced category expansion of the models to three dimensions to investigate the layered flow in the Chesapeake Bight is desirable. However, the cost of developing and using a model of this type may be prohibitive. Further, sufficient field data on the tidal and non-tidal circulation in the coastal zone during a typical summer and winter condition are needed to calibrate both the two- and three-dimensional models. The size and cost of a field program of this nature would depend on the area of interest and extent of modeling undertaken.

APPENDIX A
ORDER OF MAGNITUDE ESTIMATE

Compare the magnitudes of

$$-\frac{gH^2}{\bar{\rho}L} \frac{\partial \bar{\rho}}{\partial x} \quad \text{A.1}$$

and

$$-\frac{g}{\bar{\rho}} \frac{\partial}{\partial x} \int_{-h}^{\delta} \left(\int_3^{\delta} \rho' dz \right) dz. \quad \text{A.2}$$

By using the first two terms of Taylor series, let

$$\rho(z) \approx \bar{\rho} + \left. \frac{\partial \rho}{\partial z} \right|_{z=z_0} (z-z_0) \quad \text{A.3}$$

where z_0 is the position in the vertical at which the density equals $\bar{\rho}$. Now using 2.21 and A.3 and evaluating $\partial \rho / \partial z$ at

$z = z_0$ gives

$$\rho' = \rho - \bar{\rho} \approx \left. \frac{\partial \rho}{\partial z} \right|_{z_0} (z-z_0) \quad \text{A.4}$$

Integrating A.4 from z to δ yields

$$\int_3^{\delta} \rho' dz \approx \left. \frac{\partial \rho}{\partial z} \right|_{z_0} \left[\frac{(\delta-z_0)^2}{2} - \frac{(z-z_0)^2}{2} \right]. \quad \text{A.5}$$

Integrating A.5 from $-h$ to δ and combining terms gives

$$\int_{-h}^{\delta} \left(\int_3^{\delta} \rho' dz \right) dz \approx \left. \frac{\partial \rho}{\partial z} \right|_{z_0} \left[\frac{2}{3} (\delta-z_0)^2 + \frac{1}{3} (\delta-z_0)(h+z_0) - \frac{1}{3} (h+z_0)^2 \right] \quad \text{A.6}$$

Assuming $z_0 = (-h + \delta)/2$ and substituting into A.6 gives

$$\int_{-h}^{\delta} \left(\int_3^{\delta} \rho' dz \right) dz \approx \frac{H^3}{12} \left. \frac{\partial \rho}{\partial z} \right|_{z_0}. \quad \text{A.7}$$

Now substituting A.7 into A.2 yields A.8, a form of A.2 whose magnitude can be evaluated

$$-\frac{g}{\rho} \frac{\partial}{\partial x} \left(\frac{H^3}{12} \frac{\partial \rho}{\partial z} \right) \approx \frac{g}{\rho} \frac{H^2}{12} \frac{\partial}{\partial x} \Delta \rho \quad \text{A.8}$$

where $\Delta \rho$ is the density variation over the water column.

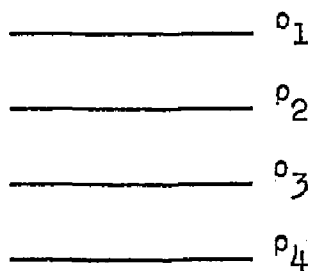
The relative magnitude of A.8 and A.1 is then

$$\frac{-\frac{g}{\rho} \frac{H^2}{12} \frac{\partial \Delta \rho}{\partial x}}{-\frac{g}{\rho} \frac{H^2}{2} \frac{\partial \bar{\rho}}{\partial x}} = \frac{1}{6} \frac{\frac{\partial}{\partial x} \Delta \rho}{\frac{\partial \bar{\rho}}{\partial x}} = R. \quad \text{A.9}$$

Equation A.9 is a ratio of A.2 to A.1. If this ratio is ≤ 0.1 (A.1 $>$ A.8 by a factor of 10 or more), then equations 2.39 and 2.40 are valid. Simple examples of density distributions where term A.2 can be ignored are shown below:

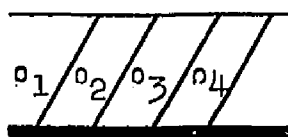
$\rho = \text{constant}$	$R = \frac{1}{6} \frac{0}{0} = \frac{0}{0}$
--------------------------	---

<table style="border-collapse: collapse; width: 100%;"> <tr> <td style="border-right: 1px solid black; padding: 5px; text-align: center;"> $\rho_1 = \text{constant}$ </td> <td style="padding: 5px; text-align: center;"> $\rho_2 = \text{constant}$ </td> </tr> </table>	$\rho_1 = \text{constant}$	$\rho_2 = \text{constant}$	$R = \frac{1}{6} \frac{0}{\frac{\partial \rho}{\partial x}} = 0$
$\rho_1 = \text{constant}$	$\rho_2 = \text{constant}$		
$\rho_1 \neq \rho_2$			



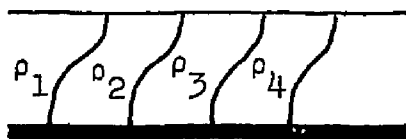
$$R = \frac{1}{6} \frac{0}{0} = \frac{0}{0}$$

$$\rho_1 < \rho_2 < \rho_3 < \rho_4$$



$$R = \frac{1}{6} \frac{0}{\frac{\partial \rho}{\partial x}} = 0$$

$$\rho_1 < \rho_2 < \rho_3 < \rho_4$$



$$\rho_1 < \rho_2 < \rho_3 < \rho_4$$

The general cases where the surfaces of constant density are approximately parallel.

If the density distribution in the water column gives a ratio $R > 0.1$, then term A.2 cannot be ignored and equations 2.39 and 2.40 are not valid. The case $R > 0.1$ would imply the existence of relatively strong vertical stratification and the simulation by a vertically integrated two-dimensional model will not be applicable. Therefore, in the framework

of two-dimensional approximation, it may be assumed that equations 2.39 and 2.40 are valid.

APPENDIX B
TABLE OF EQUIVALENTS

<u>Text Notation</u>	<u>Computer Notation</u>	<u>Text Notation</u>	<u>Computer Notation</u>
f	FC	A _j	1/2DT
g	G	B _j	BX, BY
h	H	C _j	CX, CY
\bar{h}	HAVG	D _j	DX, DY
m	J	E _j	EX, EY
n	K	F _j	G/2L
x	X	H _j	HGX, HGY
y	Y	P _j	PX, PY
C	C*	Q _j	QX, QY
D _i	DX, DY*	R _j	RX, RY
H _{jF} ^{it} , H _{jB} ^{it}	HXF, HYF, HXB, HYB*	T _j	TX, TY
S	S*	A _j [!]	AA _X , AA _Y
\bar{U}	U1A	B _j [!]	BB _X , BB _Y
U	U*	C _j [!]	CC _X , CC _Y
\bar{V}	V1A	D _j [!]	DD _X , DD _Y
V	V*	E _j [!]	EE _X , EE _Y
α	A1	F _j [!]	FF _X , FF _Y
δ	HL*		
ρ	R*		
T _x ^S , T _y ^S	WSX, WSY		
ΔL	L		
Δt	DT		

NOTE: Notations with an asterisk may have a 1 or 2 with them; i.e., S1, U2, HXF1. The variables without a 1 or 2 are the variables at the future time. With a 1 attached they are the variables at the present time, and with a 2 at the past time.

APPENDIX C
COMPUTER PROGRAM

```

PROGRAM MODEL(INPUT=128,OUTPUT=128,TAPE4=1024,TAPES=INPUT,
1 TAPE6=OUTPUT)
REAL L,L1,L2,L3,L4
DIMENSION U(30,50),U1(30,50),U2(30,50)
DIMENSION V(30,50),V1(30,50),V2(30,50)
5 DIMENSION HL(30,50),HL1(30,50),HL2(30,50)
DIMENSION HAVG(30,50),PX(50),QX(50),RX(50),TX(50)
DIMENSION EEX(50),FFX(50)
DIMENSION PY(50),QY(50),RY(50),TY(50)
10 DIMENSION EY(50),FFY(50)
DIMENSION S(30,50),S1(30,50),H(30,50),S2(30,50)
DIMENSION UAN(50)
DIMENSION TITLE(8)
COMMON HJMKH,HL1JK,HJKM1,JM1,KM1,JP1,KP1,HJK,MJM1K,
15 IBX,CX,DCX,E1,E2,E3,EX,HC1A,HC1B,HC1D,HC1,HC2,HC3,HC4A,HC4B,HC4C,
HC4D,HC4,HC5,HC6,HC7,HCX,G,FC, H,HL1,HL2,U, U2,V, V2,S,
IS1,DX,DY,DX1,DY1,R1,C1,HXB1,HXF1,HYB1,HYF1,C,HXF,HXB,HAUG,V1A,A,
IF,L1,L2,L3,L4,WSX,AA1,AA2,AA3,AA4,AA5,BB1,BB2,BB3,CC1,CC2,CC3,CC4,
19 ICCX,DD1,DD2,DD3,DDX,C2,HL,S2,TX,EEX,FFX,RX,L,J,K
COMMON BY,CY,DCY,EY,HCY,AA5,BB3,CCY,DDY,HYF,HYB,WSY,U1A,
20 IC1JP,R1JP,DXJM,DY1KM,CJM,C1KM,C1KP,R1KP,DYKM,DX1JM,CKM,C1JM
EQUIVALENCE (PX,EEX,PY,EY)
EQUIVALENCE (QX,FFX,QY,FFY)
EQUIVALENCE (RX,RY),(TX,TY)
25 EQUIVALENCE (U,U1),(V,V1)
G=980.
HAUG(1,1)=30.
PX(1)=1.
QX(1)=1.
30 RX(1)=0
TX(1)=1.
HL(1,1)=-3
S(2,1)=30.00
UAN(1)=0
35 FC=0
C INPUT OF INITIAL CONDITIONS
READ(5,4)TITLE
4 FORMAT(8A10)
READ(5,5)JMAX,KMAX
40 5 FORMAT(14,14)
WRITE(6,50)JMAX,KMAX
50 FORMAT(11INPUT DATA## JMAX =#14/# KMAX =#14)
READ(5,6)DT,L
6 FORMAT(2F7.0)
45 WRITE(6,60)DT,L
60 FORMAT(1# DT =#F7.0/# L =#F7.0)
READ(5,7)ITMAX
7 FORMAT(14)
WRITE(6,70)ITMAX
50 70 FORMAT(1# ITMAX=#14)
READ(5,8)WSX,WSY
8 FORMAT(2F8.2)
80 FORMAT(1# WSX =#F8.2/# WSY =#F8.2)
WRITE(6,80)WSX,WSY
55 C TAPE WRITING STATEMENTS
WRITE(4)TITLE
WRITE(4)JMAX,KMAX,DT,L,ITMAX,WSX,WSY
MODEL 2
MODEL 3
MODEL 4
MODEL 5
MODEL 6
MODEL 7
MODEL 8
MODEL 9
MODEL 10
MODEL 11
MODEL 12
MODEL 13
MODEL 14
MODEL 15
MODEL 16
MODEL 17
MODEL 18
MODEL 19
MODEL 20
MODEL 21
MODEL 22
MODEL 23
MODEL 24
MODEL 25
MODEL 26
MODEL 27
MODEL 28
MODEL 29
MODEL 30
MODEL 31
MODEL 32
MODEL 33
MODEL 34
MODEL 35
MODEL 36
MODEL 37
MODEL 38
MODEL 39
MODEL 40
MODEL 41
MODEL 42
MODEL 43
MODEL 44
MODEL 45
MODEL 46
MODEL 47
MODEL 48
MODEL 49
MODEL 50
MODEL 51
MODEL 52
MODEL 53
MODEL 54
MODEL 55
MODEL 56
MODEL 57
MODEL 58

```

	DO 3400 K=1,KMAX	MODEL	59
	DO 3300 J=1,JMAX	MODEL	60
60	V1(J,K)=0	MODEL	61
	V2(J,K)=0	MODEL	62
	U1(J,K)=0	MODEL	63
	U2(J,K)=U1(J,K)	MODEL	64
	HL1(J,K)=0	MODEL	65
65	HL2(J,K)=HL1(J,K)	MODEL	66
	H(J,K)=1000.0	MODEL	67
	S1(J,K)=30.00	MODEL	68
	S2(J,K)=30.00	MODEL	69
	3300 CONTINUE	MODEL	70
70	3400 CONTINUE	MODEL	71
	JMAX=JMAX-1	MODEL	72
	KMAX=KMAX-1	MODEL	73
	L3=1./(2.*(L**2))	MODEL	74
75	L4 = 1./(8.*L)	MODEL	75
	L2 = L4 + L4	MODEL	76
	L1 = L2 + L2	MODEL	77
	A=1./DT	ES75001	1
	F = G/(2.*L)	MODEL	79
	DO 200 K=2,KMAX	MODEL	80
80	DO 100 J=2,JMAX	MODEL	81
	HAVG(J,K) = (H(J,K) + H(J,K-1) + H(J-1,K-1) + H(J-1,K))/4.	MODEL	82
	100 CONTINUE	MODEL	83
	200 CONTINUE	MODEL	84
85	DO 300 IT=1,ITMAX	MODEL	85
	C INPUT OF BOUNDARY CONDITIONS	MODEL	86
	LT=IT	MODEL	87
	DO 3000 K=1,KMAX	MODEL	88
	HL(JMAX,K)=0	MODEL	89
90	U(1,K)=0	MODEL	90
	S(1,K)=30.00	MODEL	91
	S(JMAX,K)=30.00	MODEL	92
	3000 CONTINUE	MODEL	93
	C JET START UP	MODEL	94
95	DO 3001 K=23,25	ES75001	2
	U(1,K)=25*(1-(((L*2.5)-((L/2)*(K-23)*L))**2)/((L*2.5)**2))	ES75001	3
	1SIN(.0001405*DT*((2*LT)-1))	ES75001	4
	U(1,50-K)=U(1,K)	ES75001	5
	3001 CONTINUE	MODEL	100
100	C CALCULATION OF CONSTANTS FOR U,HL	MODEL	108
	DO 600 K=2,KMAX	MODEL	109
	DO 700 J=2,JMAX	MODEL	110
	CALL INDEX	MODEL	111
	CALL CONUH	MODEL	112
105	RX(J)=0	MODEL	113
	TX(J)=U(1,K)	MODEL	114
	PX(J)=BX/(A-CX*RX(JM1))	MODEL	115
	QX(J)=(OCX-CX*TX(JM1))/(A-CX*HX(JM1))	MODEL	116
	RX(J)=F/(EX*PX(J)*F)	MODEL	117
	TX(J)=(F*QX(J)+HCX)/(EX*PX(J)*F)	MODEL	118
110	700 CONTINUE	MODEL	119
	C CALCULATION OF U,HL	MODEL	120
	140 J=JMAX	MODEL	121
	110 U(J,K)=TX(J)-RX(J)*HL(J,1,K)	MODEL	122
	HL(J,K)=QX(J)-PX(J)*U(J,K)	MODEL	123

115	J=J-1	MODEL	174
	IF(J-2) 120,110,110	MODEL	125
	120 CONTINUE	MODEL	126
	600 CONTINUE	MODEL	127
	C EXTRAPOLATION OF U,HL	MODEL	128
120	DO 801 K=2,KMAX	MODEL	129
	U(JMAX,K)=U(JMAXH,K)	ES75001	6
	801 CONTINUE	MODEL	131
	DO 800 K=23,27	ES75001	7
125	HL(1,K)=(HL(2,K)-HL(3,K))*HL(2,K)	MODEL	133
	800 CONTINUE	MODEL	134
	DO 900 J=1,JMAXH	MODEL	135
	JP1=J+1	MODEL	136
	HL(J,1)=0	ES75001	8
	U(JP1,1)=0	ES75001	9
130	HL(JP1,KMAX)=0	MODEL	139
	U(JP1,KMAX)=0	ES75001	10
	900 CONTINUE	MODEL	141
	C PRINT STATEMENTS	MODEL	142
	C VELOCITY IN THE X DIRECTION	MODEL	143
135	TMX=((2*IT-1)*DT)/60.	MODEL	144
	IF(IMOD(IT,3).NE.0) GO TO 4100	ES75001	11
	WRITE(6,91)TMX	MODEL	145
	91 FORMAT(1 TIME(MIN.) FOR HALF TIME STEP X-DIRECTION= #F6.1)	MODEL	146
	WRITE(6,51)IT,DT	MODEL	147
140	51 FORMAT(1 COMPUTED FROM IT,DT=#I5,F10.5)	MODEL	148
	WRITE(6,95)	MODEL	149
	95 FORMAT(1,1 VELOCITY IN X DIRECTION#)	MODEL	150
	DO 902 IK=1,KMAX	MODEL	151
	WRITE(6,92) (U(IJ,IK),IJ=1,JMAX)	MODEL	152
145	902 CONTINUE	MODEL	153
	92 FORMAT(1,1,30F4.0)	MODEL	154
	LT=IT	MODEL	155
	C TIDAL HEIGHT FOR THE X DIRECTION.	MODEL	156
	WRITE(6,96)	MODEL	157
150	96 FORMAT(1,1 TIDAL HEIGHT IN X DIRECTION#)	MODEL	158
	DO 903 IK=1,KMAX	MODEL	159
	WRITE(6,92) (HL(IJ,IK),IJ=1,JMAX)	MODEL	160
	903 CONTINUE	MODEL	161
	4100 CONTINUE	MODEL	162
155	C TAPE WRITING STATEMENTS	MODEL	163
	IDIR=1HX	MODEL	164
	WRITE(4)IDIR,TMX	MODEL	165
	WRITE(4) ((U(IJ,K),J=1,JMAX),K=1,KMAX)	MODEL	166
	WRITE(4) ((HL(IJ,K),J=1,JMAX),K=1,KMAX)	MODEL	167
160	GO TO 4200	ES75001	12
	C CALCULATION OF CONSTANTS FOR S,X-DIRECTION	MODEL	168
	DO 1000 K=2,KMAXH	MODEL	169
	DO 1100 J=2,JMAXH	MODEL	170
	CALL INDEX	MODEL	171
165	CALL CONSX	MODEL	172
	EEX(1)=0	MODEL	173
	FFX(1)=S(1,K)	MODEL	174
	EEX(J)=CCX/(BBX-AAX*EEX(JM1))	MODEL	175
	FFX(J)=(DDX-AAX*FFX(JM1))/(BBX-AAX*EEX(JM1))	MODEL	176
170	1100 CONTINUE	MODEL	177
	C CALCULATION OF S,X-DIRECTION	MODEL	178

	180 J=JMAXM	MODEL	179
	150 S(J,K)=FFX(J)-EEX(J)*S(J+1,K)	MODEL	180
	J=J-1	MODEL	181
175	IF(J-2) 160,150,150	MODEL	182
	160 CONTINUE	MODEL	183
	1000 CONTINUE	MODEL	184
	C EXTRAPOLATION OF S	MODEL	185
	DO 400 J=1,JMAX	MODEL	186
180	S(J,1)=30.00	MODEL	187
	S(J,KMAX)=30.00	MODEL	188
	400 CONTINUE	MODEL	189
	C PRINT STATEMENTS	MODEL	190
	C SALINITY FOR THE X DIRECTION	MODEL	191
185	IF(MOD(IT,3).NE.0) GO TO 4200	ES75001	13
	WRITE(6,98)	MODEL	192
	98 FORMAT(#1 SALINITY FOR X-DIRECTION#)	MODEL	193
	DO 904 IK=1,KMAX	MODEL	194
	WRITE(6,92) (S(IJ,IK),IJ=1,JMAX)	MODEL	195
190	904 CONTINUE	MODEL	196
	4200 CONTINUE	MODEL	197
	C TAPE WRITING STATEMENTS	MODEL	198
	GO TO 4250	ES75001	14
	WRITE(4) ((S(J,K),J=1,JMAX),K=1,KMAX)	MODEL	199
195	4250 CONTINUE	ES75001	15
	DO 1200 J=1,JMAX	MODEL	200
	DO 1300 K=1,KMAX	MODEL	201
	S(J,K)=30.0	ES75001	16
	S2(J,K)=S1(J,K)	MODEL	202
200	S1(J,K)=S(J,K)	MODEL	203
	HL2(J,K)=HL1(J,K)	MODEL	204
	HL1(J,K)=HL(J,K)	MODEL	205
	V2(J,K)=V1(J,K)	MODEL	206
	1300 CONTINUE	MODEL	207
205	1200 CONTINUE	MODEL	208
	C INPUT OF BOUNDARY CONDITIONS	MODEL	209
	LT=IT	MODEL	210
	DO 4000 J=1,JMAX	MODEL	211
	S(J,1)=30.00	MODEL	212
210	S(J,KMAX)=30.00	MODEL	213
	HL(J+1,1)=0	ES75001	17
	HL(J+1,KMAX)=0	ES75001	18
	HL(J,KMAX)=0	MODEL	215
	4000 CONTINUE	MODEL	216
215	4050 CONTINUE	MODEL	217
	C CALCULATION OF CONSTANTS FOR V,HL	MODEL	218
	DO 1400 J=2,JMAXM	MODEL	219
	K=1	ES75001	19
	CALL INDEX	ES75001	20
220	CALL CONVM	ES75001	21
	E1=A/2*(L1*2*(V2(J,K)-V2(J,KP1)))	ES75001	22
	E2=((V2(J,K))**2)+(.0625)*((U1A)**2)**0.5	ES75001	23
	E3=(HYB1*((C1KP+C1)/2)**2)	ES75001	24
	EY=((E2/E3)*6)+E1	ES75001	25
225	PY(1)=0	ES75001	26
	RY(1)=-F/(EY-PY(1)*F)	ES75001	27
	TY(1)=(HCY-F*HL(J,1))/(EY-PY(1)*F)	ES75001	28
	DO 1500 K=2,KMAXM	MODEL	220

	CALL INDEX	MODEL	221
230	CALL CONVH	MODEL	222
	PY(K)=CY/(A-BY*RY(KH1))	MODEL	225
	QY(K)=(DCY-BY*TY(KH1))/(A-BY*RY(KH1))	MODEL	226
	RY(K)=-(F/(EY-PY(K)*F))	MODEL	227
	TY(K)=(HCY-F*QY(K))/(EY-PY(K)*F)	MODEL	228
235	1500 CONTINUE	MODEL	229
	C CALCULATION OF V,HL	MODEL	230
	240 K=KMAXM	MODEL	231
	210 CONTINUE	MODEL	232
	KP1=K+1	MODEL	233
240	V(J,K)=TY(K)-RY(K)*HL(J,KP1)	MODEL	234
	HL(J,K)=QY(K)-PY(K)*V(J,K)	MODEL	235
	K=K-1	MODEL	236
	IF(K=2) 220,210,210	MODEL	237
	V(J,1)=TY(1)-RY(1)*HL(J,2)	ES75001	29
245	220 CONTINUE	MODEL	238
	1400 CONTINUE	MODEL	239
	C EXTRAPOLATION OF V,HL	MODEL	240
	DO 2100 J=2,JMAXM	MODEL	241
	HL(J,1)=0	ES75001	30
250	V(J,1)=V(J,2)	ES75001	31
	V(J,KMAX)=V(J,KMAXM)	ES75001	32
	2100 CONTINUE	MODEL	244
	DO 2200 K=1,KMAXM	MODEL	245
	KP1=K+1	MODEL	246
255	HL(1,K)=0	MODEL	247
	V(1,K)=0	MODEL	248
	HL(JMAX,K)=0	MODEL	249
	V(J,KMAX)=V(JMAX,1)	ES75001	33
260	2200 CONTINUE	MODEL	251
	DO 2300 K=23,27	ES75001	34
	HL(1,K)=(HL(2,K)-HL(3,K))+HL(2,K)	MODEL	253
	V(1,K)=0	MODEL	254
	2300 CONTINUE	MODEL	255
	C PRINT STATEMENTS	MODEL	256
265	TMY=(IT*DT*2)/60.	MODEL	257
	IF(MOD(IT,3).NE.0) GO TO 4300	ES75001	35
	WRITE(6,93) TMY	MODEL	258
	93 FORMAT(1 TIME(MIN.) FOR HALF TIME STEP Y-DIRECTION= #,F6.1)	MODEL	259
	WRJTE(6,51)IT,DT	MODEL	260
270	C VELOCITY V IN THE Y DIRECTION	MODEL	261
	101 FORMAT(/, # VELOCITY Y DIRECTION#)	MODEL	262
	WRITE(6,101)	MODEL	263
	DO 905 IK=1,KMAX	MODEL	264
	WRITE(6,92) (V(IJ,IK),IJ=1,JMAX)	MODEL	265
275	905 CONTINUE	MODEL	266
	C TIDAL HEIGHT FOR THE Y DIRECTION	MODEL	267
	103 FORMAT(/, # TIDAL HEIGH IN Y DIRECTION#)	MODEL	268
	WRITE(6,103)	MODEL	269
	DO 906 IK=1,KMAX	MODEL	270
280	WRITE(6,92) (HL(IJ,IK),IJ=1,JMAX)	MODEL	271
	906 CONTINUE	MODEL	272
	4300 CONTINUE	MODEL	273
	C TAPE WRITING STATEMENTS	MODEL	274
	IDIR=JHY	MODEL	275
285	WRITE(4)IDIR,TMY	MODEL	276

	WRITE(4) ((V(J,K),J=1,JMAX),K=1,KMAX)	MODEL	277
	WRITE(4) ((HL(J,K),J=1,JMAX),K=1,KMAX)	MODEL	278
	GO TO 4400	ES75001	36
	C CALCULATION OF CONSTANTS FOR S,Y-DIRECTION	MODEL	279
290	DO 1900 J=2,JMAX	MODEL	280
	DO 2000 K=2,KMAX	MODEL	281
	CALL INDEX	MODEL	282
	CALL CONSY	MODEL	283
	EEY(1)=0	MODEL	284
295	FFY(1)=S(J,1)	MODEL	285
	EEY(K)=CCY/(BBY-AAY*EEY(KM1))	MODEL	286
	FFY(K)=(DDY-AAY*FFY(KM1))/(BBY-AAY*EEY(KM1))	MODEL	287
	2000 CONTINUE	MODEL	288
	C CALCULATION OF S,Y-DIRECTION	MODEL	289
300	280 K=KMAX	MODEL	290
	250 CONTINUE	MODEL	291
	S(J,K)=FFY(K)-EEY(K)*S(J,K+1)	MODEL	292
	K=K-1	MODEL	293
	IF(K=2) 260,250,250	MODEL	294
305	260 CONTINUE	MODEL	295
	1900 CONTINUE	MODEL	296
	C EXTRAPOLATION OF S	MODEL	297
	DO 500 K=1,KMAX	MODEL	298
	S(1,K)=30.00	MODEL	299
310	S(JMAX,K)=30.00	MODEL	300
	500 CONTINUE	MODEL	301
	C PRINT STATEMENTS	MODEL	302
	C SALINITY FOR THE Y DIRECTION	MODEL	303
	IF(MOD(IT,3).NE.0) GO TO 4400	ES75001	37
315	WRITE(6,105)	MODEL	304
	105 FORMAT(1 SALINITY FOR Y-DIRECTION#)	MODEL	305
	DO 907 IK=1,KMAX	MODEL	306
	WRITE(6,92) (S(IJ,IK),IJ=1,JMAX)	MODEL	307
	907 CONTINUE	MODEL	308
320	4400 CONTINUE	MODEL	309
	C TAPE WRITING STATEMENTS	MODEL	310
	GO TO 4450	ES75001	38
	WRITE(4) ((S(J,K),J=1,JMAX),K=1,KMAX)	MODEL	311
325	4450 CONTINUE	ES75001	39
	DO 2500 K=1,KMAX	MODEL	312
	DO 2600 J=1,JMAX	MODEL	313
	S(J,K)=30.0	ES75001	40
	HL2(J,K)=HL1(J,K)	MODEL	314
330	HL1(J,K)=HL(J,K)	MODEL	315
	S2(J,K)=S1(J,K)	MODEL	316
	S1(J,K)=S(J,K)	MODEL	317
	U2(J,K)=U1(J,K)	MODEL	318
	2600 CONTINUE	MODEL	319
	2500 CONTINUE	MODEL	320
335	WRITE(6,90) IT	MODEL	321
	90 FORMAT(# CYCLES COMPLETED= #,I4)	MODEL	322
	300 CONTINUE	MODEL	323
	WRITE(6,7852)	MODEL	324
	7852 FORMAT(# THIS IS THE END#)	MODEL	325
340	C TAPE WRITING STATEMENTS	MODEL	326
	I1=10HTHIS IS TH	MODEL	327
	I2=10HE END	MODEL	328

345

```
WRITE(4)11.12  
ENDFILE4  
REWIND4  
STOP  
END
```

```
MODEL 329  
MODEL 330  
MODEL 331  
MODEL 332  
MODEL 333
```

	SUBROUTINE CONUH	CONUH	2
	RFAL L,L1,L2,L3,L4	CONUH	3
	DIMENSION U(30,50),U1(30,50),U2(30,50)	CONUH	4
	DIMENSION V(30,50),V1(30,50),V2(30,50)	CONUH	5
5	DIMENSION HL(30,50),HL1(30,50),HL2(30,50)	CONUH	6
	DIMENSION HAVG(30,50),PX(50),QX(50),RX(50),TX(50)	CONUH	7
	DIMENSION EEX(50),FFX(50)	CONUH	8
	DIMENSION PY(50),QY(50),RY(50),TY(50)	CONUH	9
	DIMENSION EY(50),FFY(50)	CONUH	10
10	DIMENSION S(30,50),S1(30,50),H(30,50),S2(30,50)	CONUH	11
	COMMON HJHKM,HL1JK,HJKM1,JM1,KM1,JP1,KP1,HJK,HJM1K,	CONUH	12
	1BX,CX,DCX,E1,E2,E3,EX,HC1A,HC1B,HC1D,HC1,HC2,HC3,HC4A,HC4B,HC4C,	CONUH	13
	1HC4D,HC4,HC5,HC6,HC7,HCX,G,FC, H,HL1,HL2,U, U2,V, V2,S,	CONUH	14
	1S1,DX,DY,DX1,DY1,R1,C1,HXB1,HXF1,HYB1,HYF1,C,HXF,HXB,HAvg,V1A,A,	CONUH	15
15	1F,L1,L2,L3,L4,WSX,AA1,AA2,AA3,AA4,AA5,AB1,BB2,BB3,CC1,CC2,CC3,CC4,	CONUH	16
	1CCX,DD1,DD2,DD3,DDX,C2,HL,S2,TX,EEX,FFX,RX,L,J,K	CONUH	17
	COMMON BY,CY,DCY,EY,HCY,AA,BBY,CCY,DDY,HYF,HYB,WSY,U1A,	CONUH	18
	1C1JP,R1JP,DXJM,DY1KM,CJM,C1KM,C1KP,R1KP,DYKM,DX1JM,CKM,C1JM	CONUH	19
20	EQUIVALENCE (PX,EEX,PY,EY)	CONUH	20
	EQUIVALENCE (QX,FFX,QY,FFY)	CONUH	21
	EQUIVALENCE (RX,RY),(TX,TY)	CONUH	22
	EQUIVALENCE (U,U1),(V,V1)	CONUH	23
	C1=400.0	EST5001	41
25	R1=1.00*(.007945*S1(J,K))	CONUH	25
	C1JP=C1	EST5001	42
	R1JP=1.00*(.007945*S1(JP1,K))	CONUH	27
	V1A=(V1(JP1,K)+V1(JP1,KM1)+V1(J,KM1)+V1(J,K))	CONUH	28
	BX=L1*HXF1	CONUH	29
	CX=-(L1*HXB1)	CONUH	30
30	DCX=-1*((-HL1(J,K))*A)+(L1*(HYF1*V1(J,KM1)-HYB1*V1(J,K)))	EST5001	43
	E1=(A/2)+(L1*(U2(JP1,K)-U2(JM1,K)))	EST5001	44
	E2=((U2(J,K)**2)+(.0625)*(V1A**2))**.5	CONUH	33
	E3=(HXF1*((C1JP+C1)/2)**2)	CONUH	34
	EX=((E2/E3)*G)*E1	CONUH	35
35	HC1A=U2(J,KM1)-U2(J,KP1)	CONUH	36
	HC1B=HC1A*V1A	CONUH	37
	HC1C=HC1B*L4	CONUH	38
	HC1D=U2(J,K)*(A/2)	EST5001	45
	HC1=-HC1D*HC1C	CONUH	40
40	HC2=((HL2(JP1,K)-HL2(J,K))*F)*(R1JP-	CONUH	41
	R1)*HXF1*(1/(R1JP+R1))*F)	CONUH	42
	HC3=(FC/4.)*V1A	CONUH	43
	HC4A=2*G*U2(J,K)	CONUH	44
	HC4B=U2(J,K)**2	CONUH	45
45	HC4C=HC4B*(0.0625)*(V1A)**2	CONUH	46
	HC4D=HC4C**.5	CONUH	47
	HC4=HC4A*HC4D	CONUH	48
	HC5=(HXF1*((C1JP+C1)/2)**2)*2	CONUH	49
	HC6 = HC4 / HC5	CONUH	50
50	HC7=4*WSX/(R1JP+R1)*HXF1	CONUH	51
	HCX=-(HC1*HC2-HC3*HC6-HC7)	CONUH	52
	RETURN	CONUH	53
	END	CONUH	54

```

SUBROUTINE CONSX
REAL L,L1,L2,L3,L4
DIMENSION U(30,50),U1(30,50),U2(30,50)
DIMENSION V(30,50),V1(30,50),V2(30,50)
DIMENSION HL(30,50),HL1(30,50),HL2(30,50)
DIMENSION HAVG(30,50),PX(50),QX(50),RX(50),TX(50)
DIMENSION EEX(50),FFX(50)
DIMENSION PY(50),OY(50),RY(50),TY(50)
DIMENSION EEE(50),FFY(50)
DIMENSION S(30,50),S1(30,50),H(30,50),S2(30,50)
COMMON HJMKM,HL1JK,HJKH1,JH1,KH1,JP1,KP1,HJK,HJMK1,
IBX,CX,DCX,F1,E2,E3,EX,HC1A,HC1B,HC1D,HC1,HC2,HC3,HC4A,HC4B,HC4C,
IHC4D,HC4,HC5,HC6,HC7,HCX,G,FC, H,HL1,HL2,U, U2,V, V2,S,
IS1,DX,DY,DX1,DY1,R1,C1,HXB1,HXF1,HYB1,HYF1,C,HXF,HXB,HAvg,V1A,A,
IF,L1,L2,L3,L4,MSX,AA1,AA2,AA3,AA4,AA5,BB1,BB2,BB3,CC1,CC2,CC3,CC4,
ICCX,DD1,DD2,DD3,DDX,C2,HL,S2,TX,EEX,FFX,RX,L,J,K
COMMON BY,CY,DCY,EY,HCY,AA5,BB4,CCY,DDY,HYF,HYB,MSY,U1A,
ICJP,R1JP,DXJM,OYJ,KM,CJM,C1KM,C1KP,R1KP,DKM,DX1JH,CKH,C1JM
EQUIVALENCE (PA,EEX,PY,EEY)
EQUIVALENCE (OX,FFX,OY,FFY)
EQUIVALENCE (RX,RY),(TX,TY)
EQUIVALENCE (U,U1),(V,V1)
HXF=HJK + HJKM) + HL(JP1,K) + HL(J,K)
HXB=HJMK + HJMKM + HL(J,K) + HL(JH1,K)
C=491.9
DX=(5.93*HJK*U(J,K)+31.3049)/C
CJM=491.9
DXJM=(5.93*H(JH1,K)+U(JH1,K)*31.3049)/CJM
C1=491.9
DY1=((5.93*HJK*V1(J,K)+31.3049)/C1)
C1KM=491.9
DY1KM=((5.93*H(J,KH1)+V1(J,KH1)*31.3049)/C1KM)
AA1=HXB1*U(JH1,K)
AA2=AA1*L2
AA3=HXB*DXJM
AA4=AA3*L3
AA5=-(AA2+AA4)
BB1=(A*(HAvg(J,K)+HL(J,K)))+((HXF1*U(J,K))-
1*(HXB1*U(JH1,K)))*L2)
BB2=(HXF*DX+HXB*DXJM)*L3
BB3=BB1+BB2
CC1=HXF1*U(J,K)
CC2=CC1*L2
CC3=HXF*DX
CC4=CC3*L3
CCX=CC2-CC4
DD1A=HAvg(J,K)+HL1(J,K)
DD1B=DD1A*S1(J,K)
DD1=-DD1B*A
DD2=((HYF1* V1(J,KH1))*(S1(J,KH1)+S1(J,K)))
1-(HYB1*V1(J,K)*(S1(J,K)+S1(J,KP1))))*L2
DD3=((HYF1*DY1KM*(S1(J,KH1)-S1(J,K)))
1-(HYB1*DY1*(S1(J,K)-S1(J,KP1))))*L3)
DDX=-(DD1+DD2-DD3)
RETURN
END
CONSX 2
CONSX 3
CONSX 4
CONSX 5
CONSX 6
CONSX 7
CONSX 8
CONSX 9
CONSX 10
CONSX 11
CONSX 12
CONSX 13
CONSX 14
CONSX 15
CONSX 16
CONSX 17
CONSX 18
CONSX 19
CONSX 20
CONSX 21
CONSX 22
CONSX 23
CONSX 24
CONSX 25
CONSX 26
CONSX 27
CONSX 28
CONSX 29
CONSX 30
CONSX 31
CONSX 32
CONSX 33
CONSX 34
CONSX 35
CONSX 36
CONSX 37
CONSX 38
CONSX 39
CONSX 40
CONSX 41
CONSX 42
CONSX 43
CONSX 44
CONSX 45
CONSX 46
CONSX 47
ES75001 46
ES75001 47
CONSX 50
CONSX 51
CONSX 52
CONSX 53
CONSX 54
CONSX 55
CONSX 56
CONSX 57

```

	SUBROUTINE CONVH	CONVH	2
	REAL L,L1,L2,L3,L4	CONVH	3
	DIMENSION U(30,50),U1(30,50),U2(30,50)	CONVH	4
	DIMENSION V(30,50),V1(30,50),V2(30,50)	CONVH	5
5	DIMENSION HL(30,50),HL1(30,50),HL2(30,50)	CONVH	6
	DIMENSION HAVG(30,50),PX(50),QX(50),RX(50),TX(50)	CONVH	7
	DIMENSION EEX(50),FFX(50)	CONVH	8
	DIMENSION PY(50),QY(50),RY(50),TY(50)	CONVH	9
	DIMENSION EEY(50),FFY(50)	CONVH	10
10	DIMENSION S(30,50),S1(30,50),H(30,50),S2(30,50)	CONVH	11
	COMMON HJMK4,HL1JK,HJMK1,JM1,KM1,JP1,KP1,HJK,HJM1K,	CONVH	12
	1HC4D,HC4,HC5,HC6,HC7,HCX,G,FC, H,HL1,HL2,U, U2,V, V2,S,	CONVH	13
	1S1,DX,DY,DX1,DY1,R1,C1,HXB1,HXF1,HYB1,HYF1,C,HXF,HXB,HAVG,V1A,A,	CONVH	14
15	1F,L1,L2,L3,L4,WSX,AA1,AA2,AA3,AA4,AA5,AA6,AA7,AA8,AA9,AA0,AA1,	CONVH	15
	1CCX,DD1,DD2,DD3,DDX,S2,HL,S2,TX,EEX,FFX,RX,L,J,K	CONVH	16
	COMMON BY,CY,DCY,EY,HGY,AA1,AA2,AA3,AA4,AA5,AA6,AA7,AA8,AA9,AA0,	CONVH	17
	1C1JP,R1JP,DXJM,DY1KH,CJM,C1KH,C1KP,R1KP,DYKN,DX1JN,CKM,C1JN	CONVH	18
20	EQUIVALENCE (PX,EEX,PY,EEY)	CONVH	19
	EQUIVALENCE (QX,FFX,QY,FFY)	CONVH	20
	EQUIVALENCE (RX,RY),(TX,TY)	CONVH	21
	EQUIVALENCE (U,U1),(V,V1)	CONVH	22
	C1=400.0	CONVH	23
	C1KP=C1	EST5001	48
25	U1A=(U1(JM1,K)+U1(JM1,KP1)+U1(J,KP1)+U1(J,K))	EST5001	49
	R1=1.00+(.007945*S1(J,K))	CONVH	26
	R1KP=1.00+(.007945*S1(J,KP1))	CONVH	27
	BY=L1*HYF1	CONVH	28
	CY=-L1*HYB1	CONVH	29
30	DCY=-((-HL1(J,K))*A)+(L1*(HXF1*U1(J,K)-HXB1*U1(JM1,K)))	CONVH	30
	E1=(A/2)+(L1*(V2(J,K11)-V2(J,KP1)))	EST5001	50
	E2=((V2(J,K))**2)+(0.0625)*((U1A)**2)**0.5	EST5001	51
	E3=(HYB1*((C1KP+C1)/2)**2)	CONVH	33
	EY=((E2/E3)*G)+E1	CONVH	34
35	HC1A=V2(JP1,K)-V2(JM1,K)	CONVH	35
	HC1B=HC1A*U1A	CONVH	36
	HC1C=HC1B*L4	CONVH	37
	HC1D=V2(J,K)*(A/2)	CONVH	38
	HC1=HC1D+HC1C	EST5001	52
40	HC2=((HL2(J,K)-HL2(J,KP1))*F)+(R1-	CONVH	40
	1R1KP)*HYB1)*F*(1/(R1KP+R1))	CONVH	41
	HC3=(FC/4)*U1A	CONVH	42
	HC4A=2*G*V2(J,K)	CONVH	43
	HC4B=V2(J,K)**2	CONVH	44
45	HC4C=HC4B+(0.0625)*((U1A)**2)	CONVH	45
	HC4D=HC4C**0.5	CONVH	46
	HC4=HC4A*HC4D	CONVH	47
	HC5=(HYB1*((C1KP+C1)/2)**2)*2	CONVH	48
	HC6=HC4/HC5	CONVH	49
50	HC7=4*WSY/(R1KP+R1)*HYB1	CONVH	50
	HGY=-((HC1+HC2+HC3+HC6-HC7)	CONVH	51
	RETURN	CONVH	52
	END	CONVH	53
		CONVH	54

	SUBROUTINE CONSY	CONSY	2
	REAL L,L1,L2,L3,L4	CONSY	3
	DIMENSION U(30,50),U1(30,50),U2(30,50)	CONSY	4
	DIMENSION V(30,50),V1(30,50),V2(30,50)	CONSY	5
5	DIMENSION HL(30,50),HL1(30,50),HL2(30,50)	CONSY	6
	DIMENSION HAVG(30,50),PX(50),QX(50),RX(50),TX(50)	CONSY	7
	DIMENSION EEX(50),FFX(50)	CONSY	8
	DIMENSION PY(50),QY(50),RY(50),TY(50)	CONSY	9
	DIMENSION EY(50),FFY(50)	CONSY	10
10	DIMENSION S(30,50),S1(30,50),H(30,50),S2(30,50)	CONSY	11
	COMMON HJMKM,HL1JK,HJKM1,JM1,KM1,JP1,KP1,HJK,HJM1K,	CONSY	12
	1BX,CX,DCX,E1,E2,E3,EX,MC1A,MC1B,MC1D,MC1,MC2,MC3,MC4A,MC4B,MC4C,	CONSY	13
	1MC4D,MC4,MC5,MC6,MC7,MCX,G,FC, H,HL1,HL2,U, U2,V, V2,S,	CONSY	14
	1S1,DX,DY,DX1,DY1,R1,C1,HXB1,HXF1,HYB1,MYF1,C,HXF,HXB,HAvg,V1A,A,	CONSY	15
15	1F,L1,L2,L3,L4,WSX,AA1,AA2,AA3,AA4,AA5,BB1,BB2,BBX,CC1,CC2,CC3,CC4,	CONSY	16
	1CCX,DD1,DD2,DD3,DDX,C2,HL,S2,TX,EEX,FFX,RX,L,J,K	CONSY	17
	COMMON BY,CY,DCY,EY,HCY,AA1,BBY,CCY,DDY,HYF,HYB,WSY,U1A,	CONSY	18
	1C1JP,R1JP,DXJM,DY1KH,CJM,C1KH,C1KP,R1KP,DYKM,DX1JM,CKH,C1JM	CONSY	19
	EQUIVALENCE (PX,EEX,PY,EEY)	CONSY	20
20	EQUIVALENCE (QX,FFX,QY,FFY)	CONSY	21
	EQUIVALENCE (RX,RY),(TX,TY)	CONSY	22
	EQUIVALENCE (U,U1),(V,V1)	CONSY	23
	HYF=HJKM1+HJMKM+HLJK+HL(J,KM1)	CONSY	24
	HYB=HJK+HJM1K+HLJK+HL(J,KP1)	CONSY	25
25	C=491.9	CONSY	26
	DY=((5.93*HJK*V(J,K))*31.3049)/C	CONSY	27
	CK4=491.9	CONSY	28
	DYKM=((5.93*H(J,KM1))*V(J,KM1))*31.3049/CKM	CONSY	29
	C1=491.9	CONSY	30
30	DX1=((5.93*H(J,K))*U(J,K))*31.3049/C1	CONSY	31
	C1JM=491.9	CONSY	32
	DX1JM=((5.93*H(JM1,K))*U(JM1,K))*31.3049/C1JM	CONSY	33
	AA1=HYF1*V(J,KM1)	CONSY	34
	AA2=AA1*L2	CONSY	35
35	AA7=HYF*DYKM	CONSY	36
	AA4=AA3*L3	CONSY	37
	AA5=-AA4*AA2	CONSY	38
	BB1=(A*(HAVG(J,K)+HL(J,K)))+((HYF1*V(J,KM1))-	CONSY	39
40	1(HYB1*V(J,K)))*L2)	CONSY	40
	BB2=(HYF*DYKM-HYB*DY)*L3	CONSY	41
	BBY=BB)*BB2	CONSY	42
	CCY=(((-HYB1*V(J,K))*L2)-((HYB*DY)*L3))	CONSY	43
	DD1A=HAVG(J,K)*HL(J,K)	EST75001	53
	DD1B=DD1A*S1(J,K)	EST75001	54
45	DD1=-DD1B*A	CONSY	46
	DD2=((HXF1*U)(J,K)*(S1(JP1,K)+S1(J,K)))	CONSY	47
	1-(HXB1*U1(JM1,K)*(S1(J,K)+S1(JM1,K))))*L2	CONSY	48
	DD3=((HXF1*DX1)*(S1(JP1,K)-S1(J,K)))	CONSY	49
	1-(HXB1*DX1JM*(S1(J,K)-S1(JM1,K))))*L3)	CONSY	50
50	DDY=-DD1+DD2-DD3)	CONSY	51
	RETURN	CONSY	52
	END	CONSY	53

APPENDIX D
BOTTOM STRESS, VERTICAL EDDY VISCOSITY,
AND CHÉZY COEFFICIENT RELATIONSHIPS

To determine the relationship between values of the Chézy coefficient and the vertical eddy viscosity, we can use equation 2.33

$$-\frac{gU[U^2+V^2]^{1/2}}{C^2} = -\frac{\gamma^b}{\rho} . \quad \text{D.1}$$

Using notation from Dyer (1973), we can set

$$-\frac{\gamma^b}{\rho} = A_z \frac{\partial u}{\partial z} . \quad \text{D.2}$$

From D.1 and D.2 we now have

$$A_z \frac{\partial u}{\partial z} = \frac{gU[U^2+V^2]^{1/2}}{C^2} . \quad \text{D.3}$$

Letting $[U^2 + V^2]^{1/2} = U$ for the purpose of calculation and re-arranging D.3, we have

$$A_z = \frac{gU^2}{C^2 \frac{\partial u}{\partial z}} \quad \text{D.4}$$

If $C = 400 \text{ cm}^{1/2} \text{ sec}^{-1}$, $U = 25 \text{ cm sec}^{-1}$ (an average velocity), and the velocity has a linear variation with depth, then

$$\frac{\partial u}{\partial z} = \frac{50}{1000} = .050$$

and

$$A_z = \frac{980(25)^2}{(400)^2(.050)} = 76.6 .$$

If a vertical distribution of velocity of the form

$$u = U_{\max} \left(\frac{z}{H} \right)^{1/7} \quad \text{D.5}$$

is used (Dronkers (1964)), then $u = U_{\max}$ at the surface.

From Dronkers (1964) a value of $U = 25 \text{ cm sec}^{-1}$ gives a

$U_{\max} = 28.6 \text{ cm sec}^{-1}$. Then $\partial u / \partial z = (28.6/1000) = 0.0286$

and

$$A_z = \frac{(980)(25)^2}{(400)^2(0.0286)} = 133.9.$$

An alternate check of the bottom stress is given by the term $\gamma = g/c^2$ ($\tau_b = \rho\gamma^2U^2$) which for $g = 980 \text{ cm sec}^{-1}$ and $c = 400 \text{ cm}^{1/2} \text{ sec}^{-1}$ gives $\gamma = 6.1 \times 10^{-3}$. Dronkers reports values for their coastal work of $\gamma = 2.9 \times 10^{-3}$.

BIBLIOGRAPHY

- Abramovich, G. N. (1963) The Theory of Turbulent Jets. MIT Press, Cambridge, Mass., 671 pp.
- Albertson, M. L., Y. B. Dai, R. A. Jensen, and H. Rouse (1950) Diffusion of submerged jets. Transactions of the ASCE, 115, 639-697.
- Bates, C. C. (1953) Rational theory of delta formation. Bulletin of the American Association of Petroleum Geologists, 37, 2119-2162.
- Bickley, W. G. (1937) The plane jet. Philosophical Magazine S., 23, 727-731.
- Bigelow, H. B. (1933) Studies in the waters on the continental shelf, Cape Cod to Chesapeake Bay, I. The cycle of temperature. Papers in Physical Oceanography and Meteorology, 2, 1-135.
- Bigelow, H. B. and M. Sears (1935) Studies of the waters on the continental shelf, Cape Cod to Chesapeake Bay, II. Salinity. Papers in Physical Oceanography and Meteorology, 4, 1-94.
- Birkhoff, G. and E. H. Zarantonello (1957) Jets, Wakes and Cavities. Academic Press, Inc., New York, 353 pp.
- Boicourt, W. C. (1973) The circulation of water on the continental shelf from Chesapeake Bay to Cape Hatteras. Johns Hopkins University, PhD dissertation, 183 pp.
- Bondar, C. (1970) Considerations théoriques sur la dispersion d'un courant liquide de densité réduite et a niveau libre, dans un bassin contenant un liquide d'une plus grande densité. UNESCO Report, Symposium on the Hydrology of Deltas. 246-256.
- Borichansky, L. S. and V. N. Mikhailov (1966) Interaction of river and sea water in the absence of tides. UNESCO Report, Scientific Problems of the Humid, Tropical Zone, Deltas and their Implications, 175-180.

- Budinger, T. F., L. K. Coachman, and C. A. Barnes (1964) Columbia River effluent in the Northeast Pacific Ocean, 1961, 1962: Selected aspects of physical oceanography. University of Washington, Department of Oceanography Technical Report 99 (unpublished manuscript).
- Bumpus, D. F. (1965) Residual drift along the bottom on the continental shelf in the Middle Atlantic Bight area. Limnology and Oceanography, Supplement to 3, 48-53.
- Bumpus, D. F. (1969) Reversals in the surface drift in the Middle Atlantic Bight area. Deep Sea Research, Supplement to 16, 17-23.
- Bumpus, D. F. and L. M. Lauzier (1965) Surface circulation on the continental shelf off Eastern North America between Newfoundland and Florida. Serial Atlas of the Marine Environment Folio 7, American Geographical Society, New York, 4 pp.
- Bumpus, D. F. and E. L. Pierce (1955) The hydrography and the distribution of chaetognaths over the continental shelf off North Carolina. Deep Sea Research, Supplement to 3, 92-109.
- Douglas, J. and J. F. Gunn (1964) A general formulation of alternating direction procedures in the presence of singular operators. Numerical Mathematics, 5, 175-184.
- Dronkers, J. J. (1964) Tidal Computations. North-Holland Publishing Company, Amsterdam, 518 pp.
- Duxbury, A. C., B. A. Mare, and N. McGary (1966) The Columbia River effluent and its distribution at sea, 1961-1963. University of Washington, Department of Oceanography Technical Report 156 (unpublished manuscript).
- Dyer, K. R. (1973) Estuaries: A Physical Introduction. John Wiley and Sons, New York, 140 pp.
- Engelund, F. and F. B. Pedersen (1973) Surface jet at small Richardson numbers. Proceedings of the ASCE, HY 3, 405-416.
- Fisher, A. (1972) Entrainment of shelf water by the Gulf Stream northeast of Cape Hatteras. Journal of Geophysical Research, 77, 3248-3255.

- Ford, W. L. and A. R. Miller (1952) The surface layer of the Gulf Stream and adjacent waters. Journal of Marine Research, 1, 267-280.
- Gadgil, S. (1971) Structure of jets in rotating systems. Journal of Fluid Mechanics, 47, 417-436.
- Garvine, R. W. (1974) Physical features of the Connecticut River outflow during high discharge. Journal of Geophysical Research, 79, 831-846.
- Gibbs, R. J. (1970) Circulation in the Amazon River estuary and adjacent Atlantic Ocean. Journal of Marine Research, 28, 113-123.
- Gordon, R. and M. Spaulding (1974) A bibliography of numerical models for tidal rivers, estuaries and coastal rivers. University of Rhode Island, Marine Technical Report 32, 55 pp.
- Harrison, W., J. J. Norcross, N. A. Pore, and E. M. Stanley (1967) Circulation of shelf waters off the Chesapeake Bight. U. S. Department of Commerce, ESSA Professional Paper 3, 82 pp.
- Howe, M. R. (1962) Some direct measurements of the non-tidal drift on the continental shelf between Cape Cod and Cape Hatteras. Deep Sea Research, 9, 445-455.
- Ippen, A. I. (1966) Estuary and Coastal Hydrodynamics. McGraw Hill, New York, 744 pp.
- Iselin, C. O'D. (1955) Coastal currents and the fisheries. Deep Sea Research, Supplement to 3, 474-478.
- Leendertse, J. J. (1967) Aspects of a computational model for long-period water-wave propagation. The Rand Corporation Technical Report, RM-5294-PR, 164 pp.
- Leendertse, J. J. (1970) A water-quality simulation model for well-mixed estuaries and coastal seas: Vol. 1 principles of computation. The Rand Corporation Technical Report, RM-6230-RC, 71 pp.
- Leendertse, J. J. and E. C. Gritten (1971) Volume II computation procedures. The Rand Corporation Technical Report, R-708-NYC, 53 pp.

- Miller, A. R. (1952) A pattern of surface coastal circulation inferred from surface salinity-temperature data and drift bottle recoveries, Woods Hole Oceanographic Institution Technical Report 52-28, 14 pp.
- Neumann, G. and W. J. Pierson, Jr. (1966) Principles of Physical Oceanography. Prentice-Hall, Inc., Englewood Cliffs, N. J., 545 pp.
- Park, K. (1966) Columbia River plume identification by specific alkalinity. Limnology and Oceanography, 11, 118-120.
- Parr, A. E. (1933) A geographical-ecological analysis of the seasonal changes in temperature conditions in shallow water along the Atlantic Coast of the United States. Bulletin of the Bingham Oceanographic Collection, 4, 1-90.
- Peaceman, D. W. and H. H. Rachford, Jr. (1965) The numerical solution of parabolic and elliptic differential equations. Journal Society of Industrial and Applied Mathematics, 3, 28-41.
- Redfield, A. C. (1958) The influence of the continental shelf on the tides of the Atlantic Coast of the United States. Journal of Marine Research, 17, 432-448.
- Ryther, J. H., D. W. Menzel, and N. Corwin (1967) Influence of the Amazon River outflow on the ecology of the western tropical Atlantic. I. Hydrography and nutrient chemistry. Journal of Marine Research, 25, 69-83.
- Schlichting, H. (1933) Laminare Strahlausbreitung. Z. Angew. Math. Mech., 13, 260-263.
- Stefánsson, U. and F. A. Richards (1963) Processes contributing to the nutrient distributions off the Columbia River and Strait of Juan de Fuca. Limnology and Oceanography, 8, 394-410.
- Stefánsson, U., L. P. Atkinson, and D. F. Bumpus (1971) Hydrographic properties and circulation of the North Carolina shelf and slope waters. Deep Sea Research, 18, 383-420.
- Stommel, H. (1965) The Gulf Stream. University of California Press, Berkeley, 248 pp.

- Stommel, H. and A. Leetmaa (1972) Circulation on the continental shelf. Proceedings of the National Academy of Science, U. S. A., 69, 3380-3384.
- Sturges, W. (1974) Sea level slope along continental boundaries. Journal of Geophysical Research, 79, 825-830.
- Sverdrup, H. V., M. W. Johnson, and R. H. Fleming (1942) The Oceans. Prentice-Hall, Inc., Englewood Cliffs, N. J., 1087 pp.
- Takano, K. (1954a) On the velocity distribution off the mouth of a river. Journal of the Oceanographic Society of Japan, 10, 1-5.
- Takano, K. (1954b) On the salinity and velocity distributions off the mouth of a river. Journal of the Oceanographic Society of Japan, 10, 92-98.
- Takano, K. (1955) A complementary note on the diffusion of the seaward river flow off the mouth. Journal of the Oceanographic Society of Japan, 11, 1-3.
- Wright, L. D. and J. M. Coleman (1971) Effluent expansion and interfacial mixing in the presence of a salt wedge, Mississippi River delta. Journal of Geophysical Research, 76, 8649-8661.

VITA

Everett Michael Stanley

Born in Orangeburg, South Carolina, March 7, 1938. Graduated from Fairfax Public School, Fairfax, South Carolina, June 1956; B.S., Physics, The Citadel, June 1960; M.S., Oceanography, Massachusetts Institute of Technology, June 1964. The author is now an Oceanographer employed at the David W. Taylor Naval Ship Research and Development Center, Annapolis, Maryland.

In January 1973, the author entered the School of Marine Science of the College of William and Mary, located at the Virginia Institute of Marine Science, Gloucester Point, Virginia.